AN ABSTRACT OF THE THESIS OF

DAVID ELAM AMSTUTZ for the degree of Doctor of Philosophy

in Oceanography presented on December 20, 1976

Title: STEREOPHOTOGRAMMETRIC RECONNAISSANCE OF OCEAN WAVE/SEA ICE INTERACTION

Redacted for Privacy

Abstract approved: ______________________
Victor T. Neal

Studies of the phenomenon of ocean wave/sea ice interaction occupy a miniscule portion of the oceanographic literature. Interest in the attenuation of ocean waves by sea ice has increased during the past decade with expanding activities in the ice-covered regions.

A satisfactory explanation of the phenomenon has not been achieved through theoretical and physical modeling studies largely because of the complexities inherent with complete mathematical formulation and the absence of suitable materials for simulation of sea ice in the laboratory. As a result, investigators are forced to acquire full-scale measurements and proceed primarily by descriptive analyses. Very few observations of the interaction have been acquired and previous measurement techniques have not been able to provide simultaneous measurements of most of the relevant parameters.

A new measurement technique has been developed using airborne stereophotogrammetry. Observations have been made over the

East Greenland Drift Stream, south of Denmark Strait. The airborne technique, requiring two aircraft, utilizes an accurate measure of flying attitude obtained with an airborne laser to derive image scale. The technique provides a measure of all pertinent parameters except ice keels. The reported observations are from a single flight track extending from the ice edge to the position of immeasurable (with this technique) wave amplitude.

The wave attenuation process is dependent upon characteristics (floe size and concentration) of the ice canopy. During the time of measurement (March 11, 1974), the ice canopy was composed of relatively thick, discrete floes surrounded by thin ice. The observations indicate wave scattering to be the primary process accounting for the measured attenuation of wave amplitude. Attenuation of wave amplitude is expressed in the form of amplitude transmission coefficients, following the procedure used in studies of artificial floating breakwaters. The scattering process has a maximum effect for wavelength (λ) when the diameter (d) of the floes of greatest concentration is in a ratio (d/λ) $\geqslant 0.3 - 0.4$. The scattering process initiates for specific wavelengths upon encountering floe diameters which yield ratios $d/\lambda \geqslant 0.1 - 0.2$. Both of these ratios confirm hypotheses advanced by Robin (1963). Ice thicknesses for which the ratios apply are extended considerably from those reported by Robin (1963) and Dean (1966a). Wavelengths of greatest relative amplitude, for which floe diameters were too small to scatter using the d/λ criteria, were observed to attenuate rapidly with increasing penetration of the ice canopy. It is suggested that these wavelengths attenuate as a consequence of the mass effects of the ice.

Recommendations are made for further studies of the interaction using the airborne stereophotogrammetric technique and for examination of kindred phenomena associated with the interaction process. Existing observations, including those reported here, have been acquired under a variety of ice canopy conditions. The lack of repetitious measurements under similar ice conditions and the absence of observations for shallow water restrict constructive criticism of existing theoretical studies.

Stereophotogrammetric Reconnaissance of Ocean Wave/Sea Ice Interaction

by

David Elam Amstutz

A THESIS

submitted to

Oregon State University

in partial fulfillment of
the requirements for the
degree of

Doctor of Philosophy

Completed December 20, 1976

Commencement June 1977

APPROVED:

Redacted for Privacy

Associate Professor of Oceanography
in charge of major

Redacted for Privacy

Dean of Oceanography

Redacted for Privacy

Dean of Graduate School

Date thesis is presented December 20, 1976

Typed by Opal Grossnicklaus for David Elam Amstutz

ACKNOWLEDGMENTS

The straightforward beginning and the joyous end have been bonded by toil and the best attributes of many.

The Defense Advanced Research Projects Agency and the U.S. Naval Oceanographic Office are recognized for their sponsorship of data acquisition and processing.

I am grateful to Mr. Robert Ketchum, Jr., for patient training in the fields of sea ice and airborne remote sensing, and to Commander William Cochrane, and the Officers and Crew of VXN-8, for exercise of their skills during the measurement period.

Special appreciation for assistance and encouragement is conveyed to those who kept-the-watch during the period of toil: Dr. Victor Neal, Dr. Thomas Davis, Mr. Edward Geary, Dr. James O'Brien, Mr. Marvin Burkhart and Dr. Gordon de Q. Robin.

The necessary ingredient of inspiration has been supplied throughout by my wife, Mary Ann, to whom this effort is dedicated.

TABLE OF CONTENTS

LIST OF FIGURES

LIST OF TABLES

STEREOPHOTOGRAMMETRIC RECONNAISSANCE OF OCEAN WAVE/SEA ICE INTERACTION

I. SCOPE AND OBJECTIVES

Studies of ocean waves and sea ice have proceeded over several centuries. Studies of ocean waves span topics which precede their generation, follow their breaking and include to one degree or another all of the interim processes of alteration. Three distinct approaches have been followed: direct measurement, theoretical treatment and physical modeling. Many investigations have combined these approaches and numerous summaries of 'present knowledge' have been produced. Procedures for data analysis have improved and generally become more complex with the adaptation by wave investigators of a wide variety of mathematical and statistical techniques. The purposes of these studies have encompassed a broad range--from pursuit of understanding a specific and limited process to engineering development of offshore vehicles and structures. Within this range lies the field of wave forecasting.

Studies of sea ice have also proceeded over several centuries. Topics which have been studied precede that of formation and extend beyond disintegration and melt. The interim processes are more limited than for the case of waves but undoubtedly are no less complex. The approaches used by various investigators are similar to those used in the study of waves. The exceptions are in physical modeling largely because there are few if any materials which duplicate sea ice properties. There have been fewer investigators addressing sea ice, fewer summaries of 'present knowledge' and the subject has not attracted prominent hydrodynamicists so much as has the study of waves. Until recently, the purposes for studying sea ice have been limited. Among them, interest in climatic effects, navigation in high latitudes, and extraction of natural resources are most prominent. The latter purpose has and undoubtedly will continue to be the most influential. Interests in pursuing the forecasting of ice behavior have developed in a somewhat parallel fashion with those of wave forecasting. Again, these studies have been far fewer in number and less sophisticated.

We turn now to the more specific subject of ocean wave/sea ice interaction. This phenomenon is initiated when ocean waves, propagating over the open sea from their area of generation, encounter the seaward edge of the sea ice canopy. The spatial extent of the region of interaction may be viewed as either narrow or broad. It is narrow if one examines that zone near the ice edge in which the amplitudes of sea surface undulation are decreased very significantly. It is broad if one extends the zone to incorporate all areas of the ice canopy which are found to contain any of the wave energy initially observed at the ice edge. The zone defined in the narrow sense is presently of greatest interest to those operating in sea ice. This area is marginally navigable by surface ships, accessible to all subsurface vessels and in some locations, possessed with natural resources which are extractable with present technology. It is a region sometimes characterized by high levels of ambient noise. For this and other reasons, it is of importance in military oceanography.

Ocean wave/sea ice interaction has been studied in few regions and by even fewer investigators. If the phenomenon is to be understood, it will be necessary to acquire more field observations and under a wider variety of ice conditions than have been addressed to date. Theoretical studies are awaiting further observational information. Laboratory studies are limited not only by deficiencies in real scale observations but also in materials which simulate sea ice.

Attention in this work therefore is directed to the phenomenon of ocean wave/sea ice interaction and its measurement--not to ocean waves, per se or to sea ice, per se. My interest is confined to the seaward portion of the interaction zone, where the most rapid rate of wave amplitude attenuation is observed. Though not specifically addressed, the work is pursued toward a later formulation of predictive techniques.

The objectives are: (1) to summarize and evaluate previously used measurement techniques; (2) to develop and utilize a new measurement technique believed to be especially suited for investigation of the phenomenon (i. e., airborne stereophotogrammetry); (3) to analyze these observations and contrast the results with the findings of previous observations and their analyses; and (4) to summarize the results of existing theoretical and physical modeling studies and evaluate these results, where applicable, in light of the new observations. A final purpose is that of recommending possible future applications of the measurement technique.

This work is organized to achieve the objectives in the order they are presented above. Some digressions for sake of clarity and amplification are contained within the text. It is intended that this format will convey the findings in a concise yet thorough fashion.

II. PREVIOUS MEASUREMENT TECHNIQUES

Introduction to the Environment

There are two broad environmental circumstances required for the phenomenon of ocean wave/sea ice interaction: an expanse of open ocean surface sufficient for the generation of waves and a connected region of ocean covered by sea ice. The requirement for sea ice limits the phenomenon to areas of high latitude where either the air temperatures are sufficiently low to result in ice formation or where wind and currents will carry ice into regions where waves may be encountered.

Both hemispheres have such regions. Sea ice surrounds the Antarctic continent and is thus found in the southernmost parts of the Atlantic, Pacific and Indian Oceans. Predominant regions in the northern hemisphere are the Barents, Greenland, Labrador and Bering Seas.

Sea ice is a highly complex substance composed of water, brine solutions (containing a variety of constituents and concentrations), and atmospheric gases. The physical properties of sea ice are dependent not only on the present conditions of the ice and the *in situ* air and water temperatures, but also on its past history. The properties of sea ice are further complicated by the presence of snow cover of varying thickness and composition. The properties of sea ice and their dependence on present conditions as well as past history are discussed in a number of articles found in Kingery (1963).

In most areas and particularly in those of interest here, the sea ice canopy consists of ice of a variety of forms, stages of development and melting, arrangements, openings and surface features. The terminology used here follows that specified by the World Meteorological Organization. A brief glossary of ice terminology is presented in Appendix A.

The absence of uniformity displayed by floating ice is a consequence of its being a mixture or conglomerate of ice derived from several sources and formed at different times. The area of interest for this work, as well as for two prior studies of this phenomenon (Wadhams, 1971 and Amstutz and Ketchum, 1973), is off the east coast of Greenland, along the seaward side of the East Greenland Drift Stream. The floating ice found in the East Greenland Drift Stream derives from three distinct sources: (1) pack ice in the Arctic Basin; (2) glacier ice from Eastern Greenland; and, (3) sea ice formed locally as the canopy transits southward along the coast. The interaction of these components and their conglomeration formed through freezing, produces the complex canopy found in the interaction zone. This complexity becomes more evident through observation of floe sizes and concentrations (Figure 1).

Exposure of floating ice to ocean waves is apparent in Figure 1.

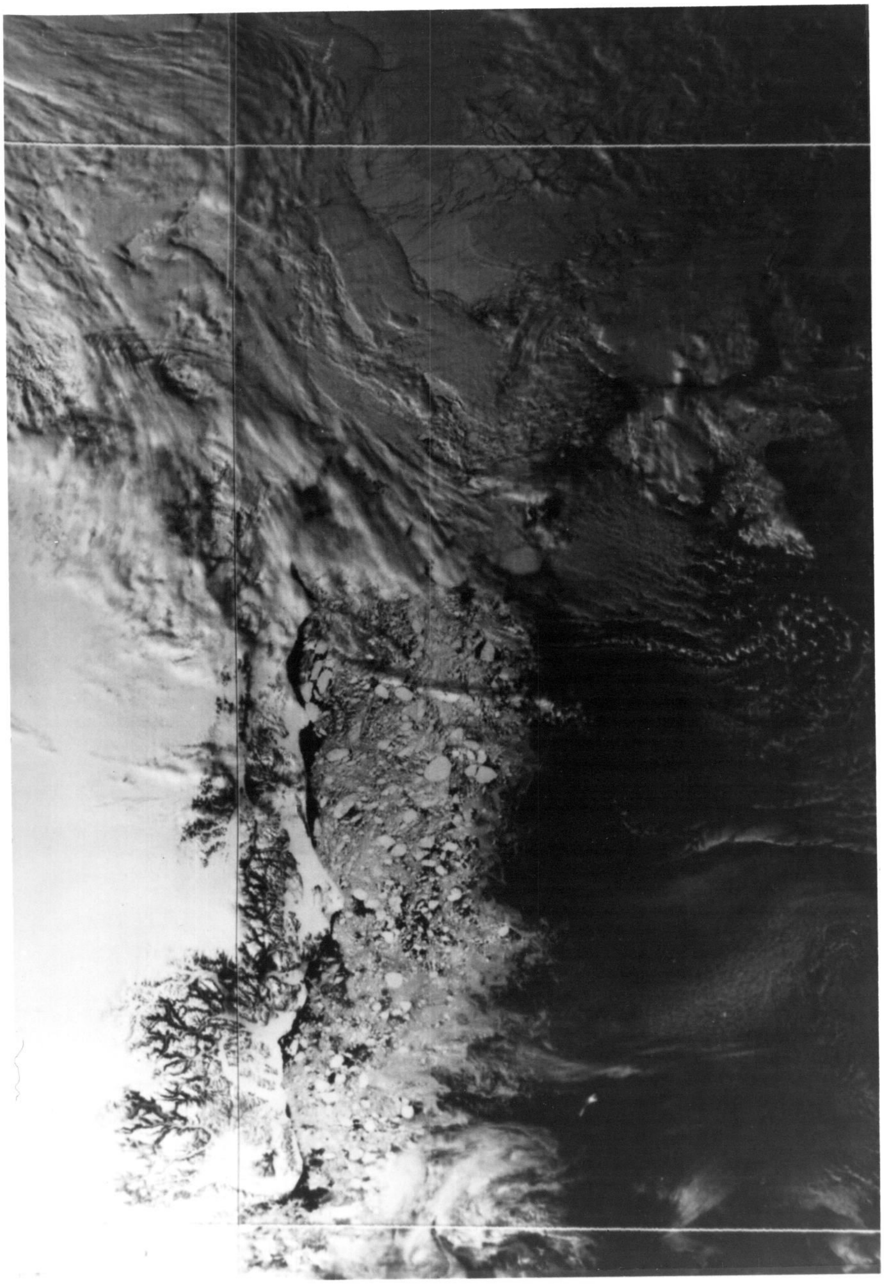

Figure 1. East Greenland area, May 1973 (NOAA/NESS--very high resolution radiometer, visible image).

Considerable wave generation within the Greenland and Norwegian Seas derives from the repeated passage of extratropical cyclones, as evidenced by the positions of their primary and secondary tracks. These intense storm systems are followed by relative calms. Ice which is fractured as a result of wind stress during the storms is believed to be reconsolidated by new ice formed during the quiescent periods. The ocean wave interaction may also produce fracturing of floes within the pack ice (Ketchum and Wittmann, 1972).

Meteorological conditions constitute the third aspect of our consideration of measurement techniques. All of the techniques used to date are dependent upon these conditions. Obviously measurement of the interaction requires observation of the ice. All present techniques require observation of the ice through the atmosphere. Dependence upon visibility, at various electromagnetic frequencies, is a limiting factor.

The interaction zone is frequently covered by clouds, especially at low level. This prevalent condition results from the juxtaposition of the open sea, sea ice canopy and alternating warm and cold air masses. As one moves away from the ice edge towards Greenland, the amount of cloud cover generally diminishes because the ice floes are generally more compacted and/or cemented together with new and young ice so there is little contact between the ocean water and atmosphere. Exceptions occur during summer months when new ice is not formed and during all months in areas of shore leads and recurring polynyas. The general circumstance just noted is favored by onshore winds and excepted during periods of offshore winds. During winter months however, the open water areas produced by the wind induced opening of the pack ice are covered rather quickly by new ice.

As a final subject of environmental conditions, preceding a review of measurement techniques, we address the characteristics of the ocean waves. All measurements of ocean wave/sea ice interaction address the distribution of wave amplitude or energy with respect to either wave frequency (period) or wave number (length). Correlations are then sought between the attenuation of energy over particular wave bands and parameters of ice thickness, floe size, etc. The amplitude or energy spectra, as observed on the open ocean generally encompass a broad range of the independent variable. Wave periods, for example, may range from the orders of 1 to 100 seconds (considering only those classified as wind generated gravity waves). Measurements of the interaction are so few in number that investigators are persently in a reconnaissance stage. This being the case one would desire that measurements be restricted to as narrow a range of wave periods as possible. A sequence of monochromatic waves, from the same direction, would be ideal. (One might also desire the floe sizes to be within a narrow range. The problem is that we don't yet know what values to desire.)

There are three environmental factors involved then in our problem, which must be considered in selecting a measurement technique--characteristics of the sea ice canopy and ocean waves, and the potentially limiting meteorological conditions which exist over the measurement site.

Specific ocean wave and sea ice conditions observed with the measurement techniques described below and conclusions obtained from the observations, are presented in the remainder of this section and in Section V.

In Situ Measurements

In situ measurements include only those made with measuring devices in contact with the undulating ocean and/or ice surfaces. Four categories of devices have been used: shipboard wave recorders (Robin, 1963 and Dean, 1966a); the theodolite bubble (Dean, 1966b); sequential surface (oblique) photography (Dean, 1966b); and, strain-meters (Goodman *et al.*, 1975 and Allan, 1975).

All observations obtained with a shipboard wave recorder have come from the Weddell Sea of the Antarctic during summer: 1959-60 (Robin, 1963 and 1963-64 (Dean, 1966a). In both of these cases, use was made of the shipborne wave recorder designed by the National Institute of Oceanography (N.I.O.), England (Tucker, 1956). For both of the investigations the standard N.I.O. wave recorder was provided with an additional direct current amplifier (amplitude gains of 2, 4 or 8). The N.I.O. wave recorder has been used extensively on the open ocean, as described by Neumann and Pierson (1966), among others.

The N.I.O. shipboard wave recorder provides a continuous measure of the vertically undulating sea surface at a reasonably fixed location (unless the ship is somehow secured against horizontal drift). Limitations in resolution of amplitude and frequency, as well as other pertinent characteristics of the N.I.O. wave recorder may be found in Robin (1963). Recordings can be made on the open sea and within the pack ice. Measurements from within the pack ice are limited to ice-free leads and polynyas accessible to the ship. Therefore, the times of year during which measurements can be made are limited. Navigation along straight tracks within the pack ice is virtually impossible--being dependent upon the spatial distribution and concentration of floe sizes as well as the degree of ice compaction. (Ice compaction can terminate the forward progress of the heaviest ice breakers.) The total time required to obtain measurements on the open sea and at several locations within the pack ice is large. This results of course from the relatively slow ship speeds obtainable while navigating through ice. If one is to be able to contrast wave energy content on the open sea with that observed within the ice all measurements should ideally be made while conditions are reasonably steady over the spatial domain. Steady conditions of course do not exceed the time for passage of envelopes of wave energies presented to the ice. The energy of a wave of say 10 second period will advance with a speed of some 7.8 m sec^{-1}. It seems reasonable to expect that the supply of this energy to the ice edge would last for at least a few hours but probably no more than a few days. One might overcome these problems by resorting to use of more than one ship or by deploying several wave measuring buoys.

Another limitation inherent to the use of shipboard wave recording is the inability to observe ice conditions. On a clear day, which does not always occur and is often of limited span, one's view is horizon limited. Additionally there are difficulties which stem from the oblique perspective obtained from the ship. However, while observing from a ship, one does have opportunity to measure directly or otherwise reliably determine, ice thicknesses.

The requirement for open water at the measurement sites within the pack ice could conceivably be overcome through use of an active ship to surface measuring device (laser or infrared transmitter/ receivers, for example) coupled with hull-mounted accelerometers. However, the resulting observations could presumably be difficult if not impossible to interpret because of the interactive effects of the ship and the ice (sensor target). Such a device was deployed by the author aboard the USCGC SOUTHWIND during March, 1974, while the ship was engaged in oceanographic research in the East Greenland Drift Stream. Unfortunately no analyzable observations were acquired because of instrument failures during the brief periods of ocean wave/sea ice interaction. After extensive efforts rendered aboard to correct matters, the ship encountered calm seas! Successful use of this device, on the open sea, is described in DeLeonibus _et al._ (1973).

The thoedolite bubble technique is predicated on the concept that the surface of large floes will slope (deviate from the horizontal) when forced to respond to a sinusoidal wave profile (Dean, 1966b). By obtaining photographs of the bubble position at 1 second intervals, Dean was able to resolve the bubble displacement to a resolution of some 23 seconds of arc. Unfortunately one of the theodolite legs settled, in what was believed to be suitably compacted snow, after a recording span of 200 seconds. Difficulties with measuring slopes produced by the longer wave lengths are said to be surmountable through use of increasingly sensitive bubbles.

The theodolite bubble technique, though interesting and unique, possesses nearly all of the disadvantages of shipboard measuring techniques. Furthermore, one is unable to observe in the open ocean.

Dean (1966b) has also used sequential photography of small objects floating beside a large floe to measure surface undulations. As with the theodolite bubble technique, it is assumed that the large floe will bend in response to the vertical component of water velocities and in so doing conform to the approximate sinusoidal profile. Given that the floe is large compared to the wave lengths and possessed of adequate inertia, the horizontal water velocities will be reduced by drag and not accelerate the large floe. The observer (photographer) on the floe then sequentially images the 'to and fro' motions of smaller pieces of ice, or bits of floating paper in Dean's case. The technique was successfully utilized for acquisition of some 300 frames, at intervals of 1 second. The duration of the experiment was limited by the effects of wind drift.

Again the technique is of interest but more importantly it bears out the validity of the initial assumptions concerning the relative behavior of large and small floes. The measurement concepts involved in both techniques are credited to Robin (1963) who observed the bending of large floes and to observations of Captain F. Worsley, master of Shackleton's ENDURANCE, who observed the 'to and fro' motion of small pieces of ice from the vantage point of a large floe (Robin, 1963).

Wire strainmeters have been used to measure ocean waves within the sea ice canopy by Goodman et al. (1975) in Bylot Sound, Thule, Greenland and by Allan (1975) in Forteau Bay, South Labrador. The instrument was fastened to the ice with ice screws and maintained in a shelter with temperature stability of ±0.5°C. The device consisted of a 2 m strand of 0.5 mm Invar wire, held in tension by a lever arm and weight. Resulting motion of the lever was detected, amplified, filtered and recorded.

In both locations, the device was attached to fast ice. The report by Allan, reveals not only that fast ice will break up due to the stresses induced by ocean waves, but also that one could conceivably develop a predictive scheme for this breakup. This technique is perhaps the most promising of the three techniques which require access to the ice. It may serve as an excellent measurement technique for those portions of the interaction zone which are removed from the ice edge. It is of doubtful utility in the more dynamic area near the ice edge. There would certainly be less risk to personnel if they were located on the larger floes.

Remote Measurements

The interaction of ocean waves and sea ice has been measured from two remote platforms--submarine and aircraft. Measurements have been acquired with: the upward-looking sonar (inverted echo sounder) described by Wadhams (1971); conventional airborne photography (Amstutz and Ketchum, 1973); and, an airborne laser (Wadhams, 1973b).

For this work the submarine platform has greater mobility than surface ships. As a result it can transit along predetermined lines and sample far from the ice edge within a matter of hours.

However, sampling distance from the ice edge and measurement duration beneath the ice are limited when diesel-electric submarines are used. The submarine has the additional advantage over a surface ship of not altering the measured environment. However, the submarine platform provides little opportunity for measuring floe sizes and concentrations, and it cannot maintain a specified depth and location during the period of measurement. Wadhams (1971) reports the necessity of maintaining a speed of about 1.5 m sec^{-1}. His observations were obtained northwest of Spitzbergen. More detailed discussions of the observations and their analysis are presented in Wadhams (1973b).

With upward-looking sonar one obtains a measure of the distance between the transducer, mounted on the hull or sail, and the underside of the ice. The underside of ice floes are generally irregular in shape and have surfaces of varying roughness elements. One must also consider the integrating effects associated with the sonar beam width as well as the difficulties in interpreting which returns are from the underside of the ice vice those from the water and upper surface of the ice. Beam widths aboard British submarines used by Wadhams (1971) and Swithinbank (1971) were 20°. To minimize the area of view it is necessary to decrease the distance below the ice. This in turn places the vessel within the oscillatory field of the waves.

Upward-looking sonar was first used by DeLeonibus (1962) for study of open ocean waves. Measurements of the underside of pack ice outside of the interaction zone, for study of the statistical properties of under-ice roughness, have been conducted by Lyon (1967), Swithinbank (1971), and others.

Observations for study of the interaction phenomenon obtained from a submarine should be acquired while viewing a relatively smooth ice region such as a refrozen lead or polynya (skylight). These features would be required at quasi-regular intervals along the track of interest. Considerable submarine time might be necessary to search for such features.

Aircraft have two significant advantages over both surface and subsurface platforms. The investigator is able to quantitatively assess the ice conditions and survey an enormous area very quickly. The latter is essential if the wave spectrum incident at the ice edge is to be related to wave spectra obtained within the ice. Limitations include the relatively brief on-station time and the dependence upon visibility (a function of the sensor used). On-station time is limited largely because of the remoteness of the interaction zone from readily available staging bases and the safety requirement of retaining sufficient reserve fuel to reach alternate landing sites.

Sensors used to date (cartographic cameras and lasers) are very much dependent upon a cloud-free and haze-free atmosphere below the aircraft. As noted above, clear skies are infrequent over the interaction zone. The locations of cloud-free regions can be determined to some degree through environmental prediction and use of satellite remote sensors. An interesting example of the airborne use of satellite infrared imagery is given by LaViolette et al. (1975). It is essential to note that though satellite observations reveal clear areas they do not delineate ceilings within cloud covered regions. The high latitude regions in which the interaction phenomenon is observed, are characterized by long periods of darkness each year. Though active transducers such as the laser are operable year round this is not the case for photography. Therefore, the advantages of acquiring a quantitative measure of the ice canopy, attributable to aircraft, are in general seasonally limited. One could make use of airborne infrared scanners, during all seasons to acquire information about the ice canopy. These devices, in addition to being severely restricted by cloud and haze, produce inherently large distortions of surface features.

Airborne observations of ocean wave/sea ice interaction were fortuitously acquired on conventional photographs and reported by Amstutz and Ketchum (1973). These observations were obtained southwest of Spitzbergen in October, 1972. Because of the low solar altitude, the investigators were able to delineate wave crests within the pack ice by their shadows (Figure 2). At the time, the aircraft was being used to obtain imagery of the ice canopy between two surface

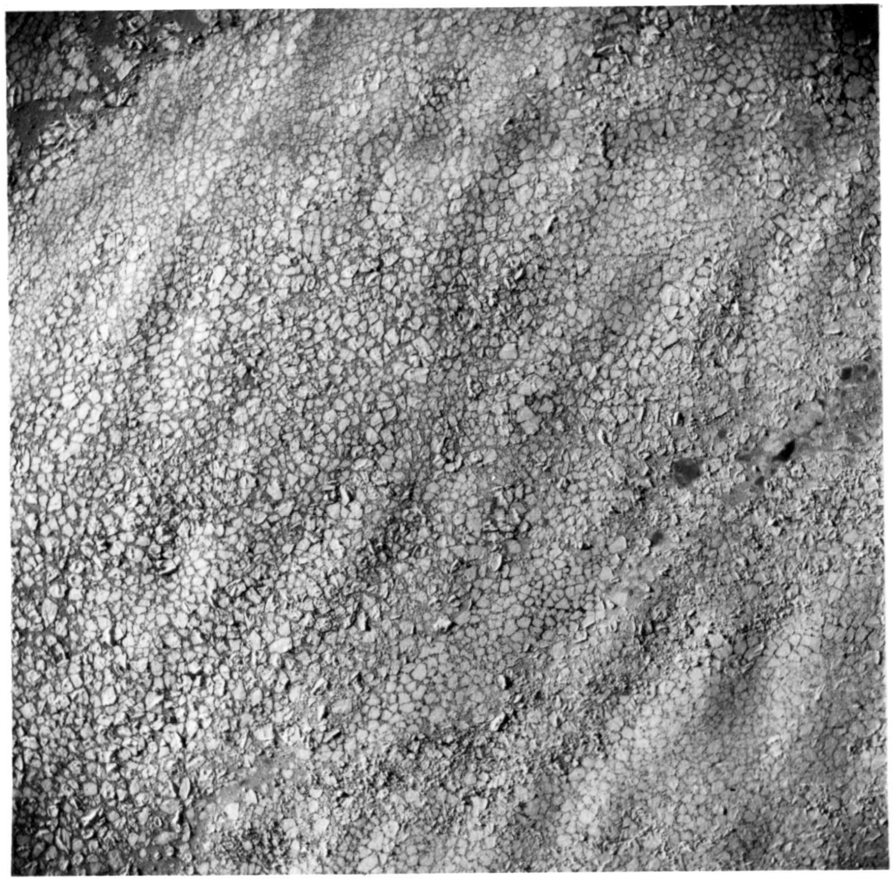

Figure 2. Ocean waves in sea ice, October 1972--79.7°N, 2.1°W--65 km from ice edge. Scale: 1 cm = 185 m (Naval Oceanographic Office, aerial photograph).

ships which were conducting acoustical research. One ship was near the ice edge while the second (an icebreaker) was within the pack ice. The photographs revealed swell of lengths between 150 and 300 meters. As these observations have not been published they will be addressed in more detail when referred to later. This measurement technique is of course not competitive with the others identified, because of the very rare opportunities for its application and the inability to distinguish other than the most predominant wavelengths (wavelengths of greatest amplitude).

Use of the airborne laser for measuring the topside roughness of sea ice was demonstrated by Ketchum (1970). The technique has been utilized in studies of pack ice such as: LeSchack _et al_. (1970), Ketchum (1971), Welsh and Tucker (1971), and Ketchum and Wittmann (1972).

The utility of measuring open ocean waves with an airborne laser was demonstrated by Ross _et al_. (1968). Examples of its use in further studies of open ocean waves may be found in Schule _et al_. (1971), and De Leonibus and Sheil (1973). The airborne laser was used to study ocean wave/sea ice interaction by Wadhams (1973b) off the coasts of Labrador and Newfoundland.

The airborne laser technique incorporates all of the advantages of the aircraft and is limited only by visibility and difficulties in interpreting the measured variation in distance between aircraft and target. The variation in distance is produced by the porpoising motion of the aircraft, the sea ice topside roughness and the vertical undulation of the sea ice canopy and water surfaces. The laser beam is extremely narrow, viewing only a few square centimeters from flying altitude. Altitudes are limited, in practice, to a maximum of about 1.5 km due to failure of phase lock during continuous operation.

The terrain profiles must of course be analyzed to remove the effects introduced by sampling from a moving platform prior to analysis of the interaction phenomenon. In order to determine the actual profile of the undulating water surface one is limited to obtaining records over areas of loosely packed ice floes; ice coverage should be less than 50%. The floes also must be of reasonably small dimension in comparison with wavelengths. A reasonably well behaved wave train advancing in one direction is highly desired.

It is essential in all airborne measurements that the undulating surface be visible from the aircraft in order to establish a line of flight normal to the wave crests. Through real time analysis of the laser terrain profile, the airborne laser serves to indicate when flight lines may be terminated.

Finally, it is noted that the records obtained with the laser represent wave information in a wavelength (or wave number) domain, unlike records obtained from fixed positions which lend themselves to analysis in the frequency (or wave period) domain. A sample wave record obtained at a fixed position for a few minutes, corresponds to a spatial record over a kilometer or more. The length (duration) of record obtainable from aircraft observations will definitely be limited because attenuation processes limit the distance of wave penetration (as detectable to the sensor at least). In the case of photography, one is limited to the field of view of the aerial camera, a function of aircraft altitude and desired image resolution. To retain some perspective of distances recall that the submarine (Wadhams, 1971) drifted nearly 100 m during each minute of sampling.

III. AIRBORNE STEREOPHOTOGRAMMETRY

Studies of ocean waves by means of stereophotography have been pursued for nearly 70 years. Some examples may be found in the texts of Kinsman (1965) and Neumann and Pierson (1966). For the early studies, referenced in these texts, the authors made their pictures from bridges and ships' masts. Not until the latter half of the present century did researchers resort to aircraft for measurement platforms (Chase *et al.*, 1957; Cote *et al.*, 1960; and Simpson, 1967). These three reports evolved from two aircraft missions, one in 1957, SWOP I and the other in 1964, SWOP II. (SWOP is the acronym for Stereo Wave Observation Project.) The intense effort and array of talent utilized for execution of SWOP I is sketchily noted by Kinsman (1965). These efforts will be described in qualitative fashion followed by a quantitative development of the procedure used for the present study.

The stereographic observation is obtained when an object is viewed from two separate locations. If the object is viewed with an airborne camera, the procedure is referred to as airborne stereophotography. If the object of interest is a building or mountain, fixed to the earth's surface, the two photographic images may be obtained from a single aircraft. Sufficient forward overlap of the images is obtained by controlling the time between successive exposures. The separation between the locations of view is equal to the product of time between exposures and the ground speed of the aircraft. This separation distance is known as the air base.

If the photographs are to be used to obtain accurate measurements of the object, the camera, lens and film must be of high quality and there must be a means for establishing an accurate image scale. Image scale may be determined if an object of known dimension is included on the imagery or if the aircraft altitude is accurately known for the instants of each exposure.

This seemingly simple procedure for obtaining airborne stereophotographs is complicated if the object is not fixed to the earth's surface, as is the case when viewing ocean surface waves. Since the ocean surface deformation varies with time, one cannot use time between exposures and aircraft ground speed to produce the desired air base. To obtain a reasonable stereophotographic field of view of the ocean surface the air base must be greater than any dimension of aircraft, consequently one must resort to using two or more aircraft. The horizontal separation between aircraft (each with an aerial camera) becomes the air base. The two exposures are made at the same time through use of a radio link between camera shutters.

In SWOP I, image scale was provided through use of RV ATLANTIS towing a raft some 152.4 m (500 ft.) astern. The two aircraft were flown in tandem at an altitude of 91.4 m (300 ft.) and an air base of 609.6 m (2000 ft.). Shipboard measurements were made at the same time using a wave pole. The project resulted in 100 stereo pairs, of which two were analyzed and combined to produce one wave number energy spectrum (Kinsman, 1965). The low altitude resulted in imagery which produced stereo models approximately 823 m (2700 ft.) by 549 m (1800 ft.). Values of sea surface elevation were read on a square grid at spatial intervals of 9.1 m (30 ft.).

The SWOP II experimental design required four aircraft and no surface ship. Three aircraft were to fly in tandem with air bases of 914 m (3000 ft.) and at an altitude of 1372 m (4500 ft.). The three aircraft were to be used to yield a large stereophotographic image for analysis. The fourth plane was to fly at an altitude of 2743 m (9000 ft.) directly above the middle of the lower three planes. The fourth plane initiated the photography, again using a radio link, and served to maintain leadership over the formation flying. Imagery from the fourth plane provides the photo scale for the experiment. Low ceilings which prevailed at the time of observation required the three aircraft to fly at less than design altitude while the fourth aircraft had to fly above the undercast. Imagery suitable for analysis was further reduced due to an excessive solar elevation. The high sun produced bright spots on the images within which elevations could not be read (Simpson, 1967).

Airborne stereophotogrammetric techniques, though potentially capable of producing invaluable measurements, are very sensitive to environmental conditions. The technique requires aircraft, cameras and radio links which all function properly at the same time and adequate visibility in terms of viewing the aircraft for formation flying and for obtaining photographs.

In the high latitudes one encounters more severe and more frequent aircraft mechanical problems. These problems result primarily from the low air temperatures experienced while the aircraft are parked. Two additional aspects of using airborne platforms for oceanographic research should be noted--speed and duration. Most oceanographers are trained in the use of ships and anchored buoys for measurement platforms. If difficulties are encountered, one can generally have the ship hove to while a solution is pursued. With aircraft it is another matter because: there are minimum speeds which must be maintained; control of alignment or formation flying can be lost in the briefest time; several minutes are required to achieve safe realignment, especially if the realignment position is a function of location; the start times for data acquisition must be precise (consider typical ground speeds of 100 m $sec.^{-1}$); and, the amount of time which may be spent over the measurement site (measurement duration) is limited. An experiment conducted in the high latitudes generally must take far less time than when performed in lower latitudes because there are fewer landing sites. As a result, the aircraft must arrive over its intended landing site with a large proportion of its total fuel in order to safely reach an alternate base. These apparent difficulties on the other hand can be viewed as assets. Maximum utilization of the assets of the airborne platform requires pre-mission planning, attentiveness to detail, practice flying and experience.

The airborne stereophotogrammetric technique used for this study was devised late in 1972 during analysis of the single aircraft observations reported by Amstutz and Ketchum (1973). For historical accuracy, it is noted that an attempt at using the two aircraft technique (described below) was made during late spring 1973. The experiment was predicated on the small chance of having a second aircraft available during a period when one aircraft was deployed to the East Greenland region exclusively for sea ice research. The second plane became available for two days. However, there were no ocean waves impacting the ice during that time even though visibility was excellent (see Figure 1). As a result, the experiment was postponed.

The most suitable time of year to measure ocean wave/sea ice interaction along East Greenland is during the period late February through early March. During this time one generally encounters considerable ocean wave activity (size and duration). Also there is a maximum or near maximum amount of sea ice, visibility is best and there are sufficient hours of daylight about local noon to carry out an airborne photographic mission. The second best time of year occurs during late September through mid October.

Performance of such an experiment requires the availability of aircraft (two in this case) as well as funding. For these experiments two aircraft were made available by the Commander, U. S. Naval Oceanographic Office and funding was provided by the Defense Advanced Research Projects Agency. The observations analyzed in this report were obtained on March 11, 1974.

The measurement technique was designed around use of the minimum number of aircraft (two) and the absence of any surface markers of known dimension. The need for an accurate image scale was satisfied by obtaining very precise measure of aircraft altitude using an airborne laser. The aircraft were RP-3A Orions (149500, the Arctic Fox and 149667, El Coyote) specially configured for oceanographic research. The cameras on each of the aircraft were Fairchild, Model CA 14. These cameras are the cartographic, mapping type and produce 22. 9 cm x 22. 9 cm (9 in. x 9 in.) images. The calibrated lenses are of 152 mm (6 in.) focal length with a vertical field of view of $73^{o}44$ (Navair, 1969). The laser altimeter was a Spectra Physics, Inc. Geodolite 3A. It uses a modulated CW laser to obtain continuous measurement of the distance between itself and the terrain. The transmitted signal, amplitude modulated at specific frequencies, was provided by a helium-neon laser. The beam spot size was approximately 3 cm in diameter from an altitude of 305 m (1000 ft.). The reflected signal was received by a 20.3 cm (8 in.) telescope and focused on the cathode of a photomultiplier tube. The resultant electrical signal was amplified and the phase delay between the modulation on this signal and that of the transmitted signal precisely measured. This phase delay is proportional to the distance travelled by the light.

The two aircraft were flown abeam of each other as opposed to the tandem or in-trail flight used during SWOP I and II. This procedure is not only safer but also enables more immediate visual detection of speed changes between the aircraft. The lead aircraft, the Arctic Fox, established altitude, course heading and ground speed. It remained for the second aircraft, El Coyote, to visually maintain a similar altitude and course heading. Speed of El Coyote was repeatedly adjusted so as to retain alignment of the wings of both aircraft. Wing alignment assured that the imagery obtained from the two aircraft was coincident in the along flight direction.

The in-flight separation of the aircraft determined the air base. The overlap of the imageries from the two aircraft (geometrically this is a side-lap) must be between 50% and 75% of the image width. Using 152 mm (6 in.) lenses each image represents a square region with side lengths measuring one and one-half times the aircraft altitude.

The arrangement of the aircraft and some example air bases are presented in Figure 3. The problem of determining and maintaining suitable air bases during flight required more time than the eventual solution might suggest. Recognition of the fact that the other aircraft is the only object of known dimension visible to the pilots, provided the answer. A transparent plastic template was marked with the lengths of the plane at its nearest and farthest acceptable distances, for each of the anticipated flight altitudes. The template was then set within a large camera viewfinder. To evaluate this tool (the aircraft lengths marked on the template were derived mathematically) and to afford some visual perspective for the pilots, the aircraft were parked on an available runway and viewed at a few of the predetermined air bases. In flight, the lead plane, Arctic Fox, was "viewed" from El Coyote. When the air base was observed to be changing, the pilot was notified and advised whether to separate or close. With a little practice the procedure was proven out. The demands placed on the flight crews were certainly greater than normal. The RP-3A aircraft is nicely suited for this procedure in that as many as five people can view what is going on from the cockpit. Aboard El Coyote, the pilot retained directional and altitude control of the aircraft, the flight engineer adjusted engine power settings to retain wing alignment, the author observed Arctic Fox through the viewfinder and the co-pilot maintained radio communications between the aircraft and

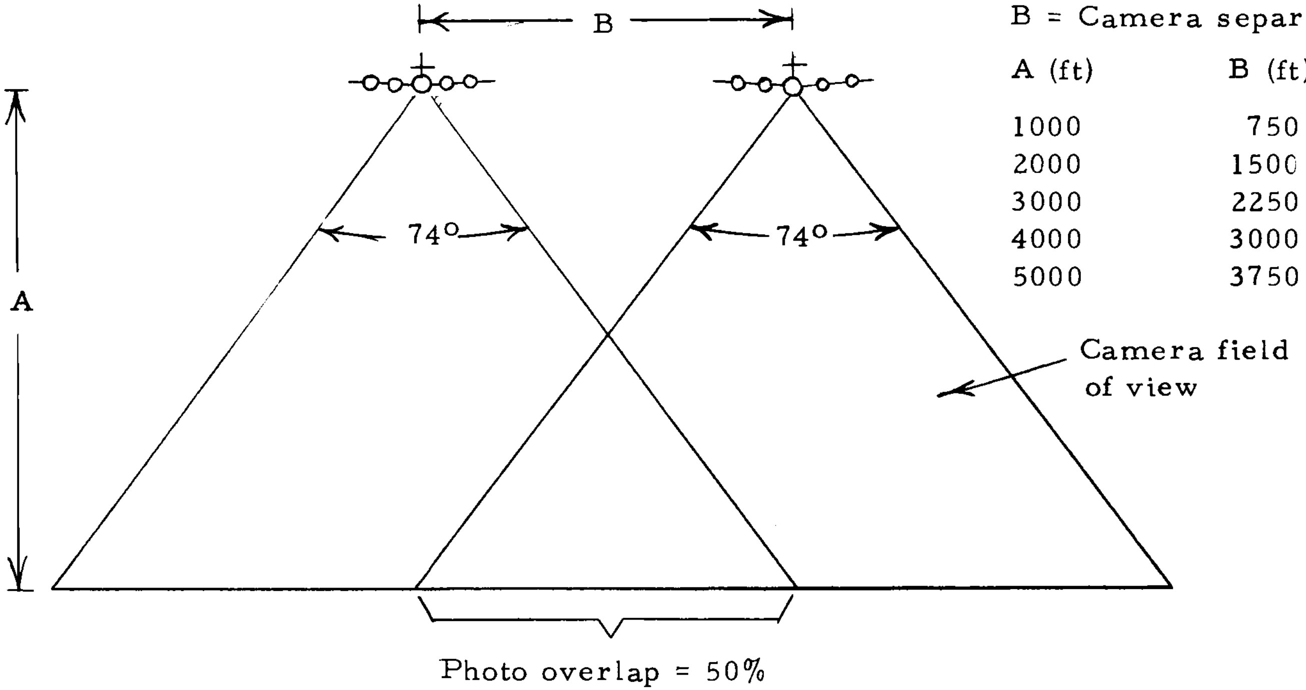

A = Aircraft altitude

B = Camera separation (air base)

A (ft)	B (ft)
1000	750
2000	1500
3000	2250
4000	3000
5000	3750

Figure 3. Camera separation (air base) versus aircraft altitude.

within the plane.

Final pre-deployment tests were conducted for crew training and to evaluate the overall technique. A test was required to assure that the imagery would not be subject to image motion. The test was accomplished by flying over a few miles of interstate highways between the Patuxent Naval Air Station, Maryland and Richmond, Virginia. An overall test of the technique was accomplished by flying over an unused runway and imaging three vehicles driving at anticipated wave phase speeds. One of these stereophotographic pairs was submitted to the Defense Mapping Agency Hydrographic Center, along with the laser determined altitude and calibrated lens focal lengths. Stereophotogrammetric determinations of the vehicle dimensions were correct within our accuracy of measurement (±2 cm) on the ground.

Aerial photogrammetry and stereophotogrammetry have experienced rapid development only during the past 40 years. A complete reference to this "science and art" is the two volume "Manual of Photogrammetry" by Thompson (1966).

For present purposes a very brief qualitative description of the procedure will be given. The original imagery, held flat by vacuum during exposure, is processed and reproduced on glass plates. These plates are projected with high illumination and great precision. The projection is achieved, in principle, as with any slide projector; however, the difference lies in the capabilities of the stereophotogrammetric system to recreate in miniature the precise interrelationships of the initial camera stations. To recreate the camera interrelationships, each projector is mounted so as to be rotated with great precision about three mutually perpendicular axes (known among those of the profession as omega, phi and kappa). Translation along one of these axes (omega) serves to establish the image scale (a function of focal length and aircraft altitude). Separation of the projectors is in proportion to the air base. The procedure to this point recovers, or establishes within the laboratory, the original perspective relationship. This process is known as relative orientation. The precise altitude was known from the laser for the lead plane (Arctic Fox). Image scale from the Arctic Fox imagery was used in conjunction with the lens focal length of the camera aboard El Coyote to adjust the second projector.

The measuring system consists of a viewing screen upon which the stereographic images are projected. The projection is viewed through two oculars. A marker, usually an illuminated point, is seen on the model and appears suspended. This marker is moved until it makes contact with the point of interest in the stereo model. The coordinates (x, y and z) of the marker are then recorded. These coordinates, in the case of the Wild B-8 Stereomat used for this study, are recorded on magnetic tape for later processing and analysis.

For the ocean wave/sea ice observations there was no absolute vertical reference or datum, as there normally would be if one obtained imagery over land. For purposes of this work the locally averaged sea level was taken for the vertical datum. During operation of the B-8 Stereomat, the marker is translated along each profile to be read and the vertical axis set so that all z (elevation) values will be positive. Similarly, the beginning x and y (horizontal) coordinates are established to produce positive increments during successive readings.

IV. AIRBORNE STEREOPHOTOGRAPHIC OBSERVATIONS

Environmental Circumstances

The two-aircraft experiment was one portion of a joint environmental-acoustical study conducted along the East Greenland coast by the U. S. Naval Oceanographic Office and the U. S. Naval Research Laboratory. Two surface ships, USNS MIZAR and USCGC EDISTO were deployed for this exercise. The aircraft staged from Keflavik Naval Air Station, Keflavik, Iceland between February 28 and March 12, 1974. During this time USCGC EDISTO was operating within the ice in the vicinity of 74°30'N, 12°E. USNS MIZAR was located east of USCGC EDISTO and outside of the ice. The aircraft performed various experiments independently and in conjunction with the surface ships.

For the first few days, the aircraft could fly together only on an opportunity basis. Determination of the time and location of the ocean wave/sea ice interaction study was to be made on the basis of: (1) satellite observations and weather forecasts obtained in Keflavik; and, (2) *in situ* observations made by the ships, particularly USCGC EDISTO. For several days there were few clear areas along the ice edge and no ocean waves of any significance within them. These circumstances were followed by reports of heavy seas, but almost no visibility, in the vicinity of USCGC EDISTO.

During the latter half of the aircraft deployment period the ocean wave/sea ice interaction study became the primary goal for the aircraft. The satellite and ship observations, as well as forecasts, remained bleak. To increase chances for success, all aircraft transits to and from their respective study sites were made over different regions of the ice edge and at lower than normal altitudes.

On March 8 the last independent aircraft studies were completed, leaving the planes totally free to pursue the interaction work. For the March 8th and later flights a new procedure was adopted. One plane flew north along the ice edge at low altitude while the other flew similarly but to the south. In the event a hole (region with suitable visibility) with ocean waves was located by either plane, the other would climb to altitude and transit rapidly to join up. On march 9th the normal procedure of having flight crews rest on alternate days was voluntarily suspended. The flights of March 10 produced no results. Requests for additional time could not be granted because of prior commitments for both aircraft. Each was required to leave Keflavik on the morning of March 12.

On the morning of March 11, USCGC EDISTO reported fog, visibility less than 0.1 nautical mile, 10/10 clouds, ceiling 30 m (100 ft.), and barometer 30.28 inches and falling. This weather report was typical for the entire East Greenland coast based upon our flight weather forecast. The planes deployed from Keflavik at 0900 local time and pursued their search plans as on prior days. In late morning a site was located by Arctic Fox in the vicinity of 65°N, 35°30' W. By 1150 the aircraft had rendezvoused, aligned and begun parallel flight along the first track.

The region of study is shown in Figure 4. The flight lines were terminated, or alternately, initiated at distances within the ice where no wave activity was detectable with the airborne laser. The laser profiles indicated that the wave activity terminated very abruptly. An example is presented in Figure 5. During the time of measurement at this site (1150 to 1325 local time) relatively thin low lying clouds were observed while looking downward from the aircraft. Undercast increased with time and rendered much of the data unsuitable for analysis. The adverse effects of this undercast were not fully realized during the flights. Later analysis indicated that the effect of the undercast increased with the viewing distance. The all-important area where the imageries overlap was thus affected more than the area directly beneath each aircraft.

The most unfortunate aspect of the experiment resulted from failure to change the camera exposure index (aperture) while flying over the open sea. The difference between the reflectivity of the snow and sea ice and that of the open ocean surface is so great that I have been unable to work with the open ocean imagery. Therefore, I have defined the wave spectra observed in the most seaward (ice edge)

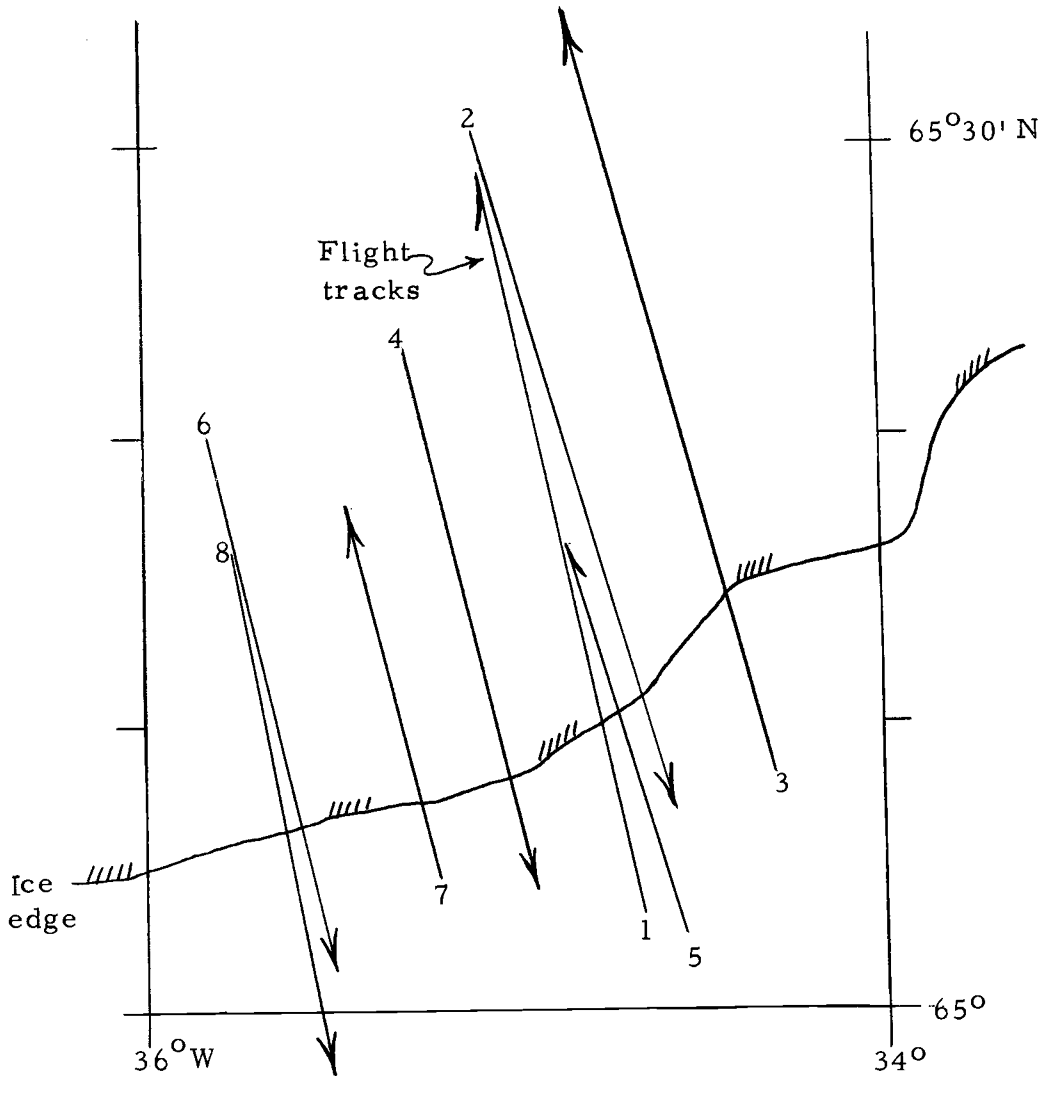

Figure 4. Measurement site, March 11, 1974.

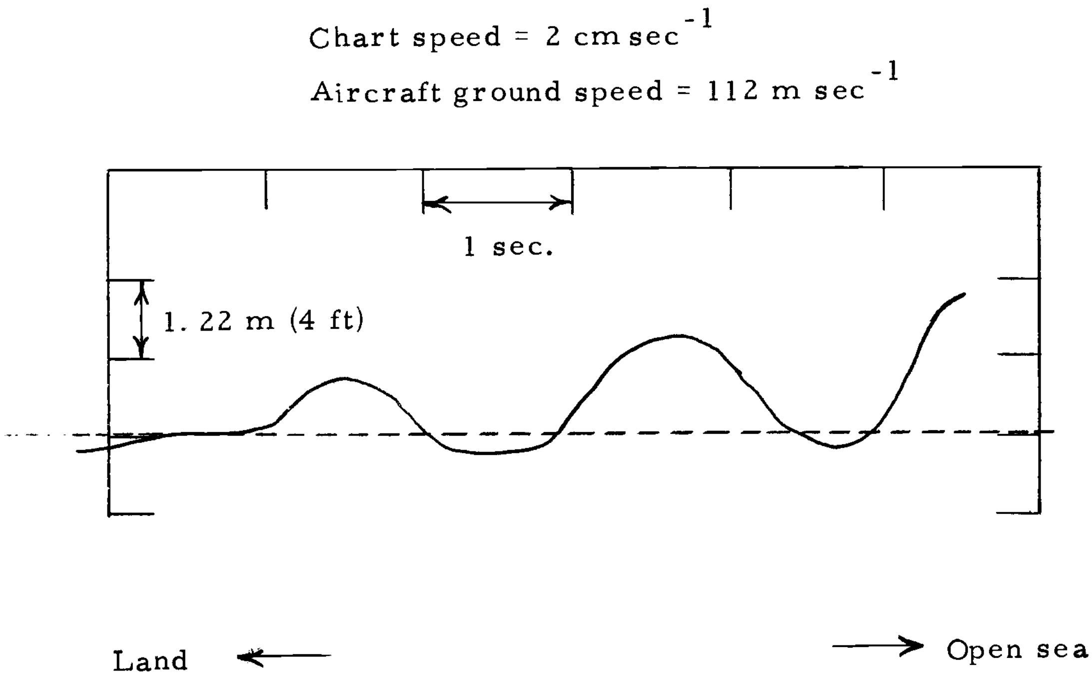

Figure 5. Laser terrain profile.

stereophotogrammetric ice model as being representative of the open ocean condition. Though this definition will not be strictly correct it seems a reasonable procedure, especially in this case where relative changes are being examined.

A second difficulty was experienced. On the first flight line the camera shutter aboard the signal receiving aircraft (El Coyote) began exposing film at a continuous and maximum rate. The cause was an incorrectly adjusted radio receiver and was soon corrected. The result was that the imageries obtained along the first track were not in synchronization. Of course stereophotogrammetric models of moving surfaces require synchronous image pairs. The rate of film exposure along the flight tracks was controlled from the lead aircraft. The intervelometer was set to provide some 20% forward overlap which allows continuous construction of the ice imagery along the flight tracks.

Of the data obtained, those along the third flight track have been analyzed and are presented here. The third track was flown at a nominal altitude of 914 m (3000 ft.).

After flying the tracks at this stie, the aircraft went in search of additional sites. A second location was found in the vicinity of 67°N, $27^{\circ}45'$ W. Visibility was less than at the first site. The ice conditions were sufficiently different however to warrant examination. Four tracks were flown over this second site--largely on the hope that at least some of the imagery might be analyzed. None of the tracks could be analyzed over sufficient distances to warrant construction of stereophotogrammetric models.

The aircraft returned to Keflavik and began homeward transit the next day. This mission terminated the two-aircraft study of ocean wave/sea ice interaction.

Data Processing

The laser records for the third track indicated that wave heights became imperceptible after 51 seconds of flight from the ice edge. The aircraft navigation logs indicated a ground speed of 112.1 m/sec (215.5 knots). While flying these tracks, positioning control was maintained from Arctic Fox through use of a Litton model LTN-51 inertial navigation system. The limit then of ocean wave penetration was taken to be 5.7 km along the flight line. Similar calculations for the other tracks establish depths of wave penetration from the ice edge, ranging from 3.4 km to 6.2 km (the average was 4.8 km). The ice conditions, floe size range and concentrations, were similar for each track. The apparent differences in depth of wave penetration result from flying perpendicular to the ice edge and not necessarily parallel to the direction of wave propagation. Though flight parallel to the direction of wave propagation was desired, and attempted, it is difficult to achieve--especially along tracks which originated over the ice and were flown towards the ice edge.

The 5.7 km distance of wave penetration determined from the laser records and track navigation log was used for selecting the number of image pairs to prepare for use in constructing stereophotogrammetric models. By measuring on the photographs the equivalent of 5.7 km along the aircraft ground track (coincident with the track measured with the laser) the region of imperceptible wave heights was located near the middle of the eighth pair of images. The first eight pairs of imagery were thus chosen for construction of stereophotogrammetric models. These eight models were numbered consecutively beginning with the first model at the ice edge.

The original observations are contained on 22.9 cm x 22.9 cm (9 in. x 9 in.) photographic negatives. These negatives were exposed through 152 mm (6 in.) focal length lenses from an accepted altitude of 914 m (3000 feet). Using the equivalence of the ratios of focal length to image size and altitude to surface image, the photographic scale is concluded to be 1 to 6000. Therefore 1 cm on the original image represents 60 meters on the earth's surface.

Positive plates were constructed from positive contact prints made from each negative (one negative from each aircraft) to prepare the stereophotogrammetric models. These plates were constructed on a scale of 1 to 3000 (a two times enlargement of the original photographic negatives). A distance of one centimeter on the constructed stereophotographic models represents 30 meters on the earth's surface.

The three-dimensional coordinate system was assigned to the positive plates and digital x, y and z values were read along the chosen profiles and recorded on magnetic tape. The profiles were identified by lines drawn on the positive contact prints. A sampling interval of 0.5 mm was chosen (equivalent to 1.5 m on the earth). The illuminated marker of the B-8 Stereomat was designed to be conveniently advanced along either of the horizontal (x, y) axes at intervals of 0.5 mm. By aligning either the x or y axis along the profile the marker could be advanced (by turning a wheel) and successive z coordinate values read (by positioning the marker on the surface).

When the eight models were first viewed stereoscopically, it was apparent that the line of flight was not parallel with the direction of wave propagation. The observed circumstance is shown in Figure 6. Lines parallel to the direction of wave propagation were then constructed on each model. The initial plan called for a single line or elevation profile for each model. In order to maximize the profile lengths, it was necessary to offset the profiles on successive models, Figure 6. Four profiles were chosen for each model in order to investigate possible differences in the along crest direction. The wave components of greatest heights, those most apparent under visual examination, appeared to be short crested.

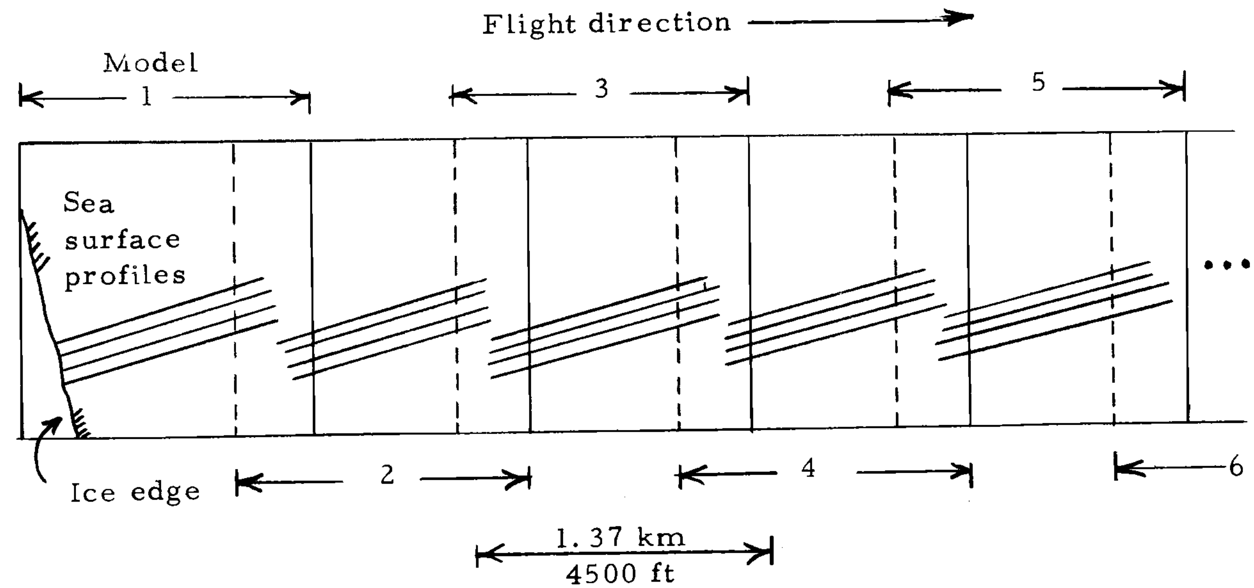

Figure 6. Stereophotogrammetric models and location of sea surface profiles.

We return now to the preparation of the stereo models and conditioning of the data for analysis. Variations in image scale and equivalent sampling intervals must be followed carefully, as will be shown. The intended simplicity of reading the models was not achieved as the profiles could not be made coincident with either the x or y axes. The actual digitized x, y and z coordinates were determined by advancing 0.5 mm along the x axis, manually moving along the y axis until contacting the profile (line on stereophotogrammetric model) and reading the z coordinate (see Figure 7). As the angle θ was constant for each line of each model, the Δy intervals between each recording should have been identical. This was the case, within resolution of the device (0.01 mm). The along line sampling interval, defined as Δs in Figure 7 was computed for each profile by applying the theorem of Pythagoras to the sums of Δx and Δy and dividing by one less than the total number of recorded z values. The resultant sampling intervals (Δs) expressed in lengths of instrument millimeters and meters on the earth's surface are presented in Table 1.

The average Δs among the eight models was 0.59 instrument mm or equivalently 1.76 m on the earth. With respect to the original photographs, this average Δs was equal to 0.3 mm. This initial sampling interval was changed later and its slight variation among lines was made uniform and constant during the initial stages of analysis.

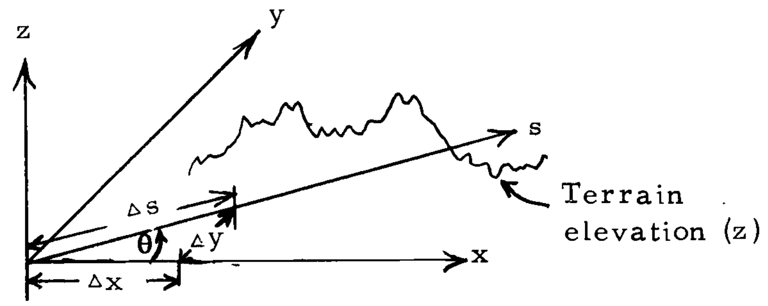

Figure 7. Recording of terrain elevation values.

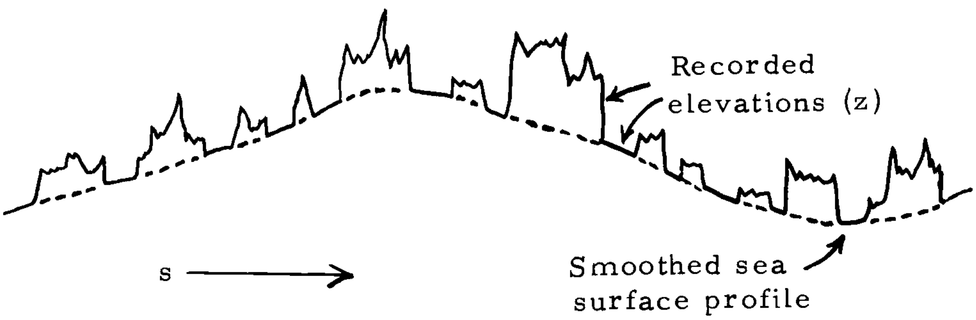

Figure 8. Recorded terrain elevation versus distance.

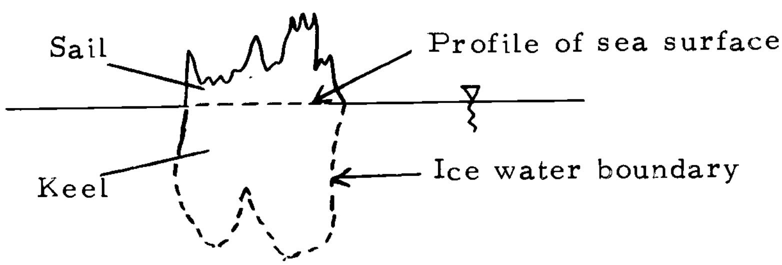

Figure 9. Profile of sea surface.

Table 1. Accepted sampling intervals ($\triangle S$).

Model	Profile	Instrument (mm)	Earth (m)
1	1	.58	1.74
	2	.57	1.71
	3	.58	1.74
	4	.57	1.71
2	1	.57	1.71
	2	.60	1.80
	3	.63	1.89
	4	.57	1.71
3	1	.58	1.74
	2	.58	1.74
	3	.56	1.68
	4	.58	1.74
4	1	.60	1.80
	2	.59	1.77
	3	.60	1.80
	4	.58	1.74
5	1	.62	1.86
	2	62	1.86
	3	.59	1.77
	4	.59	1.77
6	1	59	1 77
	2	.59	1.77
	3	.59	1.77
	4	.59	1.77
7	1	58	1.74
	2	,59	1.77
	3	.59	1.77
	4	.60	1.80
8	1	.61	1.83
	2	.57	1.71
	3	.59	1.77
	4	.58	1.74

The initially digitized z coordinates were then plotted sequentially along a line (abscissa) at the rate of 20 values per 2.54 cm (1 in.). The values of these initial z coordinates were plotted on the ordinate on the basis of 2.54 cm (1 in.) per instrument mm. An example is presented in Figure 8.

A smooth curve was constructed for each profile (Figure 8). The term profile will be used now for the sequence of elevations (initial z coordinates) plotted along the line (hypotenuse) of the (x, y) triangle. The curves were constructed to coincide with all segments of open water and with all segments of thin ice. Segments of thin ice were observed to conform to the sea surface profile implying that the thin ice regions deformed elastically. This task of construction was tedious at best--requiring nearly constant reference to the positive prints. In some instances (very few) the z coordinates were observed to be below the smooth curve (sea surface profile). This circumstance arises when the marker is moved off the edge of a relatively thick piece of ice, of light color, and onto a dark region of either open water or very thin ice. The process of constructing the sea surface profile becomes more complex as the frequency and width (along line extent) of open water/thin ice regions diminish. A similar problem exists in the processing of laser profiles, as noted above.

The process of constructing sea surface profiles could not be applied to the eighth model because of imperceptibly small wave heights. The procedure for determining the location where wave heights became imperceptibly small (laser records and track three navigation log) only provided a reasonable estimate. The actual position where wave heights became imperceptibly small was located on the landward edge of model seven rather than within the seaward half of model eight. The analysis therefore addresses only the first seven models. Wave heights within the eighth model are well within the minimum resolution of the B-8 Stereomat (1/6000 of the aircraft altitude, or 15 cm).

Delineation of the ice edge with the laser is very exact due to the significant difference in reflectivities between the open water and sea ice/snow surfaces. Since the time of flight over the ice edge was well known, the aircraft ground speed, resorted to for the initial selection of eight models, must have been overestimated. It should be noted that studies of ocean wave/sea ice interaction with airborne lasers can be very much dependent upon accurate determination of aircraft ground speed. This potential error source could be eliminated if one could locate the laser profile on concurrent aerial photographs or other imagery such as infrared. The latter has been used in studies of sea ice roughness using the airborne laser.

During development of these procedures for data processing an alternate, perhaps preferred, technique was devised. This technique amounted to identifying the regions of open water and thin ice at the time of reading the x, y and z coordinates. By viewing each point to be read, the author determined whether or not the marker was over ice or open water/thin ice. The coordinates and an identification of the surface ice condition (ice index) were recorded by hand. The values were put on computer cards and a smooth curve (sea surface profile) constructed through use of a cubic spline interpolation procedure (Davis and Kontis, 1970). The cubic spline technique will be described below with regard to its later use. The technique using a recorded ice index afforded a more quantitatively repeatable procedure than the construction process described above. The primary disadvantages, which prohibited its use on the seven stereophotogrammetric models, were the time required for two people to view the marker, hand recording of the coordinates and surface condition (ice index) and preparation and checking of the thousands of values produced. If this stereophotogrammetric analysis were to be expanded or utilized again the stereomat operator should be trained to identify surface ice conditions (a task easily performed) and the B-8 digitizing-recording electronics modified to accept input of the ice index. The latter could be most easily accomplished if the lines (profiles) were alignable with either the x or y coordinate axis thus enabling use of the unused coordinate for input of the ice index.

The term sea surface profile is deserving of some clarification.

It is equated above with the smooth curve joining all points or segments of open water and/or thin ice. This curve is taken to be the actual sea surface, i. e. that water surface (a curve in this two-dimensional sense) which separates the sea water from either the atmosphere (open water cases) or thin ice (ice of negligible thickness). But what is it in the case of intersecting sea ice of measurable thickness? Clearly, the floes extend below the water level whether the water surface is deformed or not. The actual sea surface then might be thought of as the separation between water and ice. Neglecting the porosity and small scale roughness of the underneath surface of the ice, such a surface as defined by a curve (profile) might appear as in Figure 9. This profile, however, would not be found if one were to move laterally (perpendicular to the plane of Figure 9) a distance equivalent to, at most, half the width of the floe. The sea surface, as delineated by the smooth profiles described above and used in the following analysis is viewed as being the extension of the line of zero pressure (1 atmosphere) which would exist if the ice floes were without mass. One might argue then that the profile should not be named a sea surface profile--suggesting perhaps a profile of zero pressure (taking atmospheric pressure to be uniformly equal to zero over the region for simplicity). Such renaming would be suitable except for the difficulties of describing the massless ice. It is to be noted that the actual definition of the sea surface has not been addressed in previous work. The definition would seem to be very important in all instances of measurement--especially those measurements made with upward-looking sonar and bubble theodolites. In instances of shipboard measurements it is assumed that the observations were taken in open leads or polynas and thus the measured elevations are indeed the true sea surface profile, observed at that specific location. A second question arises from this issue. If one were to construct adjacent and parallel sea surface profiles, would they differ significantly because of the construction technique and definition? It is believed that so long as the distribution of floe sizes and concentrations remains approximately the same there will be no significant difference in the measured sea surface profiles adjacent and parallel to each other. If one were dealing with ice floes of large dimension in comparison to wavelength (as would be the case in the deeper pack ice) there would be a difference. This difference would stem largely from one's inability to reconstruct the sea surface profile with regularity (quantitative repeatability) but not through any failings of the definition of sea surface profile. Agreement with the former contention is pertinent to our later discussion of within model profile coherency.

Returning to the sequence of data preparation, the sea surface profiles were digitized by following the smooth profile defined above to be the sea surface profile. The digitized data were recorded on computer cards at an along line sampling interval of 0.05 cm (0.02 in.). This resolution was finer than that used to initially produce the graphs [20 values per 2.54 cm (1 in.) yields 0.13 cm per value along the profile axis; and 0.05 cm per value along the ordinate implies 50 values per instrument mm or a resolution in elevation of 0.02 instrument mm which is equivalent to 0.06 earth m]. The digitized values of elevation and distance along the profile (abscissa) were then plotted. These plots were laid atop the graphs produced from the initial readings from the stereomat containing the smooth curves representing the sea surface profile to assure absolute coincidence.

With the latter successfully accomplished, the accepted digitized values were processed through the cubic spline interpolation referred to above. The cubic spline representation was then sampled along the profile at intervals equivalent to 2 m on the earth. At this point the resolution of elevation values exceeded the initial resolution afforded by the B-8 Stereomat. This procedure was followed in obeisance of the principle that by processing data at finer resolutions than the initial measurements, analytical round off will not dilute the results (Hildebrand, 1956).

The cubic spline interpolation is described by Davis and Kontis (1970) as a mathematical procedure which is an analog of the draftsman's plastic spline. The advantage of the method lies in its ability to not only fit the observations exactly but to maintain continuity of the first and second derivatives. The spline is constructed by first assuming the second derivative of say f(x) to be a linear function of x between pairs of adjacent points. The second derivatives are integrated twice and the two constants of integration evaluated through the requirement that f(x) match the data points (x). To solve the equation for f(x), the second derivatives must be determined at the ends of the interval $x_k \leq x \leq x_{k+1}$. This is accomplished by requiring the first derivative to be continuous at each given x. The resulting system of equations are solved subject to an appropriate set of boundary conditions. The boundary conditions used for this work state that the second derivatives at the two end points of the data record are linear extrapolations of those associated with the adjoining intervals. The interpolation formula is a cubic polynomial in x within the interval between each pair of data points. References to the original development of this method may be found in Davis and Kontis (1970).

V. ANALYSIS OF OBSERVATIONS

Stereophotogrammetric Observations

The stereophotogrammetric data analyzed consisted for four sea surface profiles from each of seven overlapping models extending from the ice edge to the position within the ice where wave heights became immeasurably small. Each of the profiles were 1.024 km long (512 values at 2 m intervals). The number of values chosen for analysis was a power of two and thus suitable for use with the fast Fourier transform (FFT) discussed below. The distances from the ice edge to the midpoint of the profiles, measured parallel to the direction of wave propagation, for each model were: model 1, 0.49 km; model 2, 1.06 km; model 3, 1.65 km; model 4, 2.36 km; model 5, 3.01 km; model 6, 3.65 km; and, model 7, 4.28 km.

Before proceeding, the purpose and objectives of this study must be recalled in addressing the phenomenon of ocean wave/sea ice interaction. The stereophotogrammetric procedure was selected because it allows one to study the interaction synoptically as it appears when all motions are instantaneously frozen in space. Another significant advantage, noted earlier, is the opportunity to quantitatively assess the character of the sea ice canopy. The procedures chosen for analysis therefore were carefully selected to maintain some balance between accurate representation of the observations and accommodation of reasonable simplifying assumptions.

With regard to the ocean waves, it is assumed that they are suitably represented with the theory of finite amplitude, at least to first order as first presented by Stokes (1847, 1880), and now found in numerous texts such as Neumann and Pierson (1966). The Airy wave solution is a first order approximate solution to the Stokes wave (McLellan, 1965). This assumption, which to first order linearizes the waves, has served well in numerous applications even though it is known not to be absolutely representative of ocean waves. This evaluation is contained in numerous texts such as Neumann and Pierson (1965), and more recently by Barnett (1972). The resultant wave,

$$\eta(x,t) = a \cos(kx - \sigma t) \tag{1}$$

where: η is the sea surface displacement; a is the wave amplitude (assumed constant); k is the radian wave number ($2\pi/\lambda$), where λ is the wavelength; σ is the radian wave frequency ($2\pi/T$), where T is the wave period; x is the horizontal axis positive in the direction of wave propagation; and t represents time. Equation (1) describes a plane wave of permanent form. The second order Stokes wave is of trochoidal form and some net fluid translation becomes apparent.

Derivation of the Airy and Stokes waves reveals the all-important dispersion relation, correct to second order,

$$\sigma^2 = gk \tanh kd \tag{2}$$

where g is the acceleration of gravity and d is the water depth. For this work the water depths are sufficiently large compared to wavelength for the term tanh kd to be taken equal to unity.

The objective of determining the amount of wave energy present within each model may be achieved by computing the amplitude spectra of each of the four profiles. The total energy (E) contained in the wave form (Equation 1) per unit surface area is given by $E = \frac{1}{2}\rho g a^2$ where ρ is the water density. In this form the total energy is composed of equivalent amounts of kinetic and gravitational potential energy. The spectra are of course expressed in terms of wavelength (wave number). These spectra may be expressed in terms of wave period (wave frequency) only if we know the dispersion relation for ocean waves propagating within sea ice. On the open sea one may use Equation 2.

The amplitude spectra have been computed using the FFT introduced by Cooley and Tukey (1965). A description may also be found in Cochran *et al.* (1967). We will now examine why this procedure was followed and what specific steps were taken.

The sea surface profiles to be analyzed represented short (brief in the time sense) segments of the longer, complex process. The short segments were but samples from the longer record. As such, it was assumed that there were wavelengths in the record which were longer than could be discriminated with the samples. Similarly there was a restriction imposed by the finite sampling interval used. These restrictions may not be severe and are almost always experienced in geophysical studies involving measurements.

The objectives of determining the change in wave energy (a function of amplitude) with propagation into the ice canopy can be addressed by determining the amount at the edge and at successive intervals within the ice. With the proposition that the alteration of wave energy content by the ice is wavelength dependent, I chose to compute an amplitude and wavelength functional representation of the samples. Such a representation is produced by computing a Fourier series for each sample and expressing the results in the form of amplitude and phase spectra.

Before proceeding, it is noted that wave investigators such as Kinsman (1965) feel this procedure is "pretentious" in that it assumes repetition of the sample outside the sampling interval. They also criticize the provision of spectra only at discrete wavelengths. These concerns stem largely from interest in the process which produces the waves in the first place. The Fourier series on the other hand does represent the sample observations exactly and at a sufficient number of wavelengths for present purposes. We must also note that many researchers who frown on harmonic analysis of wave observations will in turn compute auto-correlation functions and process them with an algorithm which computes Fourier coefficients (FFT).

Some practical matters concerning the computation of amplitude spectra will now be addressed. This development was prepared after considerable discussion with Dr. Thomas Davis of the U. S. Naval Oceanographic Office. Reference to Davis' work may be found in his published Ph. D. dissertation (Davis, 1974).

One of the problems of estimating the spectral content of a finite sample lies with the effects of the presence of wavelengths longer than the sample length. In a statistical sense these longer components contribute a non-stationary component. This is unfortunate, as noted by Kinsman (1965), since the surface of the open ocean is statistically stationary. The effects introduced, termed spectral leakage by Tukey (1967), may be reduced by pre-whitening or by modification of the data window.

For this discussion let the direct Fourier transform be defined as,

$$G(\omega) = \int_{-\infty}^{\infty} g(x) e^{-i\omega x} dx,$$

and its inverse as,

$$g(x) = \frac{1}{2\pi} \int_{-\infty}^{\infty} G(\omega) e^{i\omega x} dx$$

The acquisition of a finite sample ($-T/2 \leq x \leq T/2$) from the continuous function g(x) consists essentially of multiplying g(x) by a rectangular data window w(x) given by,

$$w(x) = \begin{cases} 1, & -T/2 \le x \le T/2 \\ 0, & \text{elsewhere} \end{cases}$$

The Fourier transform of w(x) is the sinc function,

$$W(\omega) = T\frac{\sin T\omega/2}{T\omega/2}.$$

In the frequency domain, the effect of multiplying g(x) by w(x) to obtain the sample, is equivalent to convolving $G(\omega)$ with $W(\omega)$. Therefore the Fourier transform actually computed is $G_c(\omega)$ and not $G(\omega)$, where

$$G_c(\omega) = \int_{-\infty}^{\infty} G(u)W(\omega-u)du.$$

Different data window functions have been used in attempts to obtain better estimates of $G(\omega)$ (Blackman and Tukey, 1958). In the past these window functions were applied to the sample autocorrelation function. With the emergence of the FFT as an analysis tool the window functions must be applied directly to the sampled function.

For this analysis two procedures were evaluated: use of the cosine taper window; and, prewhitening. Both of these will be explained briefly. The cosine taper is defined as,

$$W_t(x) = \begin{cases} 1/2(1+\cos\frac{2\pi x}{T}), & -T/2 \le x \le T/2 \\ 0, & \text{elsewhere} \end{cases}.$$

The Fourier transform of the $W_t(x)$ window function is given by,

$$W_t(\omega) = T/2\frac{\sin T\omega/2}{T\omega/2} + T/4\left[\frac{\sin(\pi - T\omega/2}{\pi - T\omega/2} + \frac{\sin(\pi+T\omega/2)}{\pi + T\omega/2}\right].$$

A comparison of the rectangular and cosine taper windows (Davis, 1974) reveals that the main lobe of the cosine taper is twice as wide and the amplitude of its first side lobe only some 4% of that of the rectangular window. In practice the cosine taper reduces the oscillatory character of $G_c(\omega)$.

The prewhitening procedure (Tukey, 1967) is a numerical process (also applied to the original sample) which results in a nearly uniform spectrum over the frequencies of interest (therefore the word white). The cosine taper window reduced the oscillatory character of $G_c(\omega)$ more than prewhitening, consequently the cosine taper was chosen for use in this analysis.

The Fourier transform is complex, $G(\omega) = E(\omega) + iD(\omega)$, where $E(\omega)$ is the even real part and $D(\omega)$, the odd imaginary part. The computed amplitude spectrum of $g(x)$, using the cosine taper window is given by,

$$|G_c(\omega)| = ([E(\omega) * W_t(\omega)]^2 + [D(\omega) * W_t(\omega)]^2)^{1/2}$$

where * denotes convolution. The energy or power spectrum may be defined by $|G_c(\omega)|^2$. The terminology follows convention and the inexactness of units should be noted.

Computations were made with programs prepared by the Mathematical Modeling Group of the U. S. Naval Oceanographic Office. An example of the resulting amplitude spectra is presented in Figure 10. Amplitude is used here in its general usage as the square root of the sum of the squares of the Fourier coefficients--computed for each

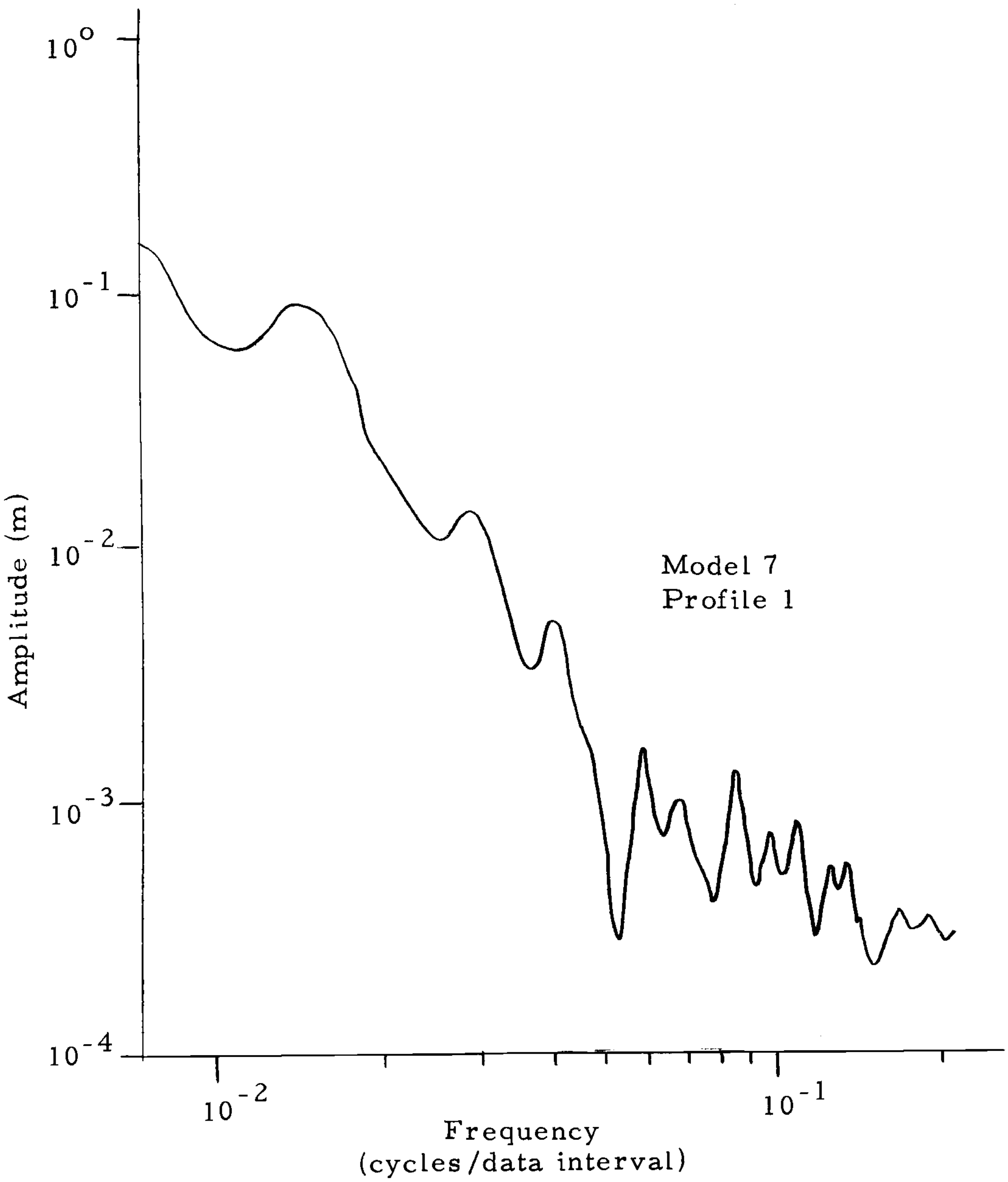

Figure 10. Amplitude spectrum using cosine taper.

frequency. All of the amplitude spectra have been computed and plotted at equal increments of normalized frequency with units of cycles per data interval. The spectra have approximately ten degrees of freedom as concluded from Tukey (1967), which result from the smoothing of seven of the amplitude estimates. The combination of (n) of the FFT values (square root of sum of squares of Fourier coefficients) yields approximately 1.36 (n) degrees of freedom.

Within each model the coherence among profiles was also computed (Figure 11). The coherence between profile number one and each of the remaining three profiles was computed by forming the ratio of the profile amplitudes at each frequency. These values are identified by the ordinate label, amplitude spectra correlation on Figure 11. The phase angle, expressed in data intervals, is the difference in phase between profiles at each frequency where phase is defined as: $\phi = \tan^{-1} \frac{b(\omega)}{a(\omega)}$, and $a(\omega)$ and $b(\omega)$ are the Fourier coefficients.

Before contrasting the spectra between successive models let us examine the spectra among the profiles within models. The distances between parallel profiles for each model are presented in Table 2. For each model the distances were measured from profile one to each of the successive profiles. In selecting these profiles one criteria used was to minimize long distances over relatively large ice floes. Avoidance of large floes facilitated a more accurate construction of the sea surface profile. As a result, the spacing of

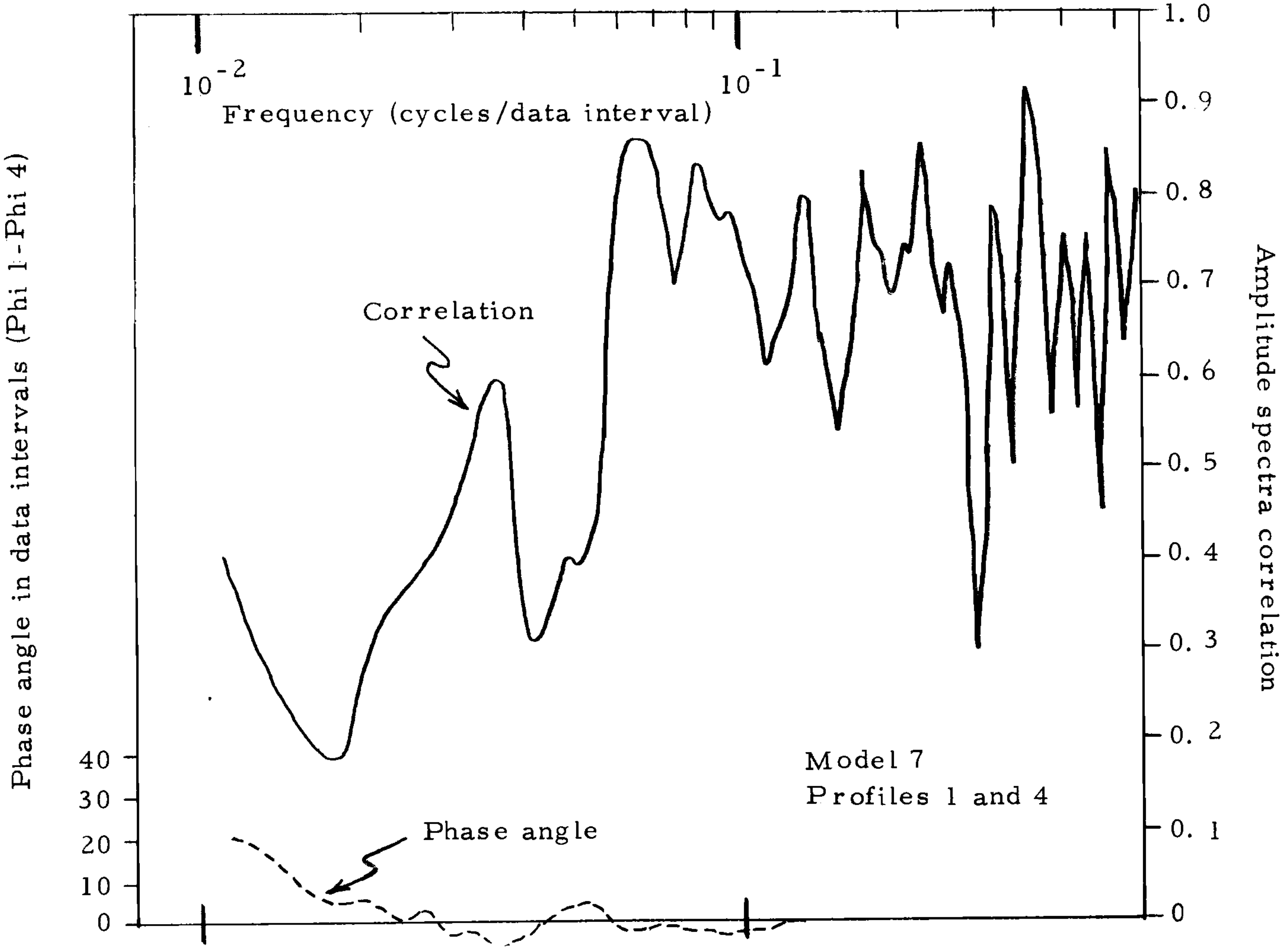

Figure 11. Coherence and phase angle between profiles.

Table 2. Distance between sea surface profiles (meters).

Model	Profiles 1-2	1-3	1-4
1	36	76	118
2	36	81	129
3	57	105	159
4	57	111	168
5	60	117	180
6	57	117	177
7	72	135	198

profiles was not uniform among models. In general the spacing between profiles 1 and 3 was twice that between 1 and 2 and the spacing between 1 and 4 was three times that between 1 and 2.

Spectra of the four profiles within each model were of course not identical. Departures from equivalence are expressed by the amplitude correlation and phase difference. Spectral equivalence among the profiles should not be expected. Most importantly because the statistical nature of the sea surface prohibits acquisition of identical records of finite length. In theory one can collect an ensemble or collection of samples of a stationary process and demonstrate an equivalence of their statistical properties. The variability of the amplitudes determined from the hypothesized collection of samples would be stable (Kinsman, 1965). One then faces the problem of what to do. To the extent that we can't obtain identical records with repetition of an experiment how can we begin to compare differences among collections of records, in this case among the models? This nagging question arises in analysis of most geophysical data--though for different reasons in many cases. For the problem at hand an average amplitude spectrum was computed for each model. The basis for this rests on the concept that the average representation of the sea surface deformation within each model is more representative, for comparison purposes, than any single sample. The amplitude spectra for each of the four profiles of each model have been averaged. The procedure was to average amplitudes for each frequency. The resulting amplitude spectra for each of the seven models are presented in Figure 12. Examination suggested similarities among several of these spectra. The spectra of Figure 12 were then combined, through averaging, to produce the four more distinctive spectra (S_i, where i = 1 to 4) shown in Figure 13. Spectra 1 is identical with that of model 1; spectra 2 is the average spectra of models 2, 3, and 4; spectra 3 is identical with that of model 5; and, spectra 4 is the average of those of models 6 and 7. The interaction phenomenon is thus characterized by four distinctive amplitude spectra spanning the ice canopy from its edge inward to the position of immeasurable (with the stereophotogrammetric technique) wave amplitudes. Further analysis will deal with these four spectra.

It is difficult to view a very large region of the model stereographically either with the B-8 Stereomat or with the much less sophisticated stereoscope. To the extent that the author could view the stereophotography (this ability improves with experience) the waves of greatest amplitude appeared to be short-crested. An illustration of short-crested waves is contained in Defant (1961). This short-crestedness is of course characteristic of most ocean waves. The waves of lesser amplitudes in the models may also have been short-crested though it was difficult to discern due to the visually predominating influence of the larger amplitudes.

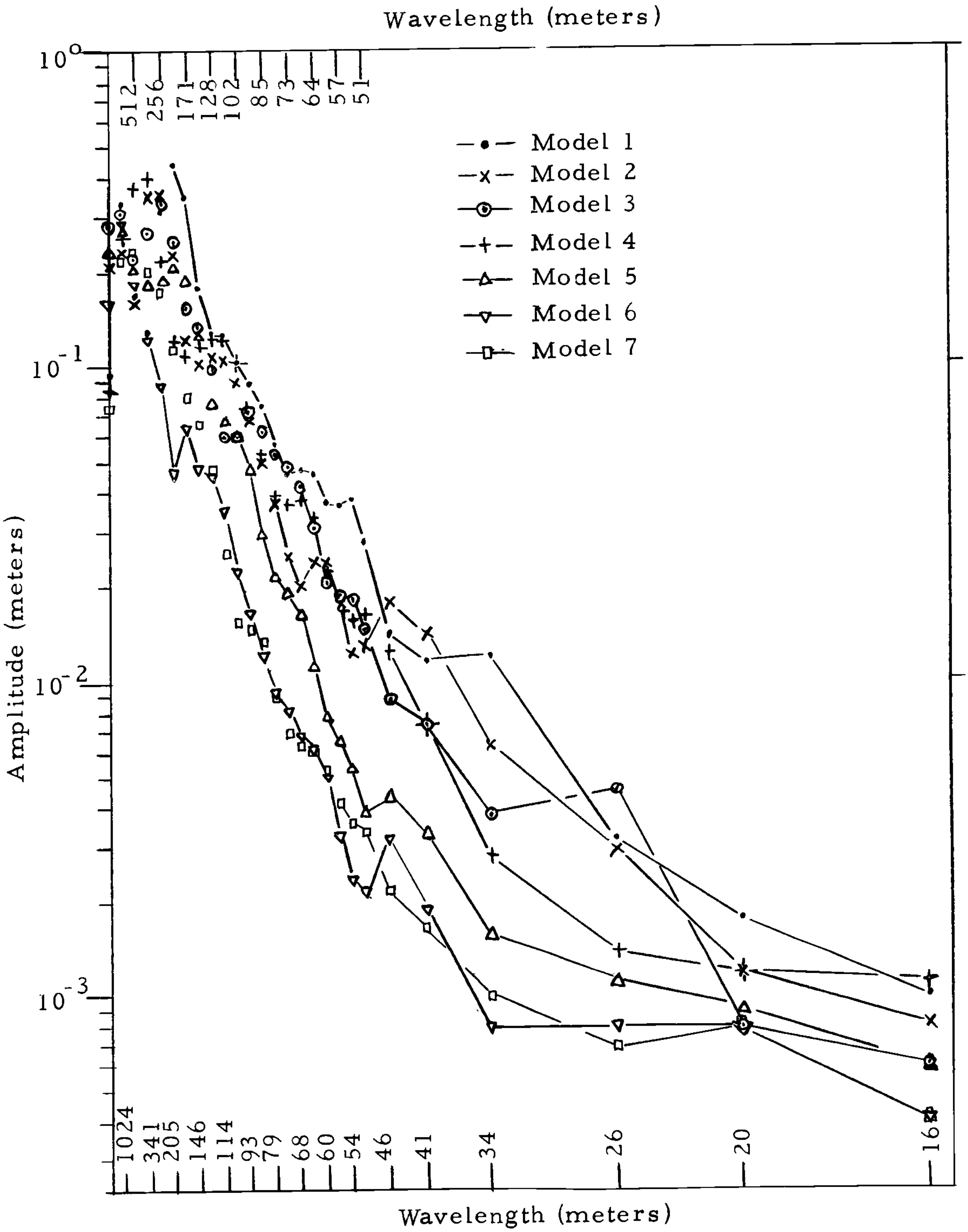

Figure 12. Averaged amplitude spectra of each model.

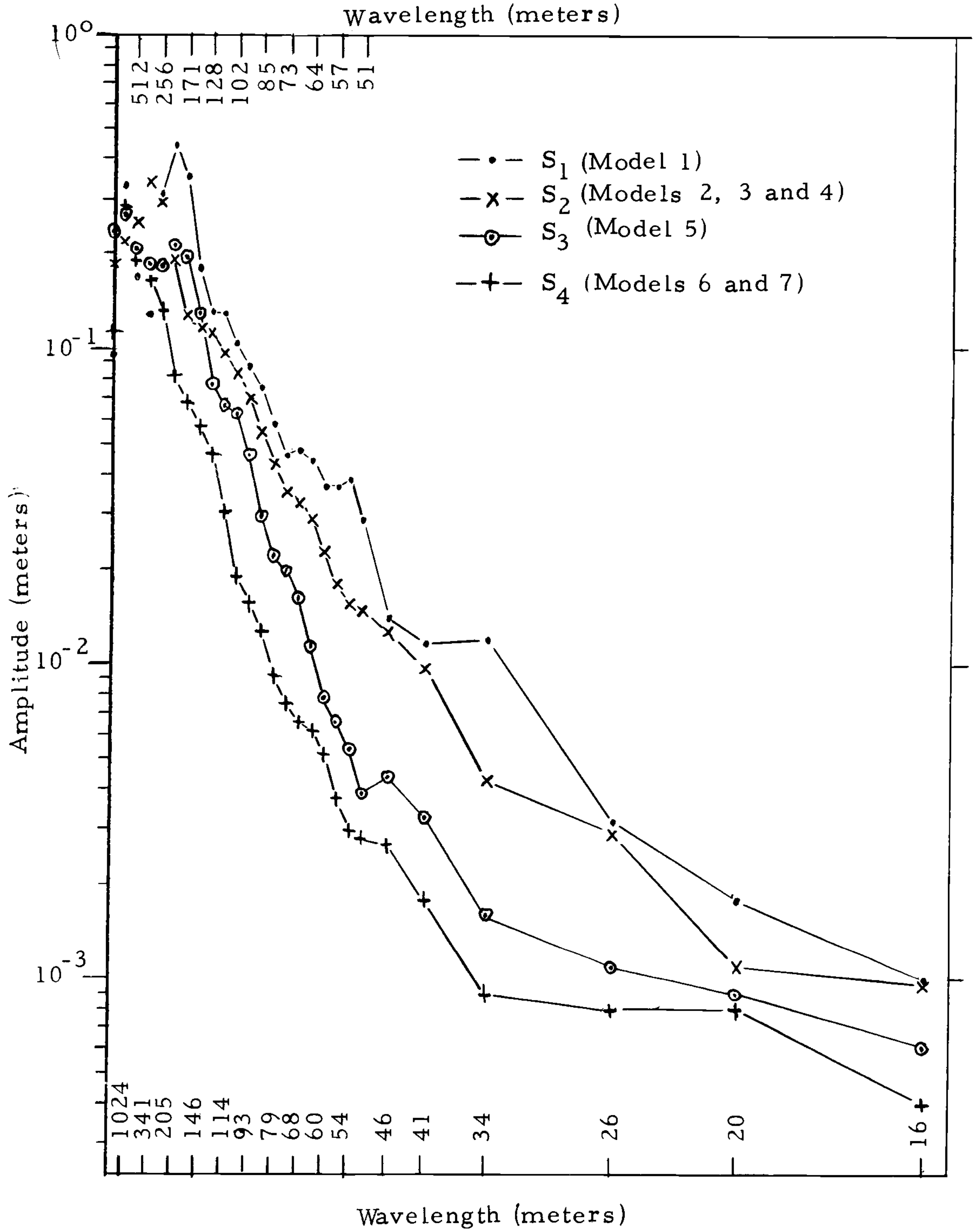

Figure 13. Averaged amplitude spectra (S_i).

For analysis of wave attenuation I chose an amplitude transmission coefficient (α_i) defined as the ratio of the amplitude measured at position (i) to the amplitude measured at the ice edge. This parameter is frequently used within the ocean engineering literature, especially as related to artificial breakwaters. Alternate expressions may be formed using wave heights or squared amplitudes--the latter being in proportion to energy attenuation.

The portion of the spectra to be analyzed is bounded by wavelengths of 256 and 50 meters. Longer wavelengths were considered to be insufficiently sampled in the 1 km record lengths. Furthermore, the 256 m wavelength was the first averaged value using the seven point spectral averaging procedure. Wavelengths shorter than 50 m are susceptible to noise derived from the measurement and data processing procedures. The effects of this noise became most evident when the α_i were computed. Further smoothing of the amplitude estimates at shorter wavelengths might alleviate this difficulty (see Figure 10). Transmission coefficients, derived from the four spectra identified above, are presented in Figure 14. The numerical values used in their computation are presented in Table 3. Wave periods calculated from Equation 2 are included for later reference. The amplitude transmission coefficients (Figure 14) are observed to reach very small values over the propagation path for nearly all wavelengths. This of course should be expected based upon our

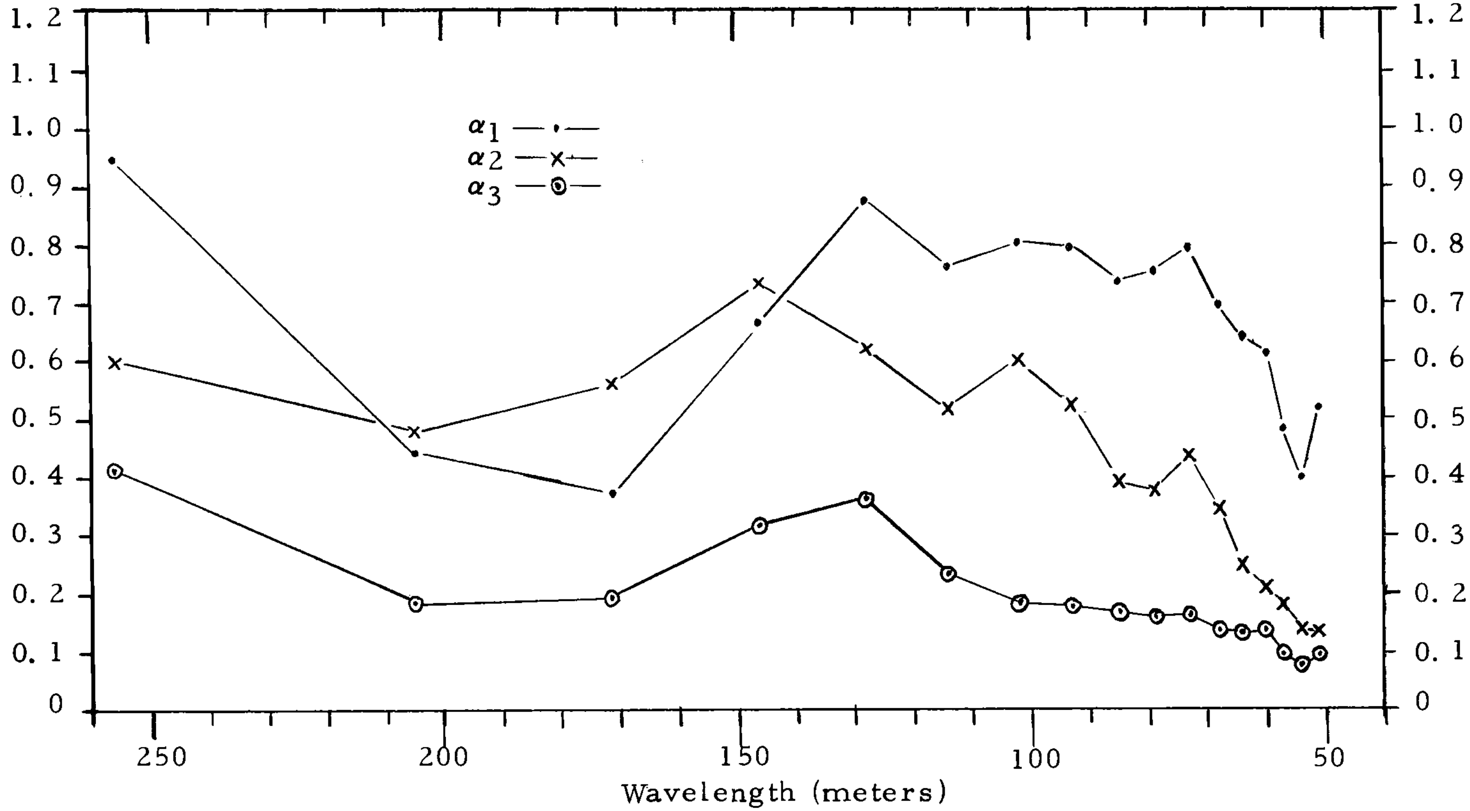

Figure 14. Amplitude transmission coefficients (α_i) versus wavelength.

Table 3. Averaged amplitude spectra [S_i (m)] and transmission coefficients (α_i).

λ (m)	S_1	S_2	S_3	S_4	α_1	α_2	α_3	T(sec)
256	.3138	.2988	.1880	.1311	.9522	.5991	.4178	12.8
205	.4396	.1956	.2112	.0820	.4449	.4804	.1865	11.5
171	.3462	.1274	.1948	.0680	.3680	.5627	.1964	10.5
146	.1776	.1181	.1298	.0570	.6650	.7308	.3209	9.7
128	.1270	.1116	.0790	.0462	.8787	.6220	.3638	9.1
114	.1274	.0969	.0668	.0304	.7606	.5243	.2386	8.5
102	.1038	.0838	.0624	.0192	.8073	.6012	.1850	8.1
93	.0884	.0704	.0465	.0159	.7964	.5260	.1799	7.7
85	.0750	.0554	.0294	.0128	.7387	.3920	.1707	7.4
79	.0580	.0438	.0219	.0094	.7552	.3776	.1621	7.1
73	.0457	.0364	.0199	.0076	.7965	.4355	.1663	6.8
68	.0478	.0335	.0164	.0066	.7008	.3431	.1381	6.6
64	.0458	.0294	.0114	.0062	.6419	.2489	.1354	6.4
60	.0372	.0230	.0078	.0052	.6183	.2097	.1398	6.2
57	.0369	.0179	.0066	.0038	.4851	.1789	.1030	6.0
54	.0388	.0155	.0054	.0030	.3995	.1392	.0773	5.9
51	.0287	.0149	.0039	.0028	.5192	.1359	.0976	5.7

Source Data	Definition
S_1 - model 1	$\alpha_1 \equiv S_2/S_1$
S_2 - models 2, 3 and 4	$\alpha_2 \equiv S_3/S_1$
S_3 - model 5	$\alpha_3 \equiv S_4/S_1$
S_4 - models 6 and 7	

observations of the laser and stereophotogrammetric observations. For comparison purposes note that $\alpha = 0.1$ and 0.32 are equivalent to wave energy attenuations of 99% and 90%, respectively.

With this development, concerning the processing of the stereophotogrammetric observations, we turn our attention to a quantitative description of the sea ice canopy.

Sea Ice Canopy Observations

The ice canopy was comprised of ice cakes and small floes which were surrounded by thin ice. The cakes and floes were judged to range from thick first year ice to multiyear ice. The stage of development was most difficult to distinguish for the cakes because of their small size. The floes which had less smooth surfaces and more angular shapes were younger than those which had smoother surfaces and more rounded edges. Some of the floes had evidence of melt puddles and flooding areas. Floe thicknesses derived from the glossary (Appendix A) may be slightly misleading. Sea ice floes in the stages of development noted above range in thickness from approximately 1.5 to 3 meters or more. Most of the observed floes contained portions of ridges and hummocks which contributed significantly to their overall thickness. It was also noted that the edges of the floes in models 1 through 5 were more deformed than those of models 7 and 8. This may indicate that the floes in the latter models were thicker and thus less apt to deform along their edges during impact with each other. Clearly, the floes were separated by thin ice and not impacting with one another on the day of observation.

The thickness of a floe (H) may be taken to be the sum of its sail (S) and keel (K). The nominal thickness cannot be judged using maximum values but rather an average for the sail and keel of a floe result from the overall equilibrium between gravitational and buoyant forces. These forces are proportional to the total ice mass and total displaced volume of water. From the available data the amount of each floe above the sea surface was estimated. It would be possible to determine the actual volume of ice above the water line if one had unlimited time for study using the B-8 Stereomat. However, if this course were pursued, the eventual determination of the submerged volume of ice would depend upon an estimate of ice density. The latter is impossible to know for it varies with ice age and past history--being very much dependent upon brine and air content. Additionally, the floes had an unknown and highly variable amount of snow coverage. There appears to be no reliable way to estimate the amount of snow coverage, either on a floe by floe or an overall basis.

Various estimates have been made of the sail to keel ratio for sea ice. The studies have resorted to various observations at large and small spatial scales and have dealt with both level and deformed ice. The question has not been resolved.

As noted earlier, sea ice is a complex substance--perhaps, according to Sater (1963), one of the world's most complex. The material is non-homogeneous and anisotropic. It is a conglomerate of fresh water crystals and cavities of brine solutions and air. These constituents are seldom, if ever, in equilibrium. Therefore, it is very difficult to determine the sail to keel ratio through measurement of ice density. Numerous measurements of ice density have been made and the values range from approximately 0.7 to 0.93 gm cm^{-3}. There are numerous references to the values of ice density (Kovacs, 1971), to the relationships between ice crystals and brine and air cavities (Assur, 1958), and the complexities of measuring ice density (Malmgren, 1927). Some interesting observations of the distribution of salinity within sea ice are found in Cox and Weeks (1973).

Older and more deformed ice tends to be less dense than newer and undeformed ice. For purposes of numerical calculation one should select the value of ice density from the known range which best represents the type of ice involved. Unfortunately, this has not always been the case. Many researchers prefer instead to adopt an average value. The most commonly reported value, or the one derivable from reported computations, is approximately 0.9 gm cm^{-3}. Swithinbank (1971) for example, estimates ice sails from measured ice keels using a sail to keel ratio of 1:7. The assumption of equilibrium between gravitational and buoyant forces yields, $S/K = (\rho - \rho_i)/\rho_i$. Using a reasonable sea water density of 1.03 gm cm^{-3}, an ice density of 0.9 is required to produce a ratio of 1:7. Multiyear ice undoubtedly has a lesser density, owing to brine drainage and inclusions of once melted snow and surface ice waters.

There are a few coincident measurements of ice sails and keels. Some examples are presented by Weeks and Kovacs (1970), Kovacs (1971), Kovacs et al. (1972) and Francois (1972). The reported values for sail to keel ratios range between 1:4 and 1:9. Extreme values as high as 1:19 (Kovacs, 1971), are attributed to local deflections induced by loading. Lower ratios have been observed, for which some theoretical accounting has been suggested through consideration of ice rubble within ridges (Parmerter and Coon, 1973). Along the East Greenland coast the value 1:5 has been measured and reported by Kozo and Diachuck (1973). Their observations were not derived from measurement of individual ridges but rather from long tracks of upward-looking sonar and nearly coincident airborne laser profiles. Similar statistical comparisons between airborne laser and upward looking sonar recordings are presently being made for the Central Arctic Basin by the British (Robin, 1976).

In nearly all measurements of ice sails one should account for snow cover. Within ice covered regions such as the Central Arctic Basin there is not much snowfall. However, when moving about on the ice it would seem to the contrary for one frequently experiences "white-out" conditions produced by blowing snow. This snow is not new but merely undergoing a redistribution. From personal experience the snow is deepest within ridges, up to a meter or more but generally less. Some bare spots are found on undeformed ice surfaces through an average cover of a few centimeters is typical. Near the open sea one should expect a greater amount of snow, because of the nearby supply of moisture for the atmosphere. Airborne laser and stereophotographic measurements of ice sails do not distinguish snow depth. The density of snow is very much a function of its compaction. The nominal value of 0.1 to 0.2 gm cm^{-3} may be representative (Yosida, 1962).

For this work, the effective water density is taken to be 1.028 (Amstutz et al., 1975). Using the sail to keel ratio of 1:5 the ice density is concluded to be 0.86 gm cm^{-3}. No numerical accounting was made for snow cover in determining ice thickness. Though estimated to be some 10-20 cm, the effect of snow cover on the ice sail to keel ratio is small in comparison to the effect of choosing a representative ice density from the measured range. The observed snow cover appeared only on the floes; there being little if any snow present on the regions of thin ice.

The average sail heights of the floes in each model and their corresponding equivalent thicknesses, based on the 1:5 ratio, are presented in Tables 4 and 5, respectively. The accepted values for

Table 4. Sail heights (meters).

Model	Profile	Range of significant values		Accepted profile value	Maximum value
1	1	.3	.8	.6	4.1
	2	.3	1.1	.8	7.5
	3	.2	1.5	.8	4.5
	4	.2	1.1	.6	3.8
2	1	.4	.8	.6	4.1
	2	.2	.6	.7	3.0
	3	.1	1.5	.8	4.5
	4	.2	1.1	.9	4.5
3	1	.6	.9	.8	8.6
	2	.8	1.9	1.2	9.7
	3	.8	1.5	1.1	8.3
	4	.8	1.5	1.1	6.0
4	1	.8	1.9	1.5	4.5
	2	.8	1.9	1.5	5.2
	3	1.5	2.2	1.9	6.0
	4	1.5	2.2	1.9	8.6
5	1	1.5	2.2	1.8	5.2
	2	1.1	1.9	1.5	4.9
	3	1.1	1.5	1.5	12.8
	4	.8	1.5	1.1	6.8
6	1	2.2	3.5	2.7	11.3
	2	1.1	1.5	1.2	3.8
	3	2.2	3.0	2.5	4.5
	4	1.5	3.0	2.3	5.2
7	1	1.5	2.2	1.9	4.5
	2	1.5	3.7	2.8	8.6
	3	1.5	3.0	2.2	6.7
	4	1.5	3.0	2.2	9.8

Table 5. Accepted ice thicknesses (meters).

Model	Accepted model values			Single point maximum model values			
	Sail	Keel	Thickness	Sail	Keel	Thickness	Observed on profile no.
1	.7	3.5	4.2	7.5	41.2	48.7	2
2	.7	3.5	4.2	4.5	23.1	27.6	3 and 4
3	1.1	5.5	6.6	9.7	48.5	58.2	2
4	1.7	8.5	10.2	8.6	43.0	51.6	4
5	1.5	2.5	9.0	12.8	64.0	76.8	3
6	2.3	11.5	13.8	11.3	56.5	67.8	1
7	2.3	11.5	13.8	9.8	49.0	58.9	4

each model lie within the range of measured values reported by Kozo and Diachuck (1973). Although the maximum reported sail heights (Table 4) are correct, the implied keel depths and consequent ice thicknesses (Table 5) are no doubt excessive. These maximum values are given only to serve as an estimate of possible extreme conditions. The sail heights have been determined through analysis of superimposed graphs of the measured profile elevations of ice and water and the smoothed accepted sea surface profile (see Figure 8). It is difficult to determine representative values of sail heights. The values in Table 4 reveal the variation in sail heights characteristic of each of the profiles. These values are averages for floes occupying significant portions of the profiles. There was a tendency for floes of larger area to have greater sail heights. Variations among profiles were evident in some of the models, which might contribute to differences in along crest wave behavior by the process of selective reflection and perhaps diffraction. The resultant effects of course will be dependent upon the spatial extent and number of these floes within a given model. The accepted characteristic sail heights and derived keels and thickness are presented in Table 5. The maximum sails for each model, equivalent to points of maximum ridge heights, are included in Table 5 for comparison. As noted, the maximum sail values are equivalent to the points of maximum ridge heights.

The ice floes were surrounded by relatively thin ice which was taken to be of negligible thickness. This thin ice was approximately 10 cm thick and appeared to be young ice. As noted above, the thin ice was observed to conform to the sea surface profile. Referring to the glossary (Appendix A), such elastic ice is identified as nilas, rather than young ice. The distinction is not great but serves to point out one of the difficulties encountered by those attempting to assign descriptive names to complex substances--especially those which are most often observed remotely.

Each of the models was covered completely by ice. The composition of the ice canopy, described in Table 6, was determined through tedious (Amstutz, 1976) accounting of each floe observed within each of three circular areas of equal diameter. The circular areas were superimposed over the four profiles of each model. The procedure is sketched in Figure 15. These circles had equivalent diameters on the earth of 312 m. There are of course numerous ways to determine the concentration of floes by size. For this study the floes were measured on positive prints and assigned to their respective size categories. The size categories (Table 6) were chosen solely because of their equivalence to metric measure in millimeters. (Recall that 1 mm on the original imagery is equivalent to 6 m on the earth.) The measure of nominal diameter used for floe classification was based on the average length and breadth of the floes. The circular area was chosen, vice any other shape, because of its geometric properties of

Table 6. Floe count by size.

Model/Circle	Average diameter (meters)									
	4	9	15	21	27	33	39	45	51	57
1/1	500	32	4	--	--	--				
2	206	57	22	7	1	--				
3	153	34	23	14	9	2				
2/1	127	39	26	7	1	--				
2	157	43	21	13	--	1				
3	115	33	21	11	1	1				
3/1	113	42	23	11	5	--				
2	137	59	25	16	9	--				
3	128	37	26	18	13	--				
4/1	80	47	25	15	4	1	--			
2	91	57	27	16	13	1	--			
3	89	41	19	12	14	--	4			
5/1	59	29	19	14	4	2	1	1		
2	34	32	30	20	9	3	1	--		
3	53	32	27	16	6	7	2	--		
6/1	13	30	14	10	6	2	2	1		
2	48	35	20	7	5	6	--	--		
3	19	29	20	12	6	6	4	--		
7/1	13	19	21	14	4	5	1	1	1	--
2	56	17	16	7	7	5	2	1	--	1
3	63	20	23	11	12	2	2	--	--	--
8/1	82	16	26	14	8	--	--	8	--	
2	36	53	20	10	17	6	--	1	1	
3	10	25	11	12	7	--	1	1	--	

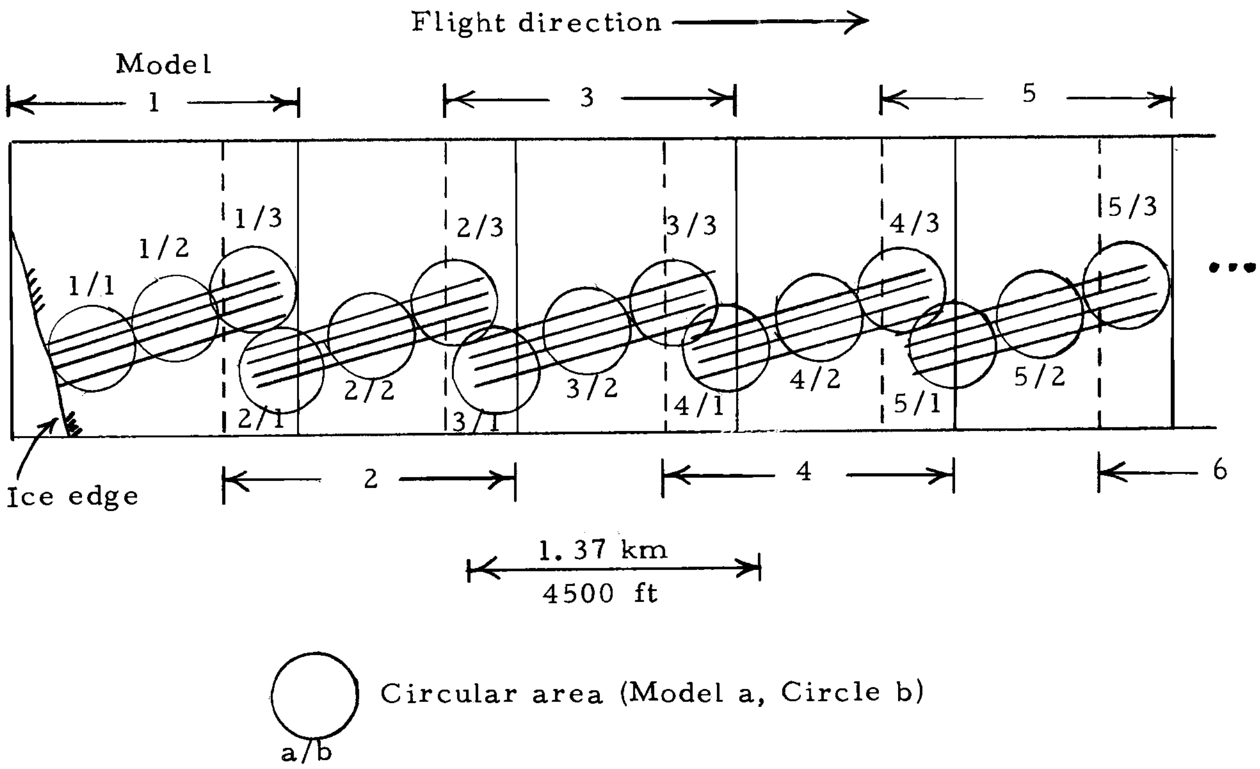

Figure 15. Procedure for counting floes.

maximum area and minimum perimeter. Floes which were contacted by the perimeter were included or excluded in the accounting procedure if a greater or lesser portion of their surface area was inside or outside of the circle.

The percentage of floes of given size observed by Dean (1966a) were similar (in distribution) to the data of able 6. Dean (1966a) describes the distribution as being half a Gaussian curve. Such an analytical description seems pointless to follow because there are zero floes of zero dimension and the half Gaussian curve cannot be zero at its mean.

The data contained in Table 6 served to quantitatively describe the ice canopy along the path of wave propagation. The distribution of circular areas, within which the count of floes was made, is sketched in Figure 15 (compare with Figure 6). Proceeding from the ice edge, the last circular area of each model was adjacent to the first circular area of the succeeding model. The floe distribution statistics of these adjacent circular areas have been combined for analysis. Values for the adjacent circular areas, e.g. model 1 circle 3 and model 2 circle 1, were determined by using the total count for each size category and dividing by an area equivalent to two of the circles.

The areal proportion of the ice canopy composed of floes of each size category is presented in Table 7, where the size categories are identified by a floe diameter. For the smallest size category

Table 7. Ice canopy composition by floe size.

Model/ Circle	Distance from edge (km)	Floe size categories (diameters in meters) 4	9	15	21	27	33	39	45	51	57	
1/1	.18	.082	.027	.009								.118
1/2	.49	.034	.047	.051	.032	.007						.171
1/3 & 2/1	.76	.023	.030	.057	.048	.037	.011					.206
2/2	1.06	.026	.036	.049	.059	--	.011					.181
2/3 & 3/1	1.37	.019	.031	.051	.050	.022	.006					.179
3/2	1.65	.023	.049	.058	.072	.067						.269
3/3 & 4/1	2.01	.017	.035	.059	.075	.064	.006					.256
4/2	2.36	.015	.047	.062	.072	.100	.011					.307
4/3 & 5/1	2.68	.012	.029	.044	.059	.067	.011	.039	.010			.271
5/2	3.01	.006	.027	.069	.091	.067	.034	.016				.310
5/3 & 6/1	3.32	.005	.026	.047	.059	.045	.050	.031	.010			.273
6/2	3.65	.008	.029	.046	.032	.037	.067					.219
6/3 & 7/1	3.97	.003	.020	.047	.059	.037	.062	.039	.010	.013		.290
7/2	4.28	.009	.014	.037	.032	.052	.056	.031	.021	--	.033	.285
7/3 & 8/1	4.54	.012	.015	.057	.057	.075	.011	.016	.083			.326
8/2	4.84	.006	.044	.046	.045	.127	.067	--	.021	.027		.383
8/3	5.21	.002	.021	.025	.054	.052	--	.016	.021			.191
		.018	.031	.048	.053	.050	.024	.011	.010	.002	.002	.249

(diameters <6 m) a diameter of 4 meters was assigned. For the remaining size categories the representative floe diameters were taken as the mid-values of the class range. The class range in each case was 6 meters. The values within Table 7 represent the proportion of each circular area occupied by the observed number of floes in each size category (summary values are presented by size category and by circular areas). Values in the bottom row of Table 7 represent the proportion of the total area covered by floes of each size category. Values in the right-hand column represent the proportion of each circular area covered by ice floes. The distances of the centers of the circular areas from the ice edge are given in column 2. From Table 7 it was concluded that some 24.9% of the total ice canopy was made up of ice floes. Measurements from model 8 were included in the summary of ice conditions to provide quantitative measure of the ice beyond the limit of significant wave propagation. Note the exception to the general tendency for increased floe coverage with increasing distance from the ice edge in passing to the third circle of model 8.

The distribution of floe sizes, based on Table 7 and presented in Figure 16, portrays the proportion of the floes in the ice canopy composed of each size category. The peak value occurs at approximately 20 m. The curve has been extended to the origin for there can be no floes of zero diameter, and to a diameter of 60 m, for there were no floes of this or greater diameter within the area of floe

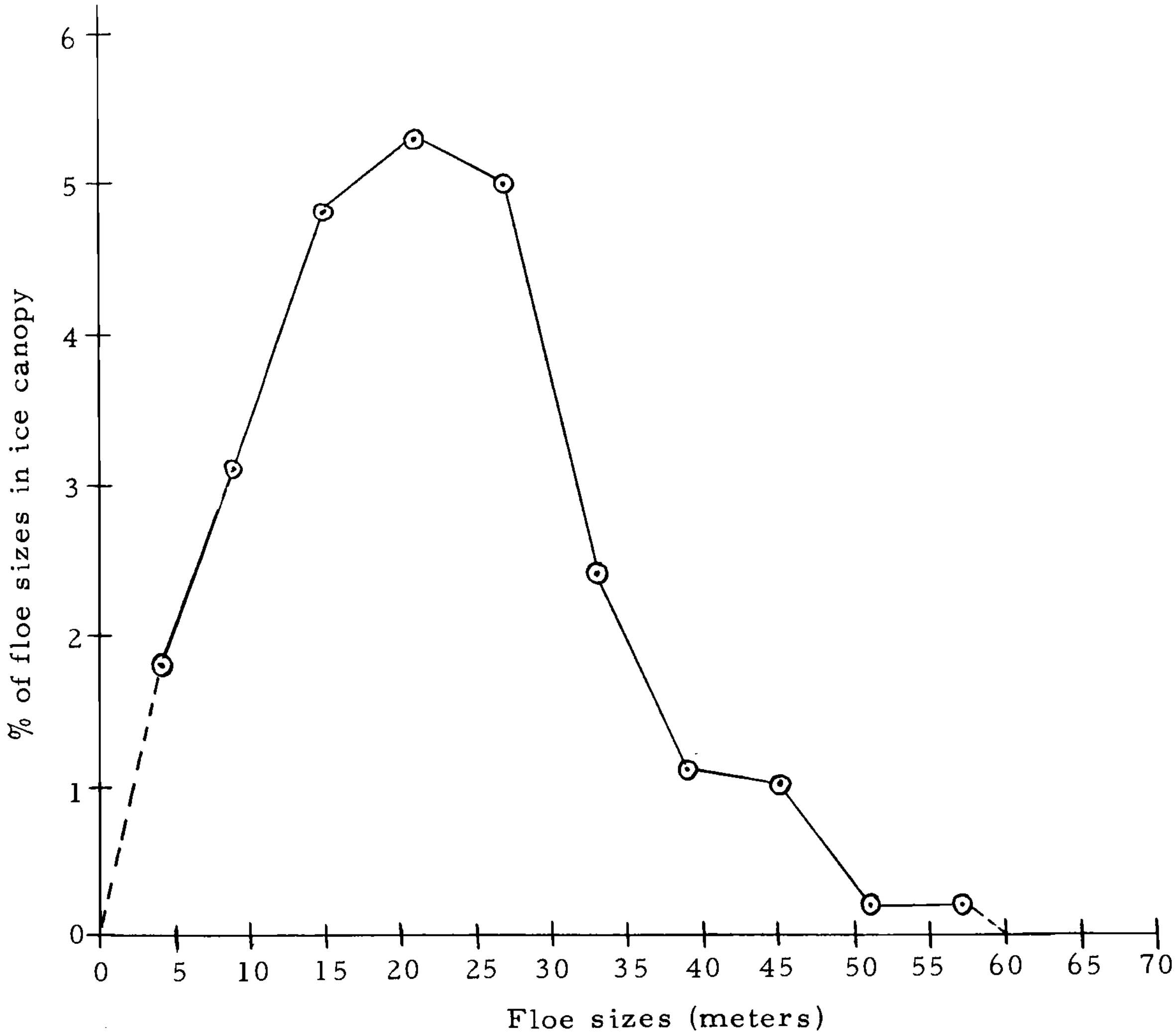

Figure 16. Distribution of floe sizes.

measurement.

The proportion of the ice canopy composed of floes, with respect to distance from the ice edge, is illustrated in Figure 17. The lower concentration of the innermost circle of model 8 is apparent. The locations of the spectra chosen for analysis (S_i) are also indicated. The location of the spectra were plotted using the center position of the model (or models) they represented.

The floe composition of the ice canopy may now be described on the basis of subareas pertinent to analysis of the amplitude transmission coefficients. Selection of these subareas is discussed in the following section.

Combined Analysis

Examination of the observations described above and those reported by Robin (1963), Dean (1966a, b) and Wadhams (1973b) has led to the formulation of a tentative or working hypothesis. The hypothesis is stated in general terms to serve as a framework for analysis of the observations. It may be refined as we proceed. We begin with the assumption that the most pertinent parameters influencing the interaction phenomenon are: the incident wave spectrum; the concentration of ice floes; the distribution of floe sizes (diameters); and, the floe thicknesses. The incident wavelength of maximum amplitude experiences the mass effects of the ice canopy. Wavelengths shorter than that of maximum amplitude are reflected (scattered) by the ice floes. The scattering process is largely a function of the ratio of wavelength to floe diameter, but will increase for wavelength to floe diameter ratios as the floe submergence extends well into the wave's water particle velocity field. The amplitude of the wavelength of maximum amplitude diminishes rapidly with increasing floe mass (thickness). With this attenuation another wavelength (probably longer than the first) becomes the wavelength of maximum amplitude. The incident amplitude spectrum is diminished over the shorter wavelengths by the scattering process, with attenuation extending to longer wavelengths as larger floes are encountered. The spectrum is also diminished at successive wavelengths of maximum amplitude through mass effects of the ice canopy. For typical ocean wave spectra and floe thicknesses this process is affecting intermediate wavelengths. With increasing distance from the ice edge the locally measured spectrum will contain only the longest wavelengths and they will be of relatively small amplitude. These longer waves will propagate deeper into the ice canopy with attenuation resulting from work performed in bending of the much larger floes existing there. Survival of the longest waves stems from the greater depths to which their water particle velocity fields extend in accord with the finite submergence of ice floes. The reflection process described for shorter waves does not apply to the longest waves for the same reason. The existence of a thinnest small floe, which would not reflect even the shorter wavelengths, is ruled out because of the physical properties of sea ice. The shorter waves are reflected by the smaller floes behaving as rigid plates (for these waves). The thinnest floe will be composed of very new and therefore elastic (non-rigid ice). The specific circumstances of an observed ocean wave/sea ice interaction will therefore depend upon the incident wave spectrum, the concentration of ice floes, the distribution of floe sizes and the floe thicknesses. With sufficient wave amplitudes there will be a fracturing of those floes which are unable to conform to the profiles of the wavelengths of maximum amplitude. Comparisons of existing observations may be difficult, due to differing circumstances for one or more of the pertinent parameters and the presence or absence of thin ice within the ice canopy. As a practical matter, for example, the thin ice between floes may serve to inhibit floe responses in surge and sway.

Before we compare the spectra with various properties of the ice canopy it should be noted that there was no evidence that any of the ice floes had been fractured by the interaction process. During the experiment, an infrared line scanner was used to obtain imagery of the ice surface to examine for ice fracturing. The presence of new fractures is readily detected on thermal imagery due to exposure of the relatively warm water. It is believed that the interaction process contributes to the production of smaller floes along the ice edge. A gradation in floe size, such as that described above, is typical of the ice regions exposed to waves and swell from the open sea.

The reflection of water waves from the ice edge and from within the ice canopy contributes significantly to the loss of energy from the interaction zone. The abruptness of final measurable wave amplitudes displayed in the laser recordings (Figure 5) is very suggestive of a reflection process. Reflection of wave energy is of course the primary ingredient in most of the theoretical studies undertaken to date. Reflection is expected also because of observed wave behavior in the presence of artificial floating bodies at sea and in wave tanks.

The reflection process is better described by the term scattering. The reflectors are not rigid plates with straight edges aligned parallel to the incident wave crests. If the floes have fairly uniform thickness, they may be viewed as short cylinders. Such would be the case for floes formed from undeformed ice. In general, and for this case, most of the floes were fragments of previously deformed ice. Beneath the water surface some may have had sills. The sides of the keel structures will slope downward and towards the vertical center plane somewhat like a wedge. The keel is generally of rough surface, being composed of blocks of ice which have been cemented with newer ice. Observations of the underside of ridges are found in Francois (1972), Weeks and Kovacs (1970) and Kovacs and Gow (1976). Theoretical studies of ridge formation (Wittmann and Schule, 1966 and Parmerter and Coon, 1973) appear to account for the observations rather well considering the complexity of ridge structures. The observed floes have keels which are composed of the remnants of multiyear pressure ridges as well as newer ridges; thus making their underside structure more complex than that of a single ridge. Ice of this type is sometimes referred to as storis, a Norwegian term.

In addition to wave reflection there also should be some wave diffraction along the direction of propagation. The resultant wave amplitudes will be diminished as a result of the diffraction process. The effects of this process have not been addressed due to the complexities of such a study. Work on the subject has been undertaken for design of nearshore breakwaters (Shore Protection Manual, 1973) for shallow water. These studies do address gap widths of less than a wavelength which are characteristic of the observed floe distributions.

Refraction of the waves is possible if the wave phase velocities are altered by the interaction process. Theoretical treatments, dealing with waves coupled to large ice sheets suggest that the incident wavelengths will be increased (Greenhill, 1887 and Wadhams, 1973a). If radian wave frequency is conserved there will of necessity be an increase in phase speed within the ice. On the other hand, theoretical treatments of interaction which assume the ice to be composed of non-interacting mass points suggest both a decrease and increase in wavelength, depending on the specific circumstances.

The only theoretical study which has been interpreted in terms of observable values (Shapiro and Simpson, 1953) does not produce results in agreement with observations. There are no measurements to date suitable for a determination of this important question.

Refraction was not observed by the author during visual observation of the interaction, nor was it apparent in the observations reported earlier (Amstutz and Ketchum, 1973). The possibility of increasing wavelengths, noted in that work, may not have resulted in any apparent refraction due to normal incidence of the waves to the ice edge and, more importantly, the nearly uniform along crest distribution of ice properties.

The amplitude transmission coefficients (Figure 14) presented for wavelengths less than 128 m have been studied for effects of reflection. The four longer wavelengths available for analysis were not incorporated, though they also exhibited significant attenuation. Examination of their attenuation has been undertaken on the hypothesis of wavelength alteration. If these four longer wavelengths were to have increased, for example, then their energy would have transferred to the left in Figure 14, resulting in an apparently large amplitude transmission coefficient. None of the theoretically derived wavelength alterations produced reasonable results. An accounting for the coverage of thin ice, some 75% of surface area, yielded equally poor results. We will return to this discussion below.

Analysis of wave reflection was undertaken through examination of wave amplitude attenuation and floe diameters. The importance of the relationship between the transmission coefficients and the ratio of floe diameter to wavelength has been amply demonstrated in studies of artificial floating breakwaters. A partial summary of these studies (Richey and Nece, 1974 and Adee, 1976), indicates little or no attenuation for beam to wavelength ratios less than 0.1, and little transmission (coefficients of approximately 0.1 to 0.2) for beam to wavelength ratios greater than 0.5. The beam width in artificial floating breakwater studies is defined as the dimension of the breakwater measured parallel to the direction of wave propagation. For the present work the beam was considered equivalent to floe diameter.

Before contrasting the spectra with the distributions of floe size, the question of which subarea effects which spectra was addressed. The supply of waves from the open sea was assumed to have been continuous and to have occurred uniformly during the measurement period and for a sufficient time before to have established a steady pattern of behavior. For sake of discussion, assume one could first measure the wave spectrum at sea, which has only those components approaching the ice edge. A second spectrum, measured near the ice edge but over open water, would include the incident waves plus all those which were reflected at the ice edge as well as those reflected from the interior. Some of the latter may have decayed to the extent that they are immeasurable. A third spectrum obtained at a point within the ice would contain only those components of the second spectrum which were not reflected prior to reaching this point plus those which were reflected beyond the point and were enroute back to the open sea. Such would be the case for spectra obtained from other points progressively deeper into the ice canopy. (The spectra measured in the interior might conceivably contain wave components which were reflected back to the interior by floes encountered during their transit to the open sea.) Eventually a point is reached within the ice canopy where no wave components are detectable with the hypothetical measuring device.

For this study we do not have measurements at a point. Clearly, the complexities of the process and the irregular nature of the ice canopy would never result in the idealized view, even if one had point measurements. In comparison with the idealized measurements described above the observations reported here consist of the third and successive spectra.

The amplitude transmission coefficients indicate the proportion of incident amplitude, for each wavelength, which has been transmitted to successive positions, proceeding from the ice edge. The amplitude transmission coefficients presented in Figure 14 were based upon averaged amplitude spectra described earlier. The ice canopy must now be described in terms of subareas pertinent to discussion of each of the transmission coefficients. The ice canopy was divided into five subareas. The first four subareas have been defined to be representative of the regions from which the four average amplitude spectra were taken. The fifth subarea represents the ice canopy of model 8 where immeasurable wave amplitudes were encountered. The exact composition of each ice canopy subarea is defined in Table 8 on the basis of model numbers and number of circular areas used for measurement of ice conditions. It is important to recall here that the ice conditions measured in sidelapping circular areas of successive models have been combined. The values in Table 8 were derived from those of Table 7 and represent the percentage composition of the floe canopy by floe size. For example, it was concluded from Table 8 that in the first circular area of the first model, 69.5% of the area covered by floes (floe canopy) is made up of floes having an average diameter of 4 meters (range 0 to 6 meters). The values from Table 8 are presented in Figure 18. An increase in both maximum floe diameter and average floe diameter, with increasing distance from the ice edge, is apparent.

A thorough inspection of Figures 14 and 18 indicates that amplitude transmission is least for waves encountering floes of maximum concentration which yield beam to wavelength ratios $\geqslant 0.3$ to 0.4. The scattering process initiates when waves encounter floes of maximum concentration which yield beam to wavelength ratios

Table 8. Percentage composition of floe canopy by subareas.

Subarea	Model/Circle	Class size by average diameter (meters)									
		4	9	15	21	27	33	39	45	51	57
1	1/1	.695	.229	.076							
1	1/2	.199	.275	.298	.187	.041					
1	1/3 & 2/1	.112	.146	.277	.233	.180	.053				
2	2/2	.144	.199	.271	.326		.061				
2	2/3 & 3/1	.106	.173	.285	.279	.123	.034				
2	3/2	.086	.182	.216	.268	.249					
2	3/3 & 4/1	.066	.137	.230	.293	.250	.023				
2	4/2	.049	.153	.202	.234	.326	.036				
2	4/3 & 5/1	.044	.107	.162	.218	.247	.040	.144	.037		
3	5/2	.019	.087	.222	.294	.216	.110	.052			
3	5/3 & 6/1	.018	.095	.172	.216	.165	.183	.114	.037		
4	6/2	.036	.132	.210	.146	.169	.306				
4	6/3 & 7/1	.010	.069	.162	.203	.128	.214	.134	.034	.045	
4	7/2	.032	.049	.130	.112	.182	.196	.109	.074		.116
4	7/3 & 8/1	.037	.046	.175	.175	.230	.034	.049	.255		

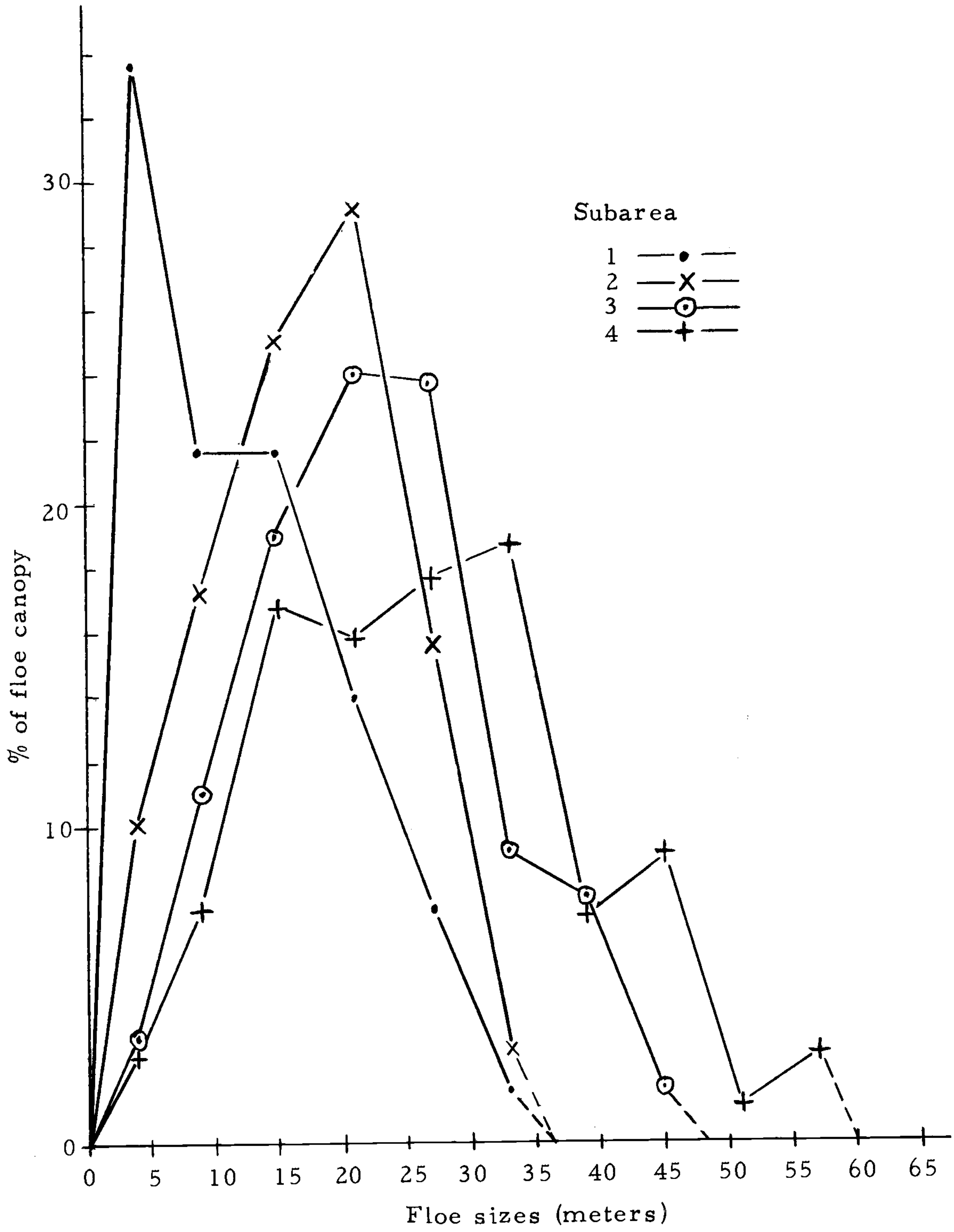

Figure 18. Percentage composition of floe canopy by subareas.

$\geqslant 0.1$ to 0.2. These ratios are in agreement with those reported above for artificial floating breakwaters. Robin (1963) and Dean (1966a) reported very similar values from their summer season Antarctic observations.

The observed beam to wavelength ratios reported here relate to amplitude attenuation without noticeable dependence upon absolute floe concentration. The observations of Robin (1963) and Dean (1966a) indicating the importance of the same ratios were made under much greater floe concentrations and in the absence of thin ice among the floes. Robin (1963) does not report a concentration value but his description of the floes being in 'loose contact' suggests a 10/10 concentration. Dean (1966a) reports 10/10 floe coverage. In both of these reports the authors determined floe sizes through visual observations and photographs taken from aboard ship. Robin (1963) reports that the most significant attenuation in wave energy was associated with floe diameters of about $\lambda/3$; little loss of energy when floe diameters were less than $\lambda/6$; and no detectable transmission when floes exceeded $\lambda/2$. Robin (1963) notes that ocean wave scattering initiates, as with electromagnetic waves, when the diameter of the scatterer exceeds $\lambda/2\pi$. The beam to wavelength ratios reported by Robin (1963) were dependent upon his increasing visual estimates of floe size by 30%. His justification for doing this stemmed from instances of concurrent visual and photographic observations.

The ice thicknesses observed by Robin (1963) ranged from 1.5 to 3 meters, while those observed by Dean (1966a) averaged about 2.5 meters. Their thickness values were derived through visual observations of portions of floes upturned in the sea. Robin (1963) notes that ridges may have extended to 10 meters. The ice thicknesses observed in this study are greater than those reported by Robin (1963) and Dean (1966a).

The submarine and laser observations reported by Wadhams (1973b) constitute the remainder of ocean wave/sea ice observations known to this author. Little is known of the ice conditions which existed during the submarine observations because of the restricted view afforded by the periscope and the nighttime conditions which existed during many of the measurement periods. The laser observations were obtained during summer with floe concentrations less than 50%. Analysis of the laser observations (Wadhams, 1973b) was undertaken through a 'rearrangement' of ice floes which effectively moves all ice towards the edge until a 100% ice cover is achieved. Wave attenuation is then examined as a function of 'effective penetration'. His finding of an exponential decay of wave energy with distance reveals the importance of a scattering process.

I have undertaken an examination of wave attenuation with respect to distance in order to contrast the results with those of Dean (1966a) and Wadhams (1973b). To accomplish this, the parameter

α_i^2 versus distance was plotted for a few wavelengths (Figure 19). The zero distance (ice edge) has been defined to be the center position of the area of model 1. This position is 0.49 km from the actual ice edge (see Table 7). Amplitude attenuation coefficients (β) have been computed for wavelengths of 54 and 128 meters. The defining expression is $\alpha_i^2 = (\frac{a_i}{a_o})^2 = \exp(-2\beta x)$, where x is the distance of penetration in kilometers. The values for wavelengths of 54 m and approximately 100 m are $\beta = 0.75\ km^{-1}$ and $0.20\ km^{-1}$, respectively. The attenuation produced by these values are included in Figure 19.

Similar coefficients, computed by Wadhams (1973b) for wavelengths of 114 m and 85 m were $0.35\ km^{-1}$ and $0.52\ km^{-1}$, respectively. Though these attenuation coefficients appear similar to those reported here it may be fortuitous. The analysis procedure used by Wadhams (1973b) involved: (1) the conversion of spatially measured wavelengths to wave periods, using the open ocean deep water dispersion relation; (2) computation of spectra; and, (3) an adjustment of the spectra frequency scale to account for forward motion of the measurement platform. The 'corrected spectra' therefore include uncertainties in ground speed.

Dean (1966a) did not present amplitude attenuation coefficients although he presented sufficient data for a comparison to be made. His observations, obtained with the shipboard wave recorder, were taken 500 m seaward of the ice edge, and at points 50 m, 100 m,

Figure 19. (Amplitude transmission)^2 versus distance.

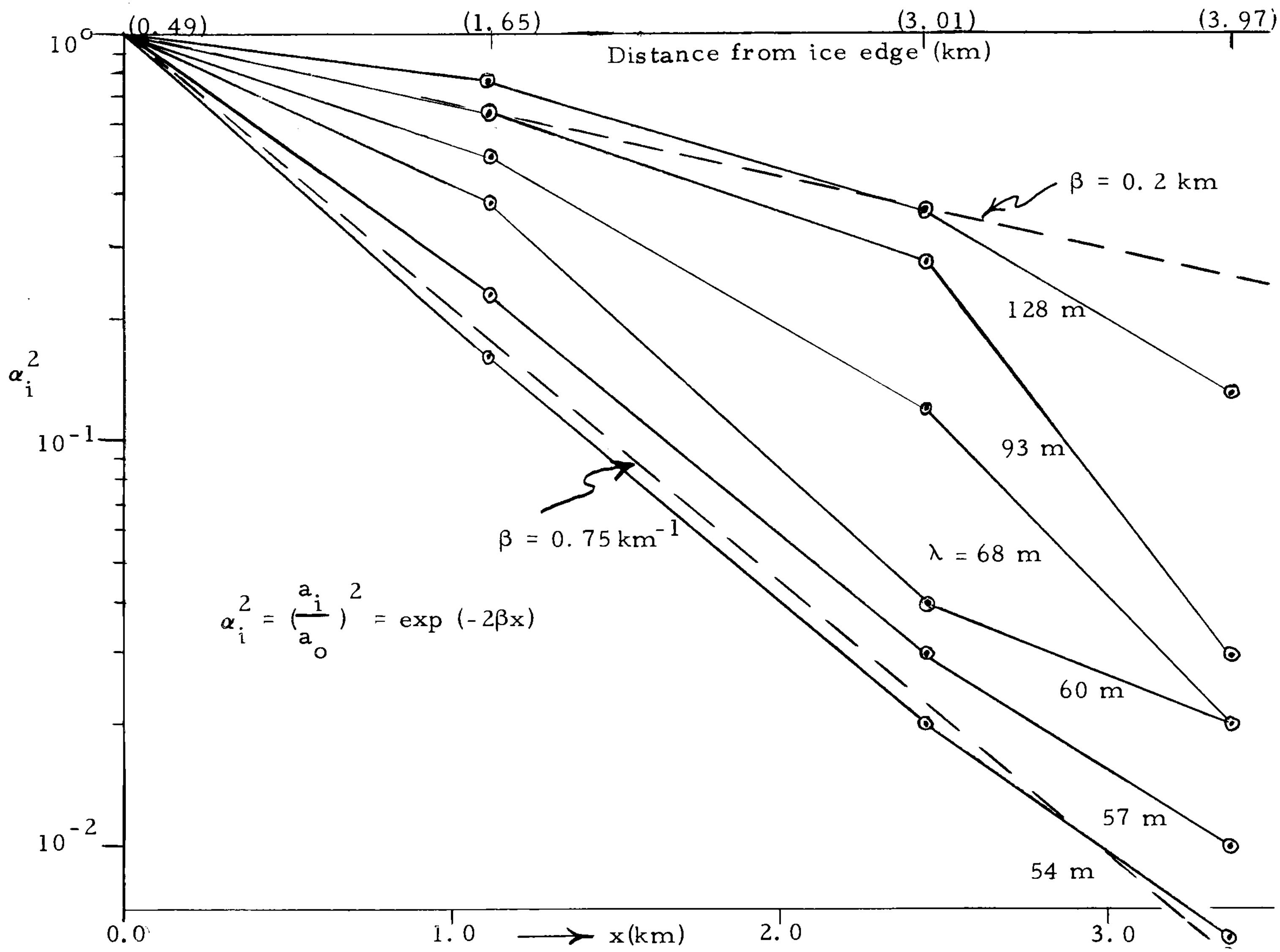
(0.49)
(1.65)
(3.01)
(3.97)
Distance from ice edge (km)
10^{0}
10^{-1}
10^{-2}
α_i^2
β = 0.2 km
128 m
93 m
λ = 68 m
60 m
57 m
54 m
β = 0.75 km^{-1}
$\alpha_i^2 = (\frac{a_i}{a_o})^2 = \exp(-2\beta x)$
0.0
1.0
2.0
3.0
x(km)

300 m, 500 m, 1000 m and 2000 m shoreward of the ice edge. These data were identified as 1963/64 (ii) by Dean (1966a). The data presented in Figure 8 of Dean (1966a) yield excellent agreement with my attenuation coefficient ($\beta = 0.4\ km^{-1}$) for wavelengths (his) of 100-114 m. This agreement extends to the 2 km limit of observation.

For shorter wavelengths (specifically, 56 m and 50 m) Dean (1966a) found the attenuation with distance to be very abrupt. On the coordinates of Figure 19, these two wavelengths reached values of $\alpha^2 \sim 2 \times 10^{-2}$ at a position 500 m within the ice. The amplitudes did not attenuate further in going to a penetration of 2 km. Dean (1966a) noted that during the three hours required to make the measurements, the open ocean spectrum was observed to have changed. This change in energy level, judged uniform over all frequencies, was linearly distributed with respect to time. A second set of observations, identified as 63/64 (i) by Dean (1966a), contained no change in the open ocean spectrum energy levels during the period of measurement. The energy attenuation with distance, determined from the 63/64 (i) and 63/64 (ii) observations, was very nearly the same. Dean (1966a) suggested that some process other than wave reflection must account for the abrupt decay of the shorter wavelengths though none was advanced. The very rapid attenuation of the 50 and 56 meter wavelengths within distances of one to two wavelengths from the ice edge would seem to suggest reflection by the ice edge itself. If this were the case the wave spectrum measured 500 m seaward of the edge may have been 'contaminated' by reflected waves--especially if the waves were of nearly normal incidence to the edge.

We return now to Figure 14 and consider the amplitude attenuation of $\lambda > 150$ m. Amplitude attenuation by wave scattering has been related to floe diameters for wavelengths less than approximately 140 m. Using the criteria that scattering is most effective when the ratio of the diameter of the floe of greatest concentration to wavelength $\geqslant 0.3$ to 0.4 has been developed using the shorter wavelengths. Assuming that it was correct, a floe of 45 m diameter from Figure 18 (subarea 4) was selected and it was determined that the longest wavelengths effected would be <150 m. Further evidence of the influence of some process, other than reflection associated with floe diameter, was found in Figure 19. Though the attenuation coefficients (β) described behavior of shorter wavelengths it appears that a different process was introduced for $\lambda > 100$ m beyond a penetration of 3 km.

It is proposed that the wavelengths of 256, 205, and 171 m have undergone very significant amplitude attenuation as a result of their being the wavelengths of maximum amplitude. These waves of maximum amplitude are viewed as carrier waves and attenuate as a consequence of the mass effects of the ice canopy. The four averaged amplitude spectra (S_i) used in this study (Figure 13 and Table 3) possessed wavelengths in descending order of maximum as follows:

S_1, 205, 171 and 256 m; S_2, 256, 205 and 171 m; S_3, 205, 171 and 256 m; and, S_4, 256, 205 and 171 m. In passing from the first subarea to the second the transmission coefficient (α_1) was lowest for the 205 and 171 m wavelengths. The transmission coefficient for the third subarea (α_2) remained nearly the same for the 205 and 171 m waves but showed a marked decrease at the 256 m length. Propagation into the fourth subarea produced minimum transmission coefficients (approximately 0.2) for wavelengths of 205 and 171 m while the coefficient for the 256 m wave diminished to only 0.4.

Though the theories of Peters (1950) and Weitz and Keller (1950) do not yield quantitatively predictable results their findings suggest the described behavior of wavelengths of maximum amplitude. This can be seen, at least qualitatively from Figure 22, if we incorporate computed wave periods (Table 3) and averaged ice thicknesses (Table 5).

The physical mechanisms producing the attenuation have not been ascertained. The existence of the wave's water particle velocity field near the surface is probably very important since the particle velocities are blocked by the submerged portions of the floes. However, the attenuation afforded through reflection from a submerged vertical plate (Ippen, 1966) does not account for the measured attenuation of these longer waves. The measured attenuation compares more favorably with the values of attenuation reported by Ippen (1966) for vertical barriers which extend upward from the sea floor to the submerged floe depths. Reflection from a vertical barrier, extending from the surface, can be shown to be much more significant if we use keels greater than the mean values (see Table 5). Ursell (1947) finds significant reflection from fixed vertical barriers, extending from the surface, when $\sigma^2 K \sim 0.4$ g. The longer waves we have observed ($T > 10$ seconds) approach this criteria upon encountering ice keels of 10 meters.

A portion of the observed amplitude attenuation for longer waves may be accounted for through wave breaking and interactions among the floes and thin ice between floes. The photographs taken nearest the edge suggest some flooding of the ice. (Flooding is used here to mean the introduction of sea water to the upper ice surface.) Lastly, as noted earlier, some energy will be expended as a result of the thin ice acting to constrain the wave induced motions of the floes.

The effects of total drag between waves and ice floes and the frequency response of floes excited by ocean wave frequencies are important factors which need to be studied. The out of phase transfer of wave momentum to ice inertia also needs further study. These topics are discussed further under recommendations.

VI. THEORETICAL AND MODELING STUDIES

Theoretical Studies

Theoretical treatments of ocean wave/sea ice interaction are few in number even though they have evolved over several decades. Before proceeding, it seems appropriate to develop a qualitative framework for this review. To accomplish this, two questions are posed: 1) what becomes of the wave energy once introduced to the ice edge; and, 2) what alterations of the ice canopy might result? This procedure hopefully reduces the complex process to some of its basic components. Excluded from consideration are such matters as waves breaking, wave-wave interaction, interactions among wave components and surface currents, and all effects which may be introduced by local winds.

All or a portion of the impacting wave energy may be reflected either at the ice edge or elsewhere within the ice canopy. Given propagation within the canopy, the waves may refract and/or experience diffraction. Pertinent parameters influencing these processes are the surface dimensions of the ice floes (nominal diameters), ice draft, wavelength and wave amplitude. It is known that wave amplitudes diminish during the interaction. It should be considered possible for wavelengths to be altered also during the interaction. If such were the case, the phase and group velocities would be altered, assuming conservation of wave frequency.

The ice, constrained by buoyant forces, will either bend to conform to the sea surface profile totally, in part, or not at all. Within these circumstances the ice may or may not fracture. Pertinent parameters are the surface dimensions and elastic properties of the ice, wavelength and wave amplitude. Work will be performed by the waves in bending floes. Thus some wave attenuation will occur. The ice may also be deformed through lateral interaction of floes. The measurable result of this would be ice ridge formation at floe boundaries (the ice being ridged is not necessarily floe ice). This interaction within the ice will be dependent upon the dimensions and concentrations of floes (compaction of ice) and wave length and amplitude. Behavior of individual floes and their resulting interactions (if in contact) may be viewed as ice floes responding to their six degrees of freedom of motion: sway, surge, heave, pitch, roll, and yaw.

The waves and ice floes are characterized by bands of pertinent dimensions. Specific effects may therefore apply only to portions of these bands. Also, if certain floes within the ice canopy were to fracture with passage of a particular wavelength succeeding waves of the same length are likely to transmit without refracturing these same floes. Put another way, the leading waves of a particular length expend portions of their energy and thereby enable passage of their following numbers without equivalent energy loss.

Wave energy will be lost due to frictional dissipation against the underside of floes, orbital characteristics of water particles may degrade to turbulent motion through interruption by ice keels, and some energy will convert to ambient noise. The ambient noise results from interaction among ice floes and from interactions involving air, ice, and water.

The work performed by the waves in moving floating ice in the earth's gravity field averages to zero over a wavelength or wave period. This work is equal to the product of the mass of the ice, the acceleration of gravity and the distance moved by the center of gravity of the ice. The latter is proportional to the wave form (Equation 1) which becomes zero upon integration over a wave length or period. The kinetic energy of the oscillating pieces of floating ice does not average to zero over a wavelength or wave period.

The kinetic energy attributed to the ice is approximated by the product of the virtual mass of the ice and the square of its vertical velocity component. The virtual mass is taken to be the sum of the mass of ice and the added mass of fluid (equated with the displaced fluid volume). Thus the virtual mass is twice the mass of ice alone. This simplification, which implies an added mass coefficient of one for ice floes, is based upon the guidelines presented by Robertson (1965). The importance of added mass to the circumstances of a heaving object is conveyed by Golovato (1957).

The vertical velocity being proportional to the square of the vertical displacement (Equation 1) exceeds zero when integrated over a wave length or period.

$$KE_{ice} = \rho_i \forall_i \int_0^T \left(\frac{\partial\eta}{\partial t}\right)^2 dt = \tfrac{1}{2}\rho_i H \delta A a^2 \sigma^2 T,$$

where $\forall_i$ is the volume of ice, H is the ice thickness and δA represents an elemental unit of area. The total energy of a surface wave over a period is given by $\frac{1}{2}\rho g a^2 \delta A T$. The ratio (r) of the kinetic energy of vertically oscillating discrete floes to the total energy of the open ocean wave is given by:

$$r = \frac{\rho_i H \sigma^2}{\rho g} = 0.033 \frac{H}{T^2},$$

where H is in cm and T in seconds. In the expression for (r) the amplitude of ice oscillation and that of the open ocean wave are equivalent. The ratio (r) serves to compare these two energies. Note that $r \to 0$ as $H \to 0$ and r is reduced with increasing period for given ice thickness. The ratio (4) is plotted in Figure 20. When $r = 1$ the kinetic energy of the vertically oscillating floes is equivalent to the total energy of the open ocean wave. For $r = 0.01$, 1% of the available surface wave energy is required for ice kinetic energy. However, a 1% loss in wave energy is equivalent to a 10% reduction in wave amplitude.

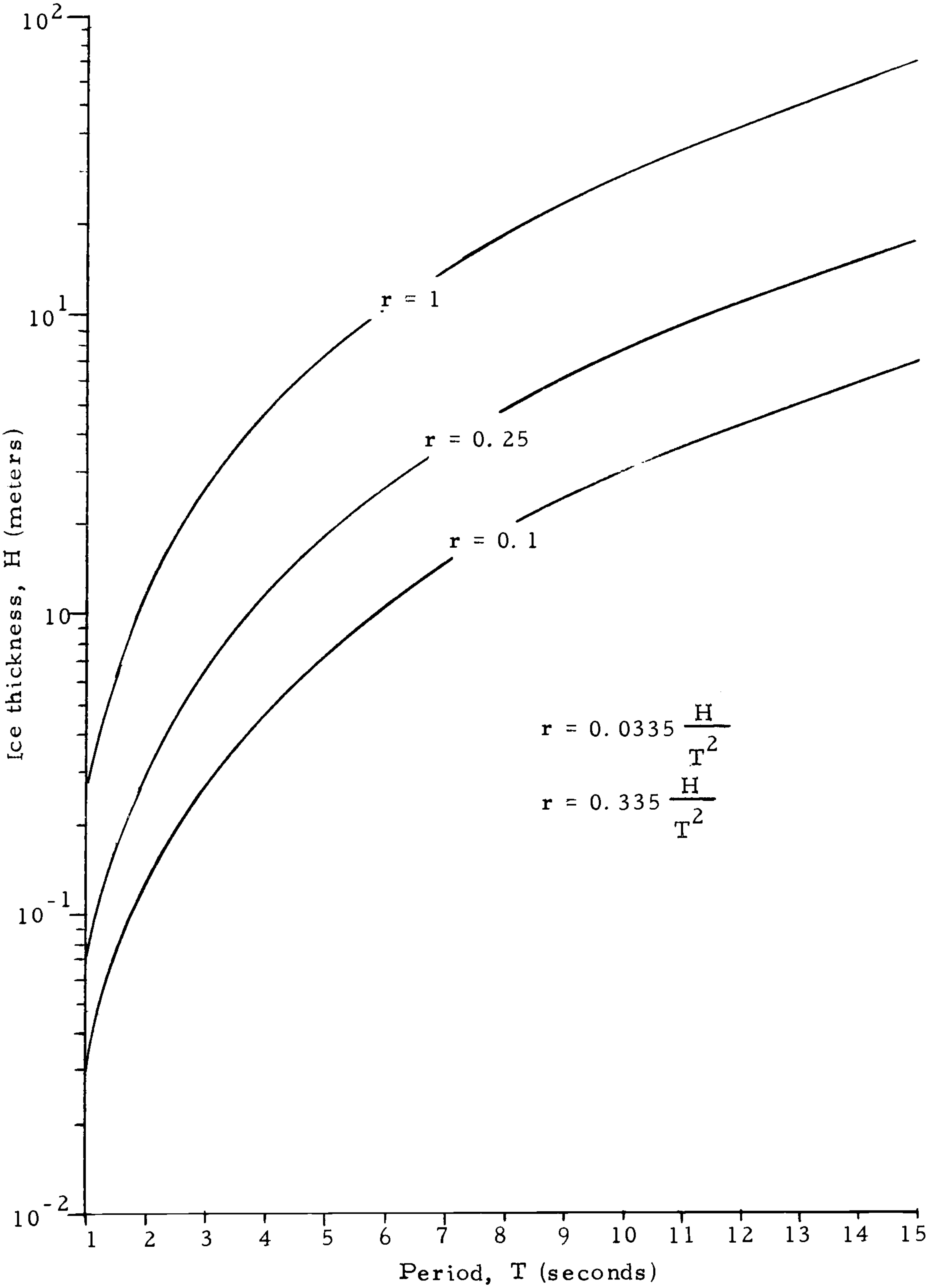

Figure 20. Kinetic energy of oscillating ice.

This rather simplistic approach reveals that an ice canopy composed of small floes (compared to λ) which do not bend or otherwise dissipate energy will have considerable attenuating effect. Very rapid attenuation should be expected as the floe thicknesses increase, as shown in Figure 20.

As will be seen later, two very elegant mathematical developments produce the above result, though in a considerably different fashion.

In describing previous studies, the terminology and symbols used follow those of the original papers. This procedure was used to ease referencing to the original papers. Where appropriate parameters or other functional representations are compared with the present observations, transformations of symbols will be made.

Theoretical examinations of the ocean wave/sea ice interaction phenomena may be made in a variety of ways and degrees of complexity. Two overall viewpoints are apparent. One is of the response of the ice or floating object to undulation of its supporting medium. Another is of the effects of floating objects upon the undulations themselves. There have been a number of studies made which exemplify both views--most of which have ultimately been associated with investigations of ship behavior. As one would expect, the degrees of complexity have been broad.

As noted at the outset, our interests are confined to works most relevant to the wave/ice interaction problem. Though there is a possibility that some studies within the literature of ship motion may apply this avenue has not been pursued in depth. The primary reason stems from the vast differences in design between ships and sea ice. The absence of similarity in shape is gradually diminishing however, with the advent of larger and larger tankers. Studies relevant to the design and behavior of these juggernauts are finding their way into the literature (Muga and Fong, 1976). Similarly, there are increasing numbers of studies addressing interaction of ocean waves and large objects relating to development of offshore oil and gas technology. To date, it appears that both areas of study have concentrated on shallow water conditions.

Our development concentrates on the behavior and effects of what may be termed discrete floes. Studies addressing other matters, such as water covered by elastic sheets and large and vast ice floes have been addressed by Greenhill (1887) and Hendrickson (1966), and Press and Ewing (1951), Hunkins (1962), Assur (1962) and LeSchack (1965), respectively. These works include theoretical and in some cases, observational studies. The observations pertinent to large and vast floes are from the Central Arctic Basin and deal with much longer wave periods than observed during this experiment.

It is possible that the observed thin ice cover may be approximated by an elastic sheet overlying an undulating water surface. The results of Greenhill (1887) suggest that under such circumstances there will be very substantial increases in wavelengths. A similar finding was made by Ofuya and Reynolds (1967), though the increases were only a few percent. The change in amplitude with distance in the ice canopy seen in Figure 14, may suggest such behavior for the longer wavelengths. It is believed that the data are insufficient to address this question. For such a study one might resort to use of an airborne laser and observe over a region covered with relatively large quantities of new ice, without the presence of floes and floebergs.

Examination of the problems of ice behavior in response to surface waves reveals that the floating object (taken to be of small surface dimension in comparison with wavelength) will oscillate with some six degrees of freedom (heave, surge, sway, roll, pitch, and yaw). The nomenclature used here follows that suggested by Kowalski (1974). The oscillation is forced through displacement of the object from its equilibrium position by pressure forces applied over its submerged surface. The equilibrium position results when buoyant and gravitational forces are the only forces acting and they are equal in magnitude but oppositely directed. Also the centers of buoyancy and gravity lie on the same vertical line. Free expression of the six motions assumes no restraint, although, induced motions are damped through friction with the water. Waves may be generated by the body as a result of its behavior.

An analytical treatment of the behavior of such rigid floating bodies is given by John (1949). The six equations of motions, to lowest order, are given by his equations (2.3.7) and (2.3.10). His work demonstrates the difficulties of treating such problems. Some simplifications are afforded by the shallow water approximation. For the shallow water case he finds that for fixed obstacles with small draught (keel) the reflection coefficient (for fixed wavelength) is independent of keel and increases with increasing diameter of the body at the water line. His Case IV, dealing with freely floating bodies, is more applicable to our circumstances. For this case he finds the reflection coefficient (for a cylinder) increases more gradually with increasing body diameter than for the fixed body case. This satisfies what John (1949) refers to as our intuitive notion of a freely floating body responding to incoming waves. More importantly to my work is his finding of dependence between the reflection coefficient and body diameter. This was not found to be the case in the modeling experiments of Wadhams (1973b). John (1949) also finds that the response, defined as the ratio of amplitude of vertical body motion to amplitude of incoming wave, diminishes (for fixed wavelength) nonlinearily as the body diameter increases. For slight immersion the response diminishes from 1 to approximately 0.1 as the body diameter increases from 0 to 1.0. For the present case, the observed floe diameters were sufficiently small, in contrast with wavelength, to occupy the region near zero--for which the response is near 1. For instances where the floes are larger in the interaction zone one might conceivably have difficulty measuring sail heights from either airborne laser or stereophotographic measurements, if John's conclusion is valid.

Theories which view the problem as the ice effects the waves have been developed by Peters (1950) and Weitz and Keller (1950). Peters (1950) addresses the effects on a surface wave produced by a thin floating mat. The wave is of sinusoidal form and progresses over water of infinite depth. The mat may be taken to be a first approximation to a canopy of broken ice or other floating material which consists of small particles which do not interact.

The formulation requires solution of a potential problem for a half plane, involving mixed boundary conditions. The only forces acting on the mat are due to gravity and the water pressure exerted beneath the mat. Introduction of dimensionless variables reveals the parameter $c = \delta g/(\delta_1 \omega^2 - \delta g)$, where δ is the water density, g the acceleration of gravity, ω the time frequency and δ_1 the density of the mat. Use of ω in the original paper implies it to be the radian wave frequency. Later in the original paper, δ_1 is referred to as the density of the mat per unit area. For our purposes it is assumed that δ_1 is a mat surface density which may be approximated by the density of ice multiplied by the ice thickness.

The author shows that the effect of the mat upon the surface waves depends upon the sign of c. If $c > 0$ the surface waves are attenuated by the mat not exponentially but as a power of $1/d$ where d is the distance inside the mat. For $c = 0$ the circumstance is equivalent to waves approaching an inflexible plate or dock. For $c < 0$ the waves transmit with altered wave length and amplitude. The changes in wave length and amplitude are functions of $|c|$. The author's equations (8.24), (8.21) and (1.12) reveal that if $|c|$ is small, waves within the mat will have longer wave lengths and smaller amplitudes than those of the open surface waves. For large $|c|$ the wave disturbance beneath the mat has a shorter wave length and smaller amplitude. For the condition $c = \infty$ there is no transmission of the waves into the mat.

The original work does not contain any numerical evaluations of c. An evaluation, using typical ocean wave periods, is presented in Figure 21. The range of ice thicknesses plotted in Figure 21 has been chosen to allow discussion of the widest range of the parameter c. The deepest ice keels observed to date are indicative of sea ice thicknesses between 30 and 50 meters. A more typical maximum thickness of deformed ice is approximately 20-25 meters. Undeformed sea ice has a maximum thickness of approximately 3 meters. With some exceptions, the thickest ice observed during the present experiment was approximately 10 meters.

From Figure 21 it is concluded that for typical ice thickness,

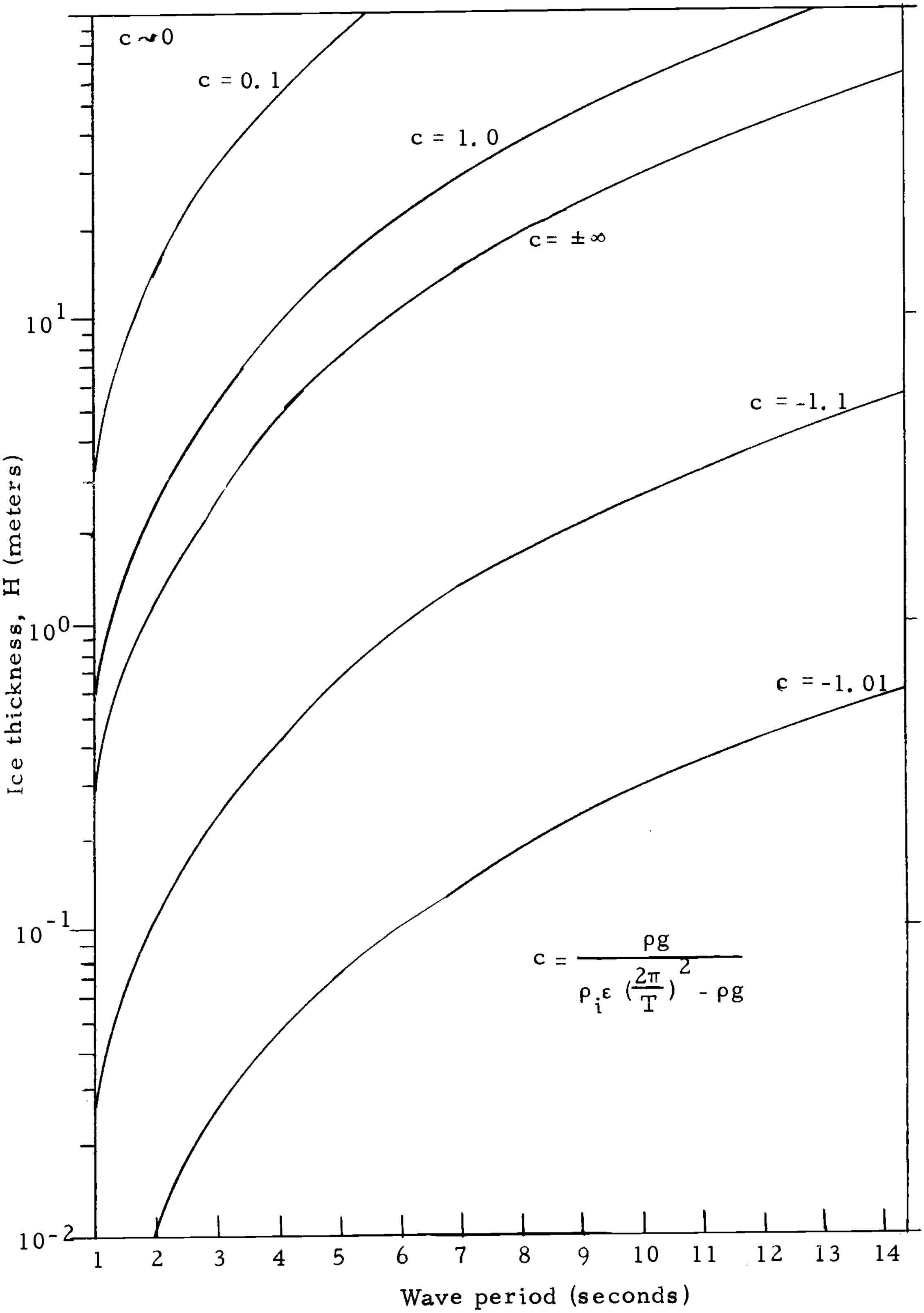

Figure 21. Coefficient c (Peters, 1950).

such as those observed during this experiment, the conditions $c=o$ and $c > o$ do not apply. $c \rightarrow \infty$ for wave periods generally less than 5 seconds. These wave periods, which Peters (1950) concluded are unable to transmit within the mat, lie within the noise region of the present experimental observations.

The pertinent portion of the ice thickness--wave period diagram to this work is characterized by $c < o$. The parameter $\delta_1 = o$ (presumably occasioned by having zero mat thickness) produces a value $c = -1$. As δ_1 cannot have values less than zero, the variable c does not apply for $c < o$ and $|c| < 1$. Values of -1.01 and -1.1 are plotted in Figure 21. We see that $c < o$ and $|c|$ is large except for very short periods and abnormally thick ice. It is expected then, according to Peters (1950), that ocean waves would transmit the mat region with decreasing wave lengths and amplitudes. These conditions arise when $\delta_1 \omega^2 < \rho g$.

The determination for $c < o$, that $|c| \sim 1$ is large based on Peters' terminology, stems from his allowing c to possess values between -1 and 0, i.e., $\delta_1 < o$.

The problem of water wave reflection with incidence on floating bodies, treated by John (1949), is simplified by the assumption that the floating material is composed of non-interacting mass points. By making that assumption an accounting for the mat may be made through modification of the boundary condition, to be satisfied by the potential function at the surface. This procedure is presented in an appendix by Weitz and Keller (1950). In essence the procedure is to combine the linearized Bernoulli equation, the surface dynamic condition and the equation of motion of one of the independent mass points. The velocity potential from linear wave theory, ϕ, satisfies the free surface boundary condition: $\phi_y = (\omega^2/g)\phi$, where ω is the radian wave frequency, and y is taken as the vertical axis. Following Weitz and Keller (1950), if the surface is covered by a rigid plate or dock the boundary condition reduces to $\phi_y = 0$. The boundary condition for a surface covered by non-interacting mass points is given by:

$$\phi_y = \phi\left(\frac{\rho\omega^2}{\rho g - m\omega^2}\right),$$

where ρ is the water density, and m the surface density of the floating material.

The work of Peters (1950) treated reflection when half the surface was covered by such a mat and the waves were normally incident at the mat edge. Goldstein and Keller (1950) have pursued a similar problem for the shallow water case but with variable angle of wave incidence with the mat edge.

The work of Weitz and Keller (1950) applies to finite depth and variable angle of incidence. They did not numerically evaluate their work though a qualitative description of wave behavior, as a function of α, was presented. The variable $\alpha = \dfrac{\rho\omega^2}{\rho g - m\omega^2}$ was described as follows: for $\alpha > o$ and sufficiently large there will be propagation within the ice; for $\alpha > o$ but not too large, there is no propagation within the ice; and, for $\alpha \leqslant o$ there is no propagation within the ice.

The variable α has been numerically evaluated over a range of ocean wave periods and ice thicknesses and is presented in Figure 22. For the majority of observed wave periods and ice thicknesses $\alpha > o$. The value of α approaches the free surface condition as ice thickness approaches zero as would be expected. Waves propagate within the ice canopy for these and larger α. The remark by Weitz and Keller (1950) that there is no propagation within the ice for $\alpha > o$ but α not too large is unclear, to this author. It would seem that the smallest positive value of α is precisely the condition $\alpha = \frac{\omega^2}{g}$.

There is no propagation within the ice when $\alpha \leqslant o$. These conditions exist (Figure 22) for abnormally thick ice and for very short wave periods. For $\alpha \rightarrow o$, m must become infinite. This condition would presumably be approached through creation of enormously thick ice. The $\alpha = o$ condition has been treated by Heins (1948). The results of Weitz and Keller (1950) are similar to those of Peters (1950) as can be seen through comparison of Figures 21 and 22.

Shapiro and Simpson (1953) simplified the mathematical theory of Weitz and Keller (1950) in order to develop a forecasting technique for sea and swell within a broken ice field. Their forecasting technique addresses wave periods from 2 to 9 seconds and ice thicknesses

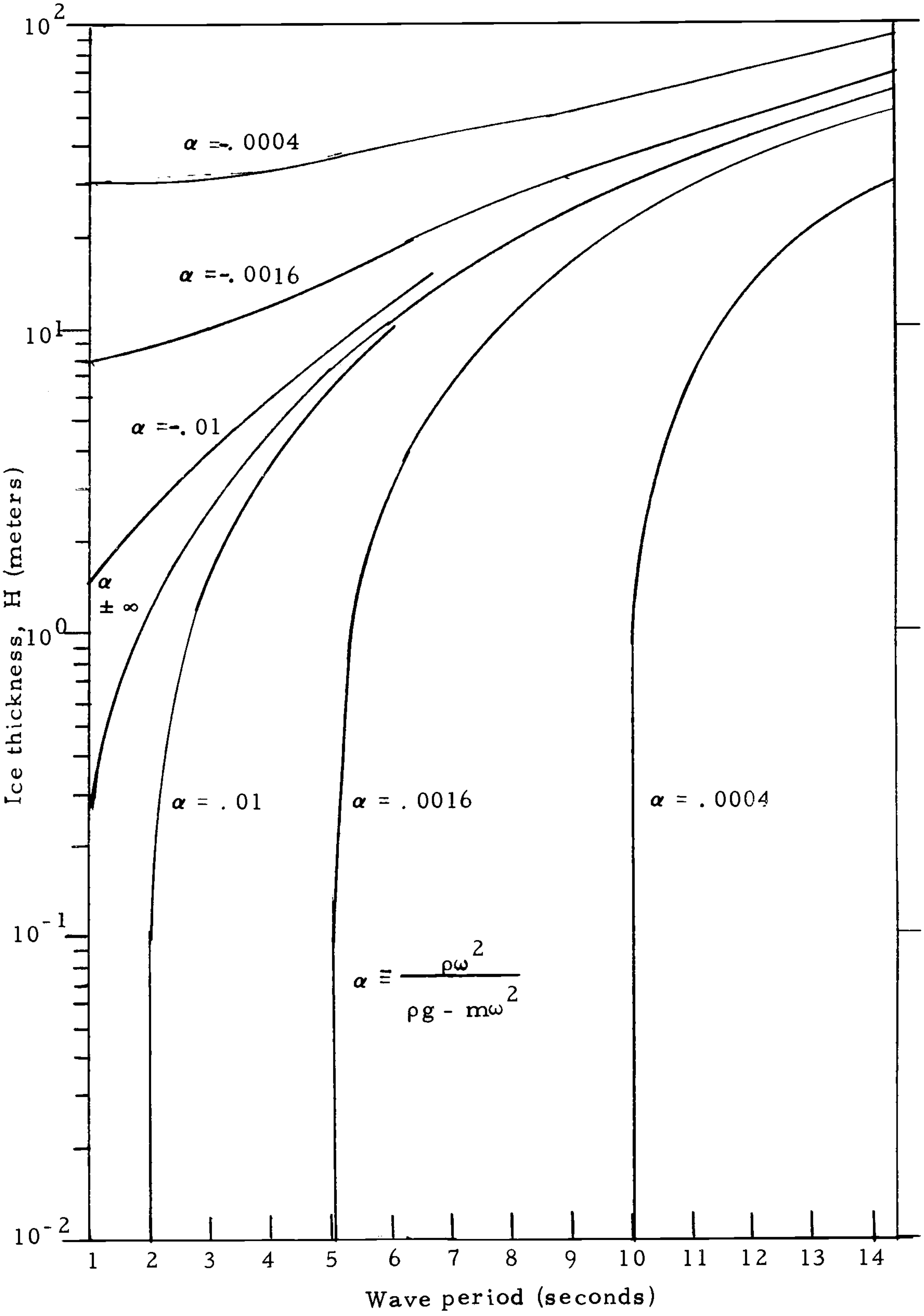

Figure 22. Coefficient α (Weitz and Keller, 1950).

1 foot (0.30 m) to 20 feet (6.1 m). The technique addresses both transmitted and reflected waves. In their development an inequality occurs between incident wave energy and the sum of reflected and transmitted wave energies. They attribute their apparent inconsistency to application of the theory of Weitz and Keller (1950). Shapiro and Simpson introduce a new factor, termed 'pressure energy', to eliminate the inconsistency. Pressure energy is considered to be a component of the transmitted energy which manifests itself as a pressure exerted against the underside of the ice.

The results of the Shapiro and Simpson (1953) forecasting technique have not agreed very well with measurements. There appears to be an error in their work as their reflection and transmission coefficients for wave energy are not related using the group (energy) velocity. This deficiency was corrected by Wadhams (1973b) though he reports the corrected functions to give equally poor agreement with field measurements.

A partial summary of the above developments may be clearer if we formulate the potential problem in equation form. The formulation presented here is contained in Hendrickson (1962) and Wadhams (1973b). The latter, chooses to orient the vertical axis to be positive downward and reverses the numbering of the pertinent regions. The parameter symbolism of Hendrickson (1962) and Wadhams (1973b) is nearly the same. Repetition of the formulation here follows the sign convention of Wadhams (1973b). The coordinates and a description of the circumstances are sketched in Figure 23.

If the flow is irrotational and occurs in an inviscid, incompressible fluid, then velocity potentials ϕ_n exist for each region n. Each potential satisfies Laplace's equation (equation of continuity):

$$\nabla^2 \phi_n = 0.$$

For regions n=1 and 3, the boundary conditions are taken to be:

$$\frac{\partial \phi_n}{\partial y} = o \Big|_{y=D} \text{ and } \frac{\partial \eta_n}{\partial t} = -\frac{\partial \phi_n}{\partial y} \Big|_{y=o}.$$

The instantaneous elevation of the free sea surface, from the Bernoulli equation, is given by:

$$\eta_n(x,t) = -\frac{1}{g} \frac{\partial \phi_n}{\partial t} \Big|_{y=o}.$$

Solutions satisfying these equations, pertinent to regions (n=1) and (n=3), are given by:

$$\phi_1 = [Be^{ikx} + Re^{-ikx}] e^{-ky} e^{-i\omega t}$$

and, $$\phi_3 = Te^{ikx} e^{-ky} e^{i\omega t}$$

where: $k = \omega^2/g = 2\pi/\lambda$, $|B|$ = amplitude of incident wave, $|R|$ = amplitude of reflected wave, $|R|/_{|B|}$ is an amplitude reflection coefficient and $|T|/_{|B|}$ is an amplitude transmission coefficient. With the assumption of no energy dissipation,

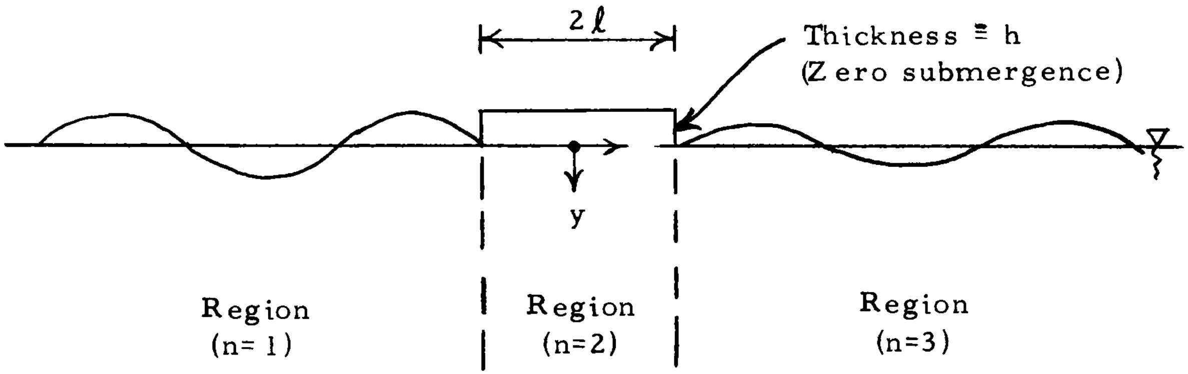

Plate extends to ∞, ⊥ page

Depth $\equiv D$
Wavelength $\equiv \lambda$
Radian wave frequency $\equiv \omega$

Plate density $\equiv \rho_i$
Fluid density $\equiv \rho$

Figure 23. Coordinates for the potential problem.

$$|R|^2 + |T|^2 = 1.$$

For region (n=2) it is assumed that the instantaneous elevation of the fluid surface, $\eta_2(x,t)$, is also the vertical floe displacement. The equation of motion for the floe (homogeneous elastic plate) is:

$$p(x,t) - L\frac{\partial^4 \eta_2}{\partial x^4} = \rho i h \frac{\partial^2 \eta}{\partial t^2}$$

where $p(x,t)$ is the pressure at the fluid/ice interface, and L the floe's flexural rigidity, equal to $Eh^3/12(1-\nu^2)$, where E is Young's modulus and ν is Poisson's ratio for sea ice. It is to be noted, following Assur (1962), that this expression for L is only valid for plates of great width. For finite floe widths Poisson's ratio need not be present, as was the case followed by Greenhill (1887).

Application of the linearized Bernoulli equation to the interface of region (n=2) yields:

$$\frac{p(x,t)}{\rho} = -g\eta_2 + \frac{\partial \phi_2}{\partial t}\Big|_{y=o}.$$

The boundary condition in region (n=2) is given by:

$$\frac{\partial \eta_2}{\partial t} = -\frac{\partial \phi_2}{\partial y}\Big|_{y=o}.$$

Considering the solution of φ_2 as a sum of potentials, it is found that:

$$\phi_2 = \sum_n [A_n e^{ik_n x} + B_n e^{-ik_n x}] e^{-k_n y} e^{i\omega t}$$

provided,

$$Lk_n^5 + (\rho g - \rho_i h\omega^2)k_n - \rho\omega^2 = o \quad (3)$$

This last expression, analogous to my Equation (2), is considered the dispersion relation for ice-coupled flexural-gravity waves. Though not noted above, this development incorporates the concept that wave period is conserved throughout.

By setting L = o, in Equation (3), the circumstance described as a mat of non-interacting mass points is produced, i.e.

$$k_n = \frac{\rho\omega^2}{\rho g - \rho_i h\omega^2}.$$

Through modification of the boundary conditions at the floe edges and by using alternate representations for the potentials, one can proceed from this outline to the works of Hendrickson (1962, 1963) and Wadhams (1973b). The latter study proceeds from Equation 3 and addresses ice-coupled flexural-gravity waves in a continuous ice cover (or one composed of giant and vast floes) leading to development of a steady state creep mechanism for attenuation of long period waves (Wadhams, 1973a). This interesting work does not apply to the circumstances of discrete floes addressed in this study.

The Hendrickson (1962) study is similarly inapplicable, due to restrictions imposed by the zero floe submergence condition and the largeness of floe width. His study includes an excellent review of the physical and elastic properties of sea ice. An attempt by Hendrickson

(1963) at treating the case of finite submergence was limited by computational costs and consequently yielded few results. The results do suggest the importance of the floe's submergence in acting as a barrier which severely alters the local flow. The barrier also serves to reflect wave energy.

For completeness I mention the work by Evans and Davies (1968), using the shallow water approximation. For water depths of order 10 meters, they found waves which transmit the ice canopy (non-interacting mass points) with undiminishing amplitude. A second model in the same report, treating the ice as an infinite elastic sheet, is of some interest as the results quantify dependence of reflection on wavelength, angle of incidence and ice thickness. The results fail to agree with the measurements obtained by Robin (1963) in the presence of big and vast floes.

Theoretical treatments of the phenomenon of ocean wave/sea ice interaction have not yielded results which have been confirmed by measurements. The necessary assumptions required to obtain solutions in some cases render the solutions inapplicable to the real world. On the other hand, the very few measurements available are deficient in many respects because of our inabilities to carry out, at one time, measurement of most of the relevant parameters. A second factor of importance is the simple fact that the available measurements have come from a variety of ice canopy conditions rather than a repetition under the same or closely similar conditions.

Modeling Studies

Only two physical models of the interaction phenomena are known to the author. These two studies (Henry, 1968 and Wadhams, 1973b) address the interaction of water waves and rigid floating objects which are intended to simulate discrete ice floes. For completeness, it is noted that two modeling studies of wave propagation in an elastic sheet have been undertaken by Szczesny and LeMehaute (1965) and Ofuya and Reynolds (1967).

The Henry (1968) model incorporated 1/4 inch (0.63 cm) polypropylene sheets cut to square shape to simulate ice floes. Wave heights were measured with a float gage. Channel bottom pressures were also monitored. Measured wave lengths, phase velocities and bottom pressure were found to be in agreement with linear wave theory, with and without the simulated ice cover. The results show an exponential decay of wave amplitude with propagation distance. The decay rate was only slightly greater for cases with simulated floes than with no simulated floes. Furthermore, the decay rates with simulated floes were found to be insensitive to either the size of floes or their total surface concentration. Undoubtedly these results stem from influences of the channel boundaries. The results of the Henry

(1968) study are inconclusive.

A second attempt at modeling the phenomena was undertaken by Wadhams (1973b). For his work, ice floes were simulated with plastic Petri dishes and 16 mm movie film cans made of aluminum. These containers were ballasted with plaster of Paris. A second Petri dish and the film can lids were set over the respective ballasted containers and attached with waterproof tape. The procedure simulated floes by setting their centers of mass below their geometric centers but produced some difficulties through container leakage. The results indicate the importance of wave reflection. Reflection from the simulated ice edge was greater than that from the interior region. Reflections from the interior floes were out of phase and, in the words of Wadhams, 'made the dominant reflection more difficut to pick out'. Although there is considerable scatter in the data, they suggest that the reflection obeys the Froude scaling criteria sufficiently to allow comparison with full scale measurements. The Froude Number, $F = \frac{v}{\sqrt{gL}}$, is a measure of the ratio of inertial to gravitational forces--where v is the characteristic velocity; g is the acceleration of gravity; and L is a characteristic dimension. The results of this study are expressed by plots of energy attenuation and a dimensionless number F_1, related to F. Energy attenuation is expressed by the ratio of the energy dissipated within the simulated ice canopy and the wave energy incident at the simulated ice edge. The term

F_1 is the product of the Froude Number (based upon a velocity given by the radian wave frequency times the wave amplitude and a characteristic length equal to the depth of immersion) and the ratio of floe thickness to wavelength. The plots contain considerable scatter and the author suggests that application of the relationship to full-scale would be a 'hazardous venture'. The relationship suggests that there is no dependence upon floe diameter which is a very significant finding.

The work in constructing the Wadhams (1973b) model and the efforts toward analysis of the results were substantial. The results were not compared quantitatively with full-scale observations. Difficulties were encountered by procedures used in tethering floes. The tethering was accomplished with strings and by attaching metal strips to the floes.

Difficulties with modeling the phenomenon stem also from inabilities to simultaneously satisfy the Froude and Reynolds criteria. The Reynolds Number is given by $R = \frac{vL}{\nu}$, where ν is the fluid kinematic viscosity. To satisfy both criteria one would presumably have to model with a fluid other than sea water. Being unable to do this, the viscous effects in the model exceed those of full-scale. As a consequence, model transmission coefficients will be less than those of full-scale.

As noted earlier in this work, attempts to model the wave/ice interaction phenomena have born little fruit--in spite of extensive and thorough efforts. In addition to the difficulties noted here and those documented in the original reports, there are the effects of impurities within the fluid which will have greatest effect upon surface phenomena. An example of surface contamination effects on wave modeling experiments has been noted by Longuet-Higgins (1960). Surface tension effects (simulated bonding of floes) may also be significant.

VII. CONCLUSIONS

The phenomenon of ocean wave/sea ice interaction is complex. There are numerous environmental parameters of a significant importance. Attempts to treat the problem mathematically and with physical models have not been very satisfactory. Theoretical treatments have been unable to simultaneously account for the number of significant environmental parameters; necessary simplifications render the results inapplicable to the real world. Construction of physical models has been hampered by several factors, particularly the absence of a suitable material for simulation of sea ice.

Given these circumstances, investigators are forced to address the problem through acquisition of full-scale measurements. Difficulties arise in making full-scale measurements because of our inabilities to simultaneously measure more than a portion of the pertinent parameters. Equally, if not more serious, are limitations imposed on measurement by weather conditions. Measurements obtained to date, including those reported here, have been made under a variety of environmental circumstances. As a consequence, it is most difficult to draw conclusive findings through comparisons of the published data sets. The variations in measurement circumstances unfortunately serve to minimize opportunities for more constructive criticism of theoretical studies.

The work reported here demonstrates the usefulness of the airborne stereophotogrammetric technique. The procedure provides an accurate measurement of the instantaneous deformation of the sea and sea ice surfaces thus enabling a determination of amplitude or energy spectra in wave number space. The technique provides a measure of all pertinent parameters except the underside ice keels. Spectra determined in this way are not subject to inexactnesses resulting from platform motion. Airborne laser and submarine upward-looking sonar observations are limited because of unresolvable platform motions and resultant effects on computed spectra of encounter. Additionally, laser and sonar observations are very limited because it is difficult to obtain measurements parallel to the wave number vector. This difficulty is even greater when submarines are used. The laser cannot be used at night due to the requirement for visibility of the ice and direction of wave propagation. To obtain long records (equivalent to those obtained with point measure in the time domain) with the stereophotogrammetric technique one must be able to increase flying altitude. Flying altitude is limited however, due to cloud ceilings and the decrease in measurement resolution with increasing altitude. The sea surface profile can be reliably constructed only if the ice floes are of the discrete type and the total profile deformation exceeds resolvable values. These two conditions are encountered only in the vicinity of the ice edge. The technique cannot be employed over regions of rapid attenuation with distance. For example, the amplitude attenuation of 50 to 75 m wavelengths over distances of one or two wavelengths reported by Dean (1966a) could not be resolved with the airborne stereophotogrammetric technique.

Airborne stereophotography does provide a means for determining numerous profiles of the sea surface and thereby enables a simultaneous collection of many records. Observations can be acquired very rapidly and significant dimensions of the ice canopy may be measured with precision. Study of wavelength alterations, suggested by theoretical studies, may require measurements of the interaction phenomenon such as these, which are in the spatial domain. The most obvious value of the stereophotogrammetric technique may be its usefulness for determining directional spectra. The questions of wave refraction may then be addressed. It may also be possible to study wave diffraction about ice floes with such observations.

The scattering of wavelengths which are in specific proportions with encountered floe diameters has been demonstrated. The observations confirm the hypothesis, first advanced by Robin (1963), and serve to define the diameter of the floe of maximum concentration as being most important in formulating the pertinent ratios. The reflection criteria is extended to greater ice thicknesses than previously observed; thereby confirming a second hypothesis suggested by Robin (1963). The absolute concentration of the floes of maximum concentration appears not to be of special importance. Although wave scattering is related to floe diameter, increasing floe thickness (or more probably floe keel) must eventually become the paramount factor in producing the reflection. The distribution of floes by size, not distance from the ice edge itself, is critical. The attenuation coefficient (β) has been determined for the stereophotogrammetric observations only to contrast my findings with those of Dean (1966a) and Wadhams (1973b). In an attempt to relate attenuation with distance Wadhams (1973b) resorted to a rearrangement of floe concentrations and the subsequent determination of attenuation as a function of effective penetration.

My analysis suggests that the rapid amplitude attenuation of wavelengths of maximum amplitude results from the mass effects of the ice canopy. Determination of the attenuation of wavelengths of maximum amplitude is of some importance. Based on earlier work alone one would grossly overestimate the depth of penetration for these wavelengths--given the general circumstances of increasing floe diameter with increasing distance from the ice edge. The observations reported by Robin (1963) were spaced at intervals that were too large to delineate the attenuation of the wavelengths of maximum amplitude. The observations reported by Dean (1966a) may agree with my finding regarding attenuation of wavelengths of maximum amplitude though a determination will require examination of the original observations. The laser observations (Wadhams, 1963b) are difficult to compare with the stereophotogrammetric observations because he had to use the spectra of encounter. Attenuation by the mass effects of the ice occurs until the longer waves encounter floe diameters which are large in comparison with wavelength, at which time the waves perform work in bending of the floes. In this study I did not address these circumstances which occur in the interior of the ice canopy. The computations made by Robin (1963) indicate that a small percentage of wave energy is required for the bending of floes; although the energy required for bending is proportional to $(H/\lambda)^3$.

VIII. RECOMMENDATIONS

A variety of measurement techniques have been used to study the interaction phenomenon. Each technique serves particular purposes and none are capable of measuring all of the relevant parameters simultaneously. Experimental work is not only costly but also taxing on the limited number of ships and aircraft available for oceanographic research, especially for the stereophotogrammetric technique which requires two aircraft. If further measurements are to be pursued, regardless of measurement technique, there may be considerable value in seeking shallow water conditions.

Very few investigators have acquired measurements of the interaction phenomenon. A re-examination of observations may be of value if similar analysis techniques could be incorporated so as to maximize comparison of findings. The differences in environmental circumstances may be accountable for, to some measure, through drag considerations. An examination of total wave drag in the presence of discrete ice floes would be of significant value. For such an examination an accounting would be required for both skin friction and pressure (form) drag, because the ice keels displace the potential flow. Small scale roughness elements may be of the order of a few millimeters. The area of the submerged portion of floes is unknown but some reasonable estimates, sufficient for evaluation of the wetted area, could be made. The frontal area of the floe keel would also have to be estimated. Various upward-looking sonar records may provide some assistance, at least for determining how streamlined the keels might be. The water particle velocities may serve as estimates of the free-stream velocity even for the small floes reported in this work which appear to be unable to surge or sway. The results of such a study may provide considerable insight. It would seem that the small floes reported here would produce considerable form drag. Studies of form drag must account for floes in three dimensions.

The oscillatory behavior of floes has not been addressed in this or other reports dealing with ocean wave/sea ice interaction. The simplified approach, which considers floes to be uniform, results in oscillation frequencies given by: $\omega_o = (g/K)^{\frac{1}{2}}$. For observed values of ice keels oscillation frequencies may be obtained if some accounting for floe shape and mass distribution can be made. Some guidelines for these studies may be found in the literature on development of ocean buoys, for example Kerr (1964). Such an undertaking might incorporate variable shape factors to enable speculation on the effects of floe sills, absence of symmetry and consequences of marginally stable configurations. The problem would be more complicated if new ice was fixed to and surrounding the floes. Analysis of the data presented in this report, indicates that floe attitudes remain constant, i.e. the central vertical axis of each floe remains in alignment with the local vertical. This observation is important for the buoyant force then varies with passage of the wave profile.

The data reported here may lend themselves to analysis of wave diffraction about floes. One or more floes might be selected for study from model 6 or 7, where attenuation of most wavelengths is reasonably complete. Elevation values read over a grid about the floe may then reveal wave behavior in the along crest direction. The detailed topography of the floe surface could also be measured and examined quantitatively for determination of the total amount of snow and ice contained in the sail.

The dependence of wave attenuation on the distribution of floe size justifies attempts to compare measured values with known distribution functions. The observation by Dean (1966a) that floe sizes were distributed as a half Gaussian curve is a step in this direction. The importance of my earlier comment, regarding the effects of zero floe diameter, is minimal in comparison with the value of knowing floe distribution in analytical form.

Studies of the distribution of floe sizes could be undertaken with existing airborne and satellite observations. It would be of interest to examine the change in floe size distributions with respect to latitude observed off East Greenland. Studies might also be made of the quantity of wave energy, and its spectral forms, which interact with the East Greenland ice over a period of time. Correlation may be found between the results of such a study and the quantity of ice existing in the region.

The number of occasions for ocean wave/sea ice interaction resulting from passage of a single extra-tropical cyclone over the Greenland-Norwegian Seas may be of interest. For example, Amstutz and Ketchum (1973) found two separate trains of ocean swell at a single location but coming from different directions. Both trains were hindcast to the same storm, which had translated rapidly between the two positions of swell generation.

The interaction of ocean waves and sea ice is deserving of further study because a great deal may be learned from Nature's floating breakwaters. The increased production of sea ice, which initiates with fracturing of floes by ocean waves, is of known importance.

There are numerous topics, associated with the phenomenon, which are open for study. The formation of pancake ice has been taken to be a consequence of ice formation in the presence of ocean surface waves. The exact sequence of events appears to be unknown. This associated phenomenon appears to have been totally overlooked. Undoubtedly the formation process itself has been observed, though no reports have come to this author's attention. Formation of pancake ice by wave interaction undoubtedly stems from the unique physical properties of the ice as well as the behavior of water particles within the wave boundary layer. The resulting surface geometry of the ice canopy will affect the further formation and growth of sea ice, simply from the fact that a compact array of equal diameter pancakes includes some 21% open water. The reported distribution of pancake diameters (up to 2 meters) seems too small for their formation to depend entirely on wavelength. Wave amplitude may be a more important factor.

A most interesting observation has been made as a result of the author's first study of ocean wave/sea ice interaction. In the first work, Amstutz and Ketchum (1973) reviewed numerous aerial photographs of sea ice near the open ocean. We observed that particular fragments of ice appear to move through the ice canopy as a result of the interaction process (see Figure 24). This phenomenon was not observed during the 1974 field experiment reported here, though one instance was observed at the second measurement site. The second site was located a few miles northward and was characterized by much less compacted ice. The motion of these pieces of ice appears to occur only when waves are present. Though few observations have been made to date, it appears that the motion is not induced by wind or current alone. The ice fragments appear to be either floebergs or pieces of glacial ice and are assumed therefore to have a considerable submerged volume. A recollection that Phillips (1966) had addressed the wave induced behavior of portions of surface films led to a review of his work. Sea ice 'covers' a portion of the ocean

Figure 24. 'Raining' of ice floes, October 1972--79. 2°N, 2°W, within diffuse ice edge. Scale: 1 cm = 130 m. (Naval Oceanographic Office, aerial photograph).

surface as does a surface film; though of course the ice is vastly different from our intuitive concept of a film (e. g. oil). The behavior of portions of surface films (slicks) related to their parallel to crest dimensions is described by Phillips (1966) on page 40. From his description, the name "raining" is suggested for the movement of particular pieces of ice through the canopy, though the mechanisms are undoubtedly dissimilar.

REFERENCES

Adee, Bruce H., 1976: A Review of Developments and Problems in Using Floating Breakwaters. Proceeding of the Offshore Technology Conference, Paper Number OTC 2543, pages 225-232.

Allan, A. J., 1975: The Breaking of Sea Ice by Ocean Waves. Scott Polar Research Institute, University of Cambridge, 20 pages.

Amstutz, D. E., and R. D. Ketchum, Jr., 1973: Observations of Swell Propagation Through Pack Ice in the East Greenland Sea. Paper read at 54th Annual Meeting, American Geophysical Union, Washington, D. C.

Amstutz, David, Donald Winfrey and Michael Longyear, 1975: An Analysis of Ocean Observations Collected Within a Small Region of the East Greenland Sea, Winter 1974. U.S. Naval Oceanographic Report, TN6140-75, 76 pages.

Amstutz, Mary Ann, 1976: Personal communication.

Assur, Andrew, 1958: Composition of Sea Ice and Its Tensile Strength. Arctic Sea Ice--Proceedings of a Conference by the National Academy of Sciences--National Research Council, Publication No. 598, pages 106-138.

Assur, Andrew, 1962: Breakup of Pack-Ice Floes. Contained in Kingery (1962), pages 335-347.

Barnett, Tim P., 1972: Observations of Wind Wave Generation and Dissipation in the North Sea: Implications for the Offshore Industry. Proceeding of the Offshore Technology Conference, Paper Number OTC 1516, pages 43-50.

Blackman, R. B., and J. W. Tukey, 1958: The Measurement of Power Spectra. Dover Publications, Inc., New York, 190 pages.

Boyle, R. J., 1965: Ice Glossary, U.S. Navy Electronics Laboratory, San Diego, 44 pages.

Chase, J., L. J. Cote, W. Marks, E. Mehr, W. J. Pierson, Jr., F. G. Rönne, G. Stephenson, R. C. Vetter, and R. G. Walden, 1957: The Directional Spectrum of a Wind Generated Sea as

Determined from Data Obtained by the Stereo Wave Observation Project. Office of Naval Research, Technical Report, Nonr 285 (03), Washington, D. C., 267 pages.

Cochran, W. T., J. W. Cooley, D. L. Favin, H. D. Helms, R. A. Kaenel, W. W. Lang, G. C. Maling, D. E. Nelson, C. M. Rader, and P. D. Welch, 1967: What is the Fast Fourier Transform? IEEE Transactions on Audio and Electroacoutics, AU-15 (2), pages 45-55.

Cooley, J. W. and J. W. Tukey, 1965: An Algorithm for the Machine Calculation of Complex Fourier Series. Mathematics of Computation, 19, pages 297-301.

Cote, L. J., J. O. Davis, W. Marks, R. J. McGough, E. Mehr, W. J. Pierson, Jr., J. F. Ropek, G. Stephenson, and R. C. Vetter, 1960: The Directional Spectrum of a Wind Generated Sea as Determined from Data Obtained by the Stereo Wave Observation Project. Meteorological Papers, New York University, College of Engineering, 2 (6), 88 pages.

Cox, F. N. and Wilford F. Weeks, 1973: Salinity Variations in Sea Ice. U.S. Army, Cold Regions Research and Engineering Laboratory, Hanover, New Hampshire, Research Report No. 310, 23 pages.

Davies, D. V. and D. V. Evans, 1968: Wave-Ice Interaction. Report Number 1313, Davidson Laboratory, Stevens Institute of Technology, Hoboken, New Jersey, 102 pages.

Davis, Thomas M. and Angelo L. Kontis, 1970: Spline Interpolation Algorithms for Track-Type Survey Data With Application to the Computation of Mean Gravity Anomalies. Naval Oceanographic Office Report, TR-226, Washington, D. C., 83 pages.

Davis, Thomas M., 1974: Theory and Practice of Geophysical Survey Design. Naval Oceanographic Office Report, NOO RP-13, Washington, D. C., 137 pages.

Dean, C. H., 1966a: The Attenuation of Ocean Waves Near The Open-Ocean/Pack Ice Boundary. Paper read at Symposium on Antarctic Oceanography, Scientific Communications on Antarctic Research, Santiago, Chile, September 13-16, 1966. (see Note after Dean (1966b).

Dean, C. H., 1966b: Wave Recording in a Field of Pack Ice--A Comparison of Three Independent Methods. This paper is believed to be unpublished. (Note: Drafts of the two excellent papers by C. H. Dean have been kindly provided to the author through the Office of the Secretary, Scott Polar Research Institute, Cambridge.)

Defant, Albert, 1961: Physical Oceanography. Pergamon Press, New York, Two Volumes, 1327 pages.

DeLeonibus, P. S., J. F. Boogaad, R. J. Sheil and B. E. Olson, 1973: Shipboard Observations of Wave Spectra With a Bow-Mounted Wave Height Sensor. Journal of Geophysical Research, 78, (15), pages 2650-2655.

Francois, R. E., 1972: New Observations of Ice Topography. Transactions of the American Geophysical Union, 53 (1018).

Goldstein, E. and J. B. Keller, 1950: Reflection of Waves in Shallow Water, unpublished. Note: This reference is found in Weitz and Keller (1950) with a note of referral to E. Goldstein's Master's Thesis, New York University. The author has not personally reviewed this Thesis.

Golovato, Paul, 1957: The Forces and Moments on a Heaving Surface Ship. Journal of Ship Research, 1, pages 19-26.

Goodman, D. J., A. J. Allan and R. G. Bilham, 1975: Wire Strainmeters on Ice. Nature, 255 (5503), pages 45-46.

Greenhill, A. G., 1887: Wave Motion in Hydrodynamics. American Journal of Mathematics, 9, pages 62-112.

Heins, A. E., 1948: Water Waves Over a Channel of Finite Depth with a Dock. American Journal of Mathematics, 70, pages 730-748.

Hendrickson, James A., Lois M. Webb and Robert J. Quigley, 1962: Study of Natural Forces Acting on Floating Ice Fields. Report NBy-32215 prepared for Naval Civil Engineering Laboratory, Port Hueneme, California, 72 pages.

Hendrickson, James A. and Lois M. Webb, 1963: Theoretical Investigation of Semi-Infinite Ice Floes in Water of Infinite Depth. National Engineering Science Company, Pasadena, California, NESCO No. P-457/SN-113, 43 pages.

Hendrickson, J. A., 1966: Interaction Theory for a Floating Elastic Sheet of Finite Length With Gravity Waves in Water of Finite Depth (Including a Comparison With Experimental Data). Report NBy-62185 prepared for U.S. Naval Civil Engineering Laboratory, Port Hueneme, California, 178 pages. (This reference is from Wadhams: 1973b).

Henry, Charles J., 1968: Wave-Ice Interaction Model Experiments. Report 1314, Davidson Laboratory, Stevens Institute of Technology, Hoboken, New Jersey, 50 pages.

Hildebrand, F. B., 1956: Introduction to Numerical Analysis. McGraw-Hill Book Company, New York, 511 pages.

H. O. Publication No. 606-d, 1968: Ice Observations, U.S. Naval Oceanographic Office, Washington, D. C. 42 pages.

Hunkins, Kenneth, 1962: Waves on the Arctic Ocean. Journal of Geophysical Research, 67(6), pages 2477-2489.

Ippen, Arthur T., 1966: Estuary and Coastline Hydrodynamics. McGraw-Hill Book Company, Inc., New York, 744 pages.

John, Fritz, 1949: On the Motion of Floating Bodies, I. Communications on Pure and Applied Mathematics, 2(1), pages 13-57.

Kerr, K. P., 1964: Stability Characteristics of Various Buoy Configurations. Buoy Technology, Transactions of the 1964 Buoy Technology Symposium, Marine Technology Society, Washington, pages 1-16.

Ketchum, R. D., Jr., 1970: Preliminary Analysis of Laser Terrain Profiles of Sea Ice Surfaces. Naval Oceanographic Office Report, IR No. 70-35, Washington, D. C., 27 pages.

Ketchum, R. D., Jr., 1971: Airborne Laser Profiling of the Arctic Pack Ice. Remote Sensing of the Environment, 2, pages 41-52.

Ketchum, R. D., and W. I. Wittmann, 1972: Recent Remote Sensing Studies of the East Greenland Pack Ice. Sea Ice Conference Proceedings, Reykjavik, Iceland, pages 213-226.

Kingery, W. D., 1963: (editor) Ice and Snow. Proceedings of a Conference held at the Massachusetts Institute of Technology.

February 12-16, 1962, The M.I.T. Press, Cambridge, Massachusetts, 684 pages.

Kinsman, Blair, 1965: Wind Waves--Their Generation and Propagation on the Ocean Surface. Prentice-Hall, Inc., Englewood Cliffs, New Jersey, 676 pages.

Kovacs, Austin, 1971: On Pressured Sea Ice. Sea Ice Conference Proceedings, Reykjavik, Iceland, pages 276-295.

Kovacs, A., W. F. Weeks, S. Ackley and W. D. Hibler, III, 1972: A Study of a Multiyear Pressure Ridge in the Beaufort Sea. Aidjex Bulletin, University of Washington, Number 12, pages 17-28.

Kovacs, Austin and Anthony J. Gow, 1976: Some Characteristics of Grounded Floebergs Near Prudhoe Bay, Alaska. U.S. Army Cold Regions Research and Engineering Laboratory, Hanover, New Hampshire, Report No. 76-34, 10 pages.

Kowalski, T., 1974: Suggested Nomenclature. Floating Breakwaters Conference Papers, Marine Technical Report Series Number 24, University of Rhode Island, Kingston, Rhode Island, pages 297-298.

Kozo, Thomas L. and Orest I. Diachuck, 1973: Spatial Variability of Topside and Bottomside Ice Roughness and Its Relevance to Underside Acoustic Reflection Loss. Aidjex Bulletin Number 19, University of Washington, Seattle, Washington, pages 113-121.

LaViolette, Paul E., Stuart Locke, Jr., and Charles Vermillion, 1975: Use of APT Satellite Infrared Data in Oceanographic Survey Operations. Transactions, American Geophysical Union, 56(5), pages 276-282.

LeSchack, L. A., 1965: On the Generation and Directional Recording of Waves in the Arctic Ocean. Naval Oceanographic Office Report, TR 179, 44 pages.

LeSchack, L. A., W. D. Hibler, III and F. H. Morse, 1970: Automatic Processing of Arctic Pack Ice Data Obtained by Means of Submarine Sonar and Other Remote Sensing Techniques. Office of Naval Research, Technical Report, NR-307-322, Washington, D.C., 45 pages.

Longuet-Higgins, M. S., 1960: Mass Transport in the Boundary Layer at a Free Oscillating Surface. Journal of Fluid Mechanics, 8(2), pages 293-306.

Lyon, Waldo K., 1967: Under Ice Profiles of Sea Ice Observed by Submarine. Proceedings of International Conference on Low Temperature Science, Hokkaido University, 1966, 1, Part 2, pages 707-711.

Malmgren, Finn, 1927: On the Properties of Sea Ice. Norwegian North Polar Expedition Aboard the Maud, 1918-1925, Scientific Results, 1(5), pages 1-67.

McLellan, Hugh, J., 1965: Elements of Physical Oceanography. Pergamon Press, New York, 151 pages.

Muga, Bruce J. and Howard Fong, 1976: Wave Forces Induced on Very Large Crude Carriers. Proceedings of the Offshore Technology Conference, Paper Number OTC 2535, pages 125-141.

Navair, 1969: Reconnaissance Reference Manual, Navair 10-1-789. Department of the Navy, Naval Air Systems Command, Washington, D. C., 208 pages.

Neumann, G., and W. J. Pierson, Jr., 1966: Principals of Physical Oceanography. Prentice-Hall, Inc., 545 pages.

Ofuya, A. O. and A. J. Reynolds, 1967: Laboratory Simulation of Waves in an Ice Floe. Journal of Geophysical Research, 72(14), pages 3567-3583.

Parmerter, R. R. and M. D. Coon, 1973: On the Mechanics of Pressure Ridge Formation in Sea Ice. Offshore Technology Conference, Paper Number OTC 1810, 10 pages.

Peters, A. S., 1950: The Effect of a Floating Mat on Water Waves. Communications on Pure and Applied Mathematics, 3, pages 319-354.

Press, Frank and Maurice Ewing, 1951: Propagation of Elastic Waves in a Floating Ice Sheet. Transactions, American Geophysical Union, 32(5), pages 673-678.

Richey, E. P. and R. E. Nece, 1974: Floating Breakwaters--State of the Art. Floating Breakwaters Conference Papers, Marine Technical Report Series Number 24, University of Rhode Island, Kingston, Rhode Island, pages 1-21.

Robertson, James M., 1965: Hydrodynamics in Theory and Application. Prentice-Hall, Inc., Englewood Cliffs, New Jersey, 652 pages.

Robin, G. deQ., 1963: Wave Propagation Through Fields of Pack Ice. Philosophical Transactions of the Royal Society of London, Series A, 255(1057), pages 313-339.

Robin, G. deQ., 1976: Personal communication.

Ross, D. B., R. A. Peloquin and R. J. Sheil, 1968: Observing Ocean Surface Waves with a Helium-Neon Laser. Fifth Symposium on Military Oceanography, Panama City, Florida, 18 pages.

Sater, John E., 1963: (coordinator) The Arctic Basin. Published by Tidewater Publishing Corporation for Arctic Institute of North America, 319 pages.

Schule, J. J., L. S. Simpson and P. S. DeLeonibus, 1971: A Study of Fetch-Limited Wave Spectra with an Airborne Laser. Journal of Geophysical Research, 76, pages 4160-4171.

Shapiro, A. and L. S. Simpson, 1953: The Effect of a Broken Ice Field on Water Waves. Transactions, American Geophysical Union, 34(1), pages 36-42.

Shore Protection Manual, 1973: U.S. Army Coastal Engineering Research Center, Fort Belvoir, Virginia, Volume 1, pages 79-98.

Simpson, Lloyd S., 1967: Preliminary Investigation of the Directional Spectrum of Ocean Wave Height as Obtained from Stereo Wave Photographs. Naval Oceanographic Office Report, IM No. 67-1, Washington, D. C., 8 pages.

Stokes, G. G., 1847: On the Theory of Oscillatory Waves. Transactions of the Cambridge Philosophical Society, 8(441).

Stokes, G. G., 1880: Supplement to a Paper on the Theory of Oscillatory Waves. Mathematical and Physical Papers, Cambridge, pages 314-326.

Swithinbank, Charles, 1971: Arctic Pack Ice From Below. Sea Ice Conference Proceedings, Reykjavik, Iceland, pages 246-254.

Szczesny, C. H. and B. LeMehaute, 1965: Experimental Investigation of Ice Floe Under Wave Action. National Engineering Science Company, Pasadena, California, Report NBy-32256 prepared for U.S. Naval Civil Engineering Laboratory, Port Hueneme, California, 34 pages.

Thompson, Morris M., 1966: (editor) Manual of Photogrammetry. Third Edition. American Society of Photogrammetry, Falls Church, Virginia, 1199 pages.

Tucker, M. J., 1956: A Shipborne Wave Recorder. Transactions of the Institute of Naval Architects, London, 98 pages 236-250.

Tukey, J. W., 1967: An Introduction to the Calculations of Numerical Spectrum Analysis. Proceedings of the Advanced Seminar on Spectral Analysis of Time Series, Wiley, New York, pages 25-46.

Ursell, F., 1947: The Effect of a Fixed Vertical Barrier on Surface Waves in Deep Water. Proceedings of the Cambridge Philosophical Society, 43, pages 374-382.

Wadhams, P., 1971: Measurement of Wave Attenuation in Pack Ice by Inverted Echo Sounding. Sea Ice Conference Proceedings, Reykjavik, Iceland, pages 254-260.

Wadhams, P., 1973a: Attenuation of Swell by Sea Ice. Journal of Geophysical Research, 78(18), pages 3552-3563.

Wadhams, P., 1973b: The Effect of a Sea Ice Cover on Ocean Surface Waves. Ph.D. Dissertation, University of Cambridge, 224 pages.

Weeks, W. F. and Austin Kovacs, 1970: On Pressure Ridges. A Report to the U.S. Coast Guard by the U.S. Army Cold Regions Research and Engineering Laboratory, Hanover, New Hampshire, 106 pages.

Weitz, Mortimer and Joseph B. Keller, 1950: Reflection of Water Waves from Floating Ice in Water of Finite Depth. Communications in Pure and Applied Mathematics, 3(3), pages 305-318.

Welsh, J. P. and W. B. Tucker, 1971: Sea Ice Laser Statistics. Proceedings of the Seventh International Symposium on Remote Sensing of the Environment, May, 1971, University of Michigan, Ann Arbor, 2, pages 1165-1175.

Wittmann, W. I. and J. J. Schule, 1966: Comments on the Mass Budget of Arctic Pack Ice. Proceedings of the Symposium on the Arctic Heat Budget and Atmospheric Circulation, the Rand Corporation (RM-5233-NSF), pages 217-246.

W. M. O., 1970: World Meteorological Organization Sea-Ice Nomenclature. WMO/OMM/BMO-No. 259, TP. 145, Parts I and II, 12 pages.

Yosida, Zyungo, 1962: Physical Properties of Snow. Contained in Kingery (1962), pages 485-527.

APPENDIX

APPENDIX A

Glossary of Ice Terminology

The words listed below are defined in accordance with the World Meteorological Organization (WMO, 1970). Sea ice nomenclature, rather like the substance, is subject to frequent change. One can only trust that changes in terminology will one day be viewed to have been evolutionary. The terminology has increased as methods of observations and uses for the observations have increased. For example, the deployment of nuclear submarines throughout the Arctic has led to under-ice terminology, such as "ice skylights" and "hostile ice" (Boyle, 1965); also compare WMO (1970). Other examples of unique nomenclature may be found which are traceable to the advent of visual aerial observations, and to the frequent navigation by icebreakers associated with development and resupply of the Arctic Distant Early Warning radar network. Readers interested in the procedures for reporting of ice observations are referred to H. O. Pub. No. 606-d (1968).

APPENDIX A

ICE TERMINOLOGY

bergy bit: A large piece of floating glacier ice, generally showing less than 5 m above sea level but more than 1 m and normally about 100-300 square meters in area.

brash ice: Accumulations of floating ice made up of fragments not more than 2 m across, the wreckage of other forms of ice.

bummock: From the point of view of the submariner, a downward projection from the underside of the ice canopy; the counterpart of a hummock.

close pack ice: Pack ice in which the concentration is 7/10 to 8/10 (6/8 to less than 7/8), composed of floes mostly in contact.

compacted ice edge: Close, clear-cut ice edge compacted by wind or current; usually on the windward side of an area of pack ice.

compact pack ice: Pack ice in which the concentration is 10/10 (8/8) and no water is visible.

concentration: The ratio in tenths of the sea surface actually covered by ice to the total area of sea surface, both ice-covered and ice-free, at a specific location or over a defined area.

consolidated pack ice: Pack ice in which the concentration is 10/10 (8/8) and the floes are frozen together.

consolidated ridge: A ridge in which the base has frozen together.

dark nilas: Nilas which is under 5 cm in thickness and is very dark in color.

deformed ice: A general term for ice which has been squeezed together and in places forced upwards (and downwards).

diffuse ice edge: Poorly defined ice edge limiting an area of dispersed ice; usually on the leeward side of an area of pack ice.

fast ice: Sea ice which forms and remains fast along the coast, where it is attached to the shore, to an ice wall, to an ice front, between shoals or grounded icebergs. Vertical fluctuations may be observed during changes of sea-level. Fast ice may be formed in situ from sea water or by freezing of pack ice of any age to the shore, and it may extend a few meters or several hundred kilometers from the coast. Fast ice may be more than one year old and may then be prefixed with the appropriate age category (old, second-year, or multi-year).

first-year ice: Sea ice of not more than one winter's growth, developing from young ice; thickness 30 cm - 2 m. May be subdivided into thin first-year ice/white ice, medium first-year ice and thick first-year ice.

floating ice: Any form of ice found floating in water. The principal kinds of floating ice are lake ice, river ice, and sea ice, which form by the freezing of water at the surface, and glacier ice (ice of land origin) formed on land or in an ice shelf. The concept includes ice that is stranded or grounded.

floe: Any relatively flat piece of sea ice 20 m or more across.

Floes are subdivided according to horizontal extent as follows:

Giant:	Over 10 km across.
Vast:	2-10 km across.
Big:	500-2,000 m across.
Medium:	100-500 m across.
Small:	20-100 m across.

floeberg: A massive piece of sea ice composed of a hummock, or a group of hummocks, frozen together and separated from any ice surroundings. It may float up to 5 m above sea level.

fracture: Any break or rupture through very close pack ice, compact pack ice, consolidated pack ice, fast ice, or a single floe resulting from deformation processes. Fractures may contain brash ice and/or be covered with nilas and/or young ice. Length may vary from a few meters to many kilometers.

fracturing: Pressure process whereby ice is permanently deformed, and rupture occurs. Most commonly used to describe breaking across very close pack ice, compact pack ice and consolidated pack ice.

frazil ice: Fine spicules or plates of ice, suspended in water.

friendly ice: From the point of view of the submariner, an ice canopy containing many large skylights or other features which permit a submarine to surface. There must be more than ten such features per 30 nautical miles (56 km) along the submarine's track.

glacier ice: Ice in, or originating from, a glacier, whether on land or floating on the sea as icebergs, bergy bits or growlers.

grease ice: A later stage of freezing than frazil ice when the crystals have coagulated to form a soupy layer on the surface.

grey ice: Young ice 10-15 cm thick. Less elastic than nilas and breaks on swell. Usually rafts under pressure.

grey-white ice: Young ice 15-30 cm thick. Under pressure more likely to ridge than to raft.

growler: Smaller piece of ice than a bergy bit or floeberg, extending less than 1 m above the sea surface and normally occupying an area of about 20 square meters.

hostile ice: From the point of view of the submariner, an ice canopy containing no large skylights or other features which permit a submarine to surface.

hummock: A hillock of broken ice which has been forced upwards by pressure. May be fresh or weathered. The submerged volume of broken ice under the hummock, forced downwards by pressure, is termed a bummock.

ice cake: Any relatively flat piece of sea ice less than 20 m across.

ice canopy: Pack ice from the point of view of the submariner.

ice cover: The ratio of an area of ice of any concentration to the total area of sea surface within some large geographic local; this local may be global, hemispheric, or prescribed by a specific oceanographic entity such as Baffin Bay or the Barents Sea.

ice edge: The demarcation at any given time between the open sea and sea ice of any kind, whether fast or drifting. It may be termed compacted or diffuse.

ice keel: From the point of view of the submariner, a downward-projecting ridge on the underside of the ice canopy; the counterpart of a ridge. Ice keels may extend as much as 50 m below sea level.

large fracture: More than 500 m wide.

lead: Any fracture or passageway through sea ice which is navigable by surface vessels.

light nilas: Nilas which is more than 5 cm in thickness and rather lighter in color than dark nilas.

medium fracture: 200 to 500 m wide.

multi-year ice: Old ice up to 3 m or more thick which has survived at least two summers' melt. Hummocks even smoother than in second-year ice, and the ice is almost salt-free. Color, where bare, is usually blue. Melt pattern consists of large interconnecting irregular puddles and a well-developed drainage system.

new ice: A general term for recently formed ice which includes frazil ice, grease ice, slush and shuga. These types of ice are composed of ice crystals which are only weakly frozen together (if at all) and have a definite form only while they are afloat.

new ridge: Ridge newly formed with sharp peaks and slope of sides usually 40°. Fragments are visible from the air at low altitude.

nilas: A thin elastic crust of ice, easily bending on waves and swell and under pressure, thrusting in a pattern of interlocking "fingers" (finger rafting). Has a matt surface and is up to 10 cm in thickness. May be subdivided into dark nilas and light nilas.

open water: A large area of freely navigable water in which sea ice is present in concentrations less than 1/10 (1/8). When there is no sea ice present, the area should be termed ice-free, even though icebergs are present.

pack ice: Term used in a wide sense to include any area of sea ice, other than fast ice, no matter what form it takes or how it is disposed.

pancake ice: Predominantly circular pieces of ice from 30 cm - 3 m in diameter, and up to about 10 cm in thickness, with raised rims due to the pieces striking against one another. It may be formed on a slight swell from grease ice, shuga or slush or as a result of the breaking of ice rind, nilas or, under severe conditions of swell or waves, of grey ice. It also sometimes forms at some depth, at an interface between water bodies of different physical characteristics, from where it floats to the surface; its appearance may rapidly cover wide areas of water.

polynya: Any non-linear shaped opening enclosed in ice. Polynyas may contain brash ice and/or be covered with new ice, nilas or young ice; submariners refer to these as skylights. Sometimes the polynya is limited on one side by the coast and is called a short polynya or by fast ice and is called a flaw polynya. If it recurs in the same position every year, it is called a recurring polynya.

recurring polynya: A polynya wich recurs in the same position every year.

ridge: A line or wall of broken ice forced up by pressure. May be fresh or weathered. The submerged volume of broken ice under a ridge, forced downwards by pressure, is termed an ice keel.

sea ice: Any form of ice found at sea which has originated from the freezing of sea water.

second-year ice: Old ice which has survived only one summer's melt. Because it is thicker and less dense than first-year ice, it stands higher out of the water. In contrast to multi-year ice, summer melting produces a regular pattern of numerous small puddles. Bare patches and puddles are usually greenish-blue.

shore lead: A lead between pack ice and the shore or between pack ice and an ice front.

shuga: An accumulation of spongy white ice lumps, a few centimeters across; they are formed from grease ice or slush.

skylight: From the point of view of the submariner, thin places in the ice canopy, usually less than 1 m thick and appearing from below as relatively light, translucent patches in dark surroundings. The undersurface of a skylight is normally flat. Skylights are called large if big enough for a submarine to attempt to surface through them (120 m), or small if not.

slush: Snow which is saturated and mixed with water on land or ice surfaces, or as a viscous floating mass in water after a heavy snowfall.

small fracture: 50 to 200 m wide.

snow-covered ice: Ice covered with snow.

thick first-year ice: First-year ice over 120 cm thick.

thin first-year ice: First year ice 30-70 cm thick.

very small fracture: 0 to 50 m wide.

very weathered ridge: Ridge with tops very rounded, slope of sides usually 20°-30°.

weathered ridge: Ridge with peaks slightly rounded and slope of sides usually 30° to 40°. Individual fragments are not discernible.

young ice: Ice in the transition stage between nilas and first-year ice, 10-30 cm in thickness. May be subdivided into grey ice and grey-white ice.